UCLouvain

AGRO LOUVAIN

Faculté des bioingénieurs

Tropical forest type and land cover mapping from SAR-C multi-year time series (Sentinel-1)

Pokola area, Sangha Province (Rep. of Congo)

Auteur : Thibauld Collet
Promoteur(s) : Pierre Defourny (UCLouvain/ELI/ELIE)

Lecteur(s) : Patrick Bogaert (UCLouvain/ELI/ELIE)
Quentin Ponette (UCLouvain/ELI/ELIE)

Année académique 2021-2022
Mémoire de fin d'études présenté en vue de l'obtention du diplôme de Bioingénieur : Sciences et technologie de l'environnement

Acknowledgments

Je voudrais avant toute chose remercier mon promoteur le Professeur Pierre Defourny pour son encadrement de qualité, ses précieux conseils ainsi que ses enseignements qui m'ont permis de découvrir le merveilleux monde de la géomatique.

Je remercie également chaleureusement Baptiste Delhez pour sa patience, son accompagnement, ses constants encouragements et sa disponibilité tout au long de mon travail. Baptiste à fournit un encadrement technique et psychologique que tout mémorant rêverait d'avoir et je lui en suis reconnaissant.

Plusieurs chercheurs et professeur du laboratoire ELIE m'ont également apporté leur aide durant cette année académique. Pour ne citer qu'eux je remercie Nicolas et Quentin Deffense pour leur aide technique ainsi que Juliette Dalimier et Jean Bouchat. Ainsi que Patrick Bogaert pour son aide dans le domaine des statistiques. Je remercie également tous les membres de l'équipe du troisième étage qui contribue à rendent cet endroit propice au travail et à la bon humeur.

Finalement, ma famille qui m'ont accompagnés durant ces cinq années d'études, je n'aurait sans doute pas réussi sans vous. Merci à tous les proches et amis que je me suis fait durant ces cinq année à Louvain-La-Neuve, je pense particulièrement à Marco, Hugo et Maureen, mes compagnons de route durant cette belle aventure…

Content

List of figures ... 4
Acronyms table ... 7
Introduction ... 8
1.1 Geographical context ... 9
1.2 Remote sensing of tropical forest ... 11
1.3 Sentinel-1 data ... 15
1.4 Classification process ... 15
1.5 Sentinel-1 application ... 16
Chapter 2: Study area ... 20
Chapter 3 : Materials and methods ... 22
3.1 Materials ... 22
3.1.1 SLC Sentinel_1 data ... 22
3.1.3 Visualization sources ... 23
3.1.4 Other information materials ... 23
3.2 Methods ... 24
3.2.1 Sentinel-1 features computation ... 24
3.2.2 Index computation ... 24
3.2.3 Colour composite images ... 27
3.2.4 Textural features ... 28
3.2.5 Forest and land cover typology ... 29
3.2.6 Collection of training data ... 39
3.2.7 Unsupervised multiresolution segmentation algorithm (MRS) ... 40
3.2.8 Classification ... 42
3.2.9 Accuracy assessment ... 44
Chapter 4: Results and discution ... 46
4.1 Classification results and model saturation ... 46
4.2 Forest-mask and comparison with optical classification ... 47
4.3 Forest type and land cover classification (Level 3) ... 50
4.3.1 Non-textural PBIA approach ... 50
4.3.2 OBIA approach ... 51
4.3.3 Textural PBIA approach ... 52
4.3.4 Analysis of the best classification ... 53
4.3.5 Class boundaries ... 57
4.3.6 Prediction probability map ... 58
4.3.7 Complete land cover map ... 61
Conclusion ... 62
Appendices ... 63

List of figures

Figure 1 : Tropical rain forest view close to the Sangha river (dzanga-sangha.org) 8
Figure 2 : Theorical forest transition curve (Megevand and al., 2013)..... 10
Figure 3 : High-Resolution World Maps of 21st-Century Forest Cover Change (Hansen and al., 2013) 12
Figure 4 : Sentinel-1 orbitals map (ESA, no date)..... 13
Figure 5 : Schematic of the four acquisitions mode (ESA, no date)..... 14
Figure 6 : Evolution of a land cover classification performance with number of Sentinel-1 and Sentinel-2 features input. Sentinel-1 and 2 (Audreye and al. 2019)..... 16
Figure 7 : Illustration of SAR shadowing effect at the edges of a forest stand (A. Bouvet et al., 2018)..... 17
Figure 8 : Topographic map of the ROI using SRTM data. Main roads, cities and main rivers are mentioned. 20
Figure 9 : Köppen-Geiger climate classification (Beck, H. E and al. , 2018) and Pokola's ombrothermic diagram (Climate-data.org 2021)..... 21
Figure 10 : Pokola wetlands map. On the lower left the whole Cuvette centrale wetlands is represented using G.Dargie and al., (2018) classification based on SRTM, Landsat and ALOS PALSAR data. 21
Figure 11 : Orbital 7 (red) and ROI (Blue) 22
Figure 12 : Diagram of the various pre-processing steps applied on the SLC data (ESA Sen4Stat, 2021)..... 22
Figure 13 : Illustration of the Quegan filter application. The base image is in red, the filter is in green, and the final filtered image is in blue (Nicolas Deffense and al. , 2020) 23
Figure 14 : Comparison between a one day (left) one year (middle) and 4-year (right) long time series from the Mean VH polarization value. 24
Figure 15 : Illustration of the effect of the SARad transformation on A) CVVH and C) MeanVH into respectively B) SARad CVVH and D) RVI. 25
Figure 16 : Pixel value distribution from CVVH and SARad CVVH 26
Figure 17 : Plot of the correlation between SARad CVVH and his respective component : MeanVH +MeanVV (left) and CVVH (right). 26
Figure 18 : Colour composite image of the Pokola area used for photointerpretation. 27
Figure 19 : Schematic of the GLCM computation. The initial 3x3 image is centred on the pixel of interest. GLCM is build in the horizontal direction. For 9 pixels of 3 shade of grey (N) we end up with a NxN matrix filled with 6-pixel combination. On the right are presented 4 of the 14 computable features. 28
Figure 20 : Comparison of various window size on the GLCM "Mean" textural feature of RVI feature (A = 5x5, B = 11x11, C = 21x21 and D = 41x41)..... 28
Figure 21 : Comparison of 3 different visualization from Pokola and its surroundings. Colour composite is made combining 4 years long time series. Planet images were collected for the year 2020. 29
Figure 22 : A) Ouésso city centre. B) Ouésso suburbs. C) Ouésso landing strip. 1) Colour composite [RVI, SARadCVVH, SARadCVVV]. 2) Planet images [Band 4 (Red), Band 3 (Green) and Band 2 (Blue)]. 3) Maxar images (Google earth, 2022). 30
Figure 23 : A) Low density low vegetation area near Pokola. 1) Colour composite [RVI, SARadCVVH, SARadCVVV]. 2) Planet images [Band 4 (Red), Band 3 (Green) and Band 2 (Blue)]. 3) Planet images [Band 3 (Red), Band 2 (Green) and Band 1 (Blue)]..... 31
Figure 24 : A) Sparse vegetation surrounding a road in Pokola suburbs B) Crops near Pokola. C) Mixed agricultural landscape near Ouésso. 1) Colour composite [RVI, SARadCVVH, SARadCVVV]. 2) Planet images [Band 4 (Red), Band 3 (Green) and Band 2 (Blue)]. 3) Planet images [Band 3 (Red), Band 2 (Green) and Band 1 (Blue)]..... 32

Figure 25 : A) Portion of the Sangha River near Ouésso. B) Aquatic grass land on the Ndoki river. C) Floodable grass land on the Ndoki rive. 1) Colour composite [RVI, SARadCVVH, SARadCVVV]. 2) Planet images [Band 4 (Red), Band 3 (Green) and Band 2 (Blue)]. 3) Planet images [Band 3 (Red), Band 2 (Green) and Band 1 (Blue)]. 33
Figure 26 : Comparison of 3 different visualization from a portion of Djaka river. Colour composite is made combining 4 years long time series. Planet images were collected for the year 2020. In the middle of the river, we can see the Raphia stands along with the other flooded forest. Limbalis forest can be seen on the river edges surrounded by semi-deciduous forest. 34
Figure 27 : A) Raphia and B) Open flooded forest along the Djaka river. 1) Colour composite [RVI, SARadCVVH, SARadCVVV]. 2) Planet images [Band 4 (Red), Band 3 (Green) and Band 2 (Blue)]. 3) Planet images [Band 3 (Red), Band 2 (Green) and Band 1 (Blue)]. 35
Figure 28 : A) Flooded forests with mixed vegetation along the Djaka river. B) Bubinga swamp forest along the Mbouamboua river. 1) Colour composite [RVI, SARadCVVH, SARadCVVV]. 2) Planet images [Band 4 (Red), Band 3 (Green) and Band 2 (Blue)]. 3) Planet images [Band 3 (Red), Band 2 (Green) and Band 1 (Blue)]. 36
Figure 29 : A) Limbalis forest along the Mbouamboua river. B) Semi-deciduous forest near a small road on the western side of the Sangha River. 1) Colour composite [RVI, SARadCVVH, SARadCVVV]. 2) Planet images [Band 4 (Red), Band 3 (Green) and Band 2 (Blue)]. 3) Planet images [Band 3 (Red), Band 2 (Green) and Band 1 (Blue)]. 37
Figure 30 : Schematic of the various class levels. Level 1 = 2 classes, Level 2 = 9 classes and Level 3 = 16 classes. 37
Figure 31 : Schema of the relation between OFAC typology (OFAC, 2022) and the classes defined in this study. (Green) Part of the decision tree that were followed. (Red) Part of the decision tree that was not followed. (Black) Part of the decision tree that contain classes that can not be present in the ROI due to topographical and climatic condition. 38
Figure 32 : Color composite image from the ROI. The yellow points are the 400 training samples. 39
Figure 33 : Simple example of multidimensional LMBF process pixel. C will merge with pixel D. 40
Figure 34 : Schematic of the segmentation process at various scale values for three features. From top to bottom RVI, SARad CVVH and SARadCVVV. 40
Figure 35 : Various segmentations on a colour composite (RVI, SARadCVVH and SARadCVVV). The hyperparameters are respectively scale, shape, and compactness. 41
Figure 36 : Composition of the five non-textural features dataset. “Mean VH” equals to mean values of VH polarization during a 4-year long time period”, same signification for the other features. 42
Figure 37 : Description of the various textural features dataset 43
Figure 38 : Summary of the different scenarios. The legend below the table described the abbreviation contained in each scenario’s name. 44
Figure 39 : Recapitulative table of the overall accuracy from all the scenarios computed. The acronyms used are described in the bottom right corner. 46
Figure 40 : Illustration of the model saturation by Audreye and al. (2019) study on the left and from this study on the right. 46
Figure 41 : Comparison between JRC_TMF, (J. Dalimier, 2022) classification and the best produced forest-mask. The forest areas are in green and the non-forest areas are in red. . 48
Figure 42 : Comparison of the deforestation that happened between 2017 and 2020 (red) for A) JRC_TMF classification and B) PT5_Mean scenario classification. Non-forest areas before 2017 (black) and forest areas (white). 1. Pokola and its surroundings. 2. An area that encountered a brief deforestation event during the year 2018. 3. Ouésso and its surroundings. 4. Junction between the Sangha and the Ndoki river south of Pokola. 49
Figure 43 : F-score and OA comparison between the best scenario from each classification categories. (Level 3 = 16 classes) 50

Figure 44 : A comparison between A) PA and B) PAM classification that illustrate the effect of the majority filter on the classification rendering. 50
Figure 45 : A) OS_S_SEG70 + T classification map of all ROI. B) Zoom on an old logging area close to flooded forest stands. C) Zoom on a heavy deforested area west of Ouésso. ..51
Figure 46 : Recapitulative table of the Precision, Recall, Overall accuracy, and F-score for the PTC52,5,10)_All+A scenario. 53
Figure 47 : Example of predicted flooded forest. A) Around the Ndoki river. B) Big Raphia forest along the Boumbala river. C) Around the Kandeko river. D) Palm oil plantation west of Ouésso. 1. PTC(2,5,10)_All + A classification. 2. Colour composite [RVI, SARad CVVH, SARad CVVV]. 54
Figure 48 : Example of predicted monodominant forest. A) around Boumbala river. B) On a high ground near Sangha River east of Ouésso. C) Around the Djaka river tributaries. D) Square shape forest stands caused using textural features. 1. PTC(2,5,10)_All + A classification. 2. Colour composite [RVI, SARad CVVH, SARad CVVV]..... 55
Figure 49 : Example of predicted non-flooded non-forest area. A) River island and sandbank on the Sangha River. B) Aquatic grassland on the Ndoki river. C) Misclassification of the Ouésso's airfield. D) Typical case of misclassification at the class borders. In this case around a water body on the Djaka Rive. 1. PTC(2,5,10)_All + A classification. 2. Colour composite [RVI, SARad CVVH, SARad CVVV]..... 56
Figure 50 : Illustration of the road size and shape for different scenarios. A) PAM. B) PT2_Mean. C) PTC(2,5,10)_All + A. D) PTC(2,5,10,20)_All + A. E) OS_S_SEG70+T. F) Color composite [RVI, SARad CVVH, SARad CVVV]. 57
Figure 51 : Comparison between a forest succession view and the classification around the same river. A) Plant succession photography on a bank of the Ndoki River (from bottom to up respectively the aquatic grassland, the Raphia forest with R. hookeri, H. ciliata open swamp forest and dense moist semi-deciduous forest) by Gillet (2013). B) PTC(2,5,10)_All+A classification. C) OS_S_SEG70+T classification. 58
Figure 52 : Pixel distribution for each level of model certainty (left). Comparison between the model certainty, covered area and the F-score for each class (right). 59
Figure 53 : A) Probability map of the whole ROI. B) A body of water along the Djaka river. C) Recently made road west of Pokola. 60
Figure 54 : A) PTC(2,5,10)_All+A classification map of all ROI. B) Zoom on an old logging area close to flooded forest stands. C) Zoom on a heavily deforested area west of Ouésso. 61

Acronyms table

CV	Cofficient of Variation
DEM	Digital elevation model
EL	Ensemble Learning
ESA	European Space Agency
GLCM	Grey Level Co-occurrence Matrix
GRD	Ground Range Detected
IFO	Industrie Forestière de Ouésso
JRC_TMF	Vancutsem and al., map of the forest cover change between 1990 and 2019
LMBF	Local Mutual Best Fitting rule
MRS	Multi-Resolution segmentation algorithm
OA	Overall Accuracy
OBIA	Object-Based Image Annalysis
OFAC	Central African Forest Observatory
OTB	Orfeo Toolbox tools
PBIA	Pixel-Based Image Analysis
REDD+	Reduction of Emissions caused by Deforestation and Forest Degradation
ROI	Region of interest
RVI	Radar vegetation index
SARad	Features divided by MeanVV + MeanVH
Sentinel-1	Sentinel-1
Sentinel-2	Sentinel-2
SLC	Single look complex
SVM	support vector machine

Introduction

The Congo Basin Forest is one of the most preserved forest ecosystems on the planet in terms of species diversity and density (Gillet and al., 2016). Besides its role as a biodiversity reserve, the Congo Basin has an important function as long-term carbon storage especially in the wetlands and peatlands from the Cuvette Centrale. The Cuvette Central area is the biggest peatland complex in the world and is mostly lying in the Republic of Congo and the Democratic Republic of Congo. It gathers all the high organic content wetlands of the Congo River and its tributaries. The quantity of carbon contained within the forest and forest soil differs depending on the forest density, soil water content, tree species and tree heights (Biddulph and al., 2021). This highlights the importance of forest type mapping for carbon stock monitoring. Those considerations make the region one of the most critical forest areas to monitor in the climate change context and the recent decrease in biodiversity.

Even if the area is considered as well preserved in comparison with other tropical forests, the Congolese tropical moist forests are still under threats of various deforestation drivers (Gillet and al., 2016). Given the importance of those forests, a continuous large-scale monitoring must be conducting. Such an ambitious monitoring system requires to cover large remote forests usually with limited field accessibility and lack of proper infrastructure. One of the ways to overcome those limitations is to use remote satellite sensing.

The Copernicus programme provides a large number of continuous data that are available in radar (Sentinel-1) imagery both very high resolution. Those data have the potential to constitute a good data source for forest type and land cover remote sensing. In the study, the choice was made to use Sentinel-1 data only to explore the opportunities of SAR-C (Synthetic Aperture Radar in C band) in those areas where optical data are usually scare and low in quality due to cloud coverage.

This study will focus on the town of Pokola and its surroundings forest. The area has an extensive path network used by logging companies that exploit the forest. A large part of the region also included high conservation value areas where logging activities are restraint. This combination offers a good opportunity to explore the remote sensing capabilities of C-SAR data in tropical forest context. This master thesis will explore the regional Congo Basin regional context and Sentinel-1 remote sensing capabilities. The materials and the methodology used will be described. The results and limitations will be discussed. Finally, a complete land cover map will be presented.

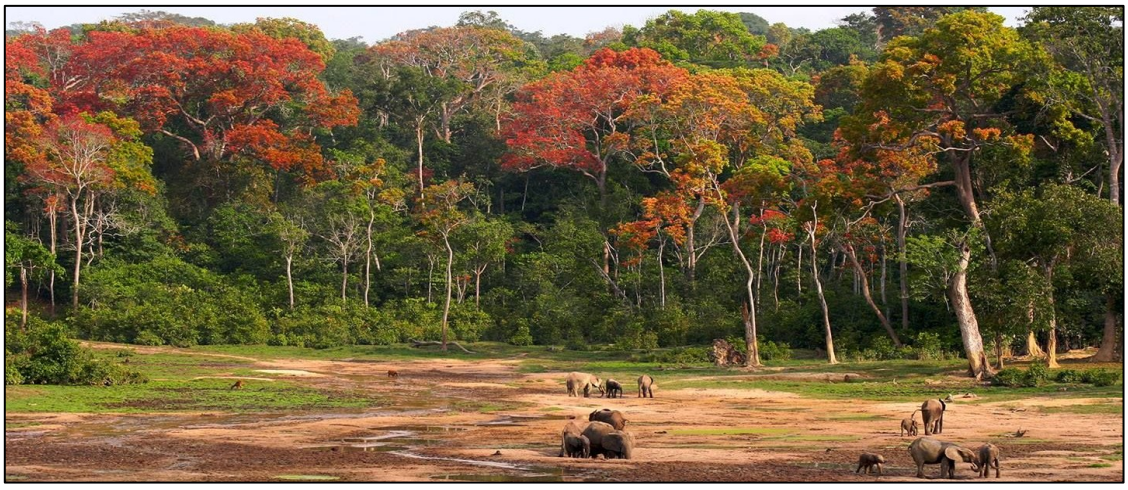

Figure 1 : *Tropical rain forest view close to the Sangha river (dzanga-sangha.org)*

Chapter 1: Literature review

1.1 Geographical context

1.1.1 State of the forest in the Congo basin

The Congo Basin rainforest covered more than 170 million hectares in 2015, that are still well preserved and has undergone low net deforestation relative to other tropical rainforests. This deforestation is about 0.14% for the period 2000–2010. This is a decrease of about 0.05% compared to the period 1990–2000 (de Wasseige and al., 2015). However, there are large disparities between countries, with rates doubling over the same period in the Republic of Congo or the Democratic Republic of Congo, rates stagnating in the Central African Republic and even declining in Cameroon and Gabon (Tchatchou et al., 2015).

The drier forests of the region are experiencing increasing net deforestation (FAO, 2021). Part of this deforestation is driven by the expansion of transport infrastructure that will likely increase deforestation in their immediate vicinity. In fact, the economic development in newly deserved areas may lead to a loss of forest cover, the current low deforestation rates may hide a future increase in deforestation if adequate protective measures and proper energetic developments (protected natural parks, replacement of firewood with alternative energy sources, ...) are not implemented by then (Tchatchou et al., 2015).

The state of degradation must also be considered when assessing the state of the Congo Basin rainforests. Indeed, between an intact and a deforested forest, there is a range of degradation levels. Degradation can, for example, take the form of selective logging or the establishment of agriculture under the canopy. Forty-five percent of degradation cases would lead to net deforestation (Lanly, 2003). In Central Africa, between 1990 and 2019, nearly 17% of tropical rainforests are estimated to have been modified, of which 9.5% were deforested, 6.8% degraded, and 0.9% regrew (Vancutsem and al., 2021). It should be noted once again that regional differences are important and that the rate of natural regeneration of rainforests varies greatly from one forest type to another. It is sometimes complicated to determine the initial natural state of a forest, depending on whether one looks at it through the prism of biodiversity, biomass content or even soil health (Lanly, 2003).

1.1.2 Deforestation drivers

The drivers of deforestation in the Congo Basin are numerous and well documented. Some are old but have recently become more important, such as shifting cultivation or the use of firewood; others are more recent, such as the large-scale monocultures that have been present since European colonization. Finally, some drivers serve as catalysts for other causes of deforestation, such as transportation infrastructures (Tchatchou and al., 2015).

The most important cause of deforestation in the Congo Basin is agriculture, and more specifically shifting agriculture. Indeed, slash-and-burn agriculture is still widely practised in the region. The increase in competition for the best land and the expansion and intensification of traditional subsistence agriculture have pushed farmers to venture into previously untouched forest areas. This phenomenon is facilitated by the still low but increasing mechanization of agriculture, by the extension of roads and by the transformation of slash-and-burn crops into permanent crops (or unsustainable reduction of the fallow time) (Tchatchou and al., 2015).

In addition, industrial rubber or palm oil farms and cash crops such as cocoa have a more limited but significant impact (Gillet and al., 2016; Tchatchou and al., 2015).

The second cause of deforestation is the use of fuelwood by both urban and rural populations. In Africa in 2007, between 70% and 95% of heating energy came from fuelwood (dry wood or charcoal). In tropical megacities such as Kinshasa or Brazzaville, wood constitutes 75% of industrial and domestic heating energy. A formal and informal economy have been developed, with the majority of fuelwood coming from the clearing of shifting cultivation, and the rest being taken directly from forests and fallow land. A complex

interaction and even interdependence exist between the different actors of deforestation around urban areas which are farmers, charcoal manufacturers and timber exporters. This complex socio-economic environment makes the problem of fuelwood even more complicated to solve (Dubiez and al., 2014).

The exploitation of timber species is not yet a major deforestation factor, but it is an important factor in the degradation of forest ecosystems. Indeed, this degradation was often the gateway to outright deforestation of degraded plots (Vancutsem et al., 2021).

Finally, the construction of industrial, energy and transportation infrastructures are a significant cause of deforestation. The underlying drivers of this deforestation are varied and complex mixing demography, economy, inequality and territory development strategies (Megevand and al., 2013; The Congo Basin Forest Partnership, 2005; Dubiez and al., 2014).

1.1.3 Forest transition theory

The theory of forest transition was established in 1992 by A.S. Mather. This theory shows that most industrialized countries have globally followed the same evolution of their forest cover. This evolution takes place in 4 stages. First, there is a vast undisturbed cover, then a brief period of massive deforestation followed by a new stagnation of the forest cover mainly composed of islands separated from each other (creation of forest mosaics) and finally there is a period of return of the forest cover (but always less extensive than before the phase of massive deforestation). This evolution also seems to have been observed in developing countries located in tropical zones. Mather suggests that population pressure is the main cause of this phenomenon. Added to this is the change in mentality brought about by the urbanization of society, which is leading to a reconsideration of the role that forests should play in society, moving from an engine of economic growth to an ecosystem service role and an aesthetic or recreational role (Mather, 1992).

With regional variation, the Congo Basin is still in the downward phase of the forest transition curve (Figure 2). Thus, the worst of deforestation in the region is yet to come, especially since everything is already in place for massive deforestation (population growth, opening of remote forest areas, energy-wood, etc.) (Tchatchou and al., 2015). However, as the different drivers of deforestation and the brakes on these drivers are clearly identified, it is quite possible that a phase jump will occur, and that the massive deforestation phase will never take place. All this will depend on the political actions and the socio-economic and climatic context that will encourage or not deforestation in the years to come (Megevand and al. 2013).

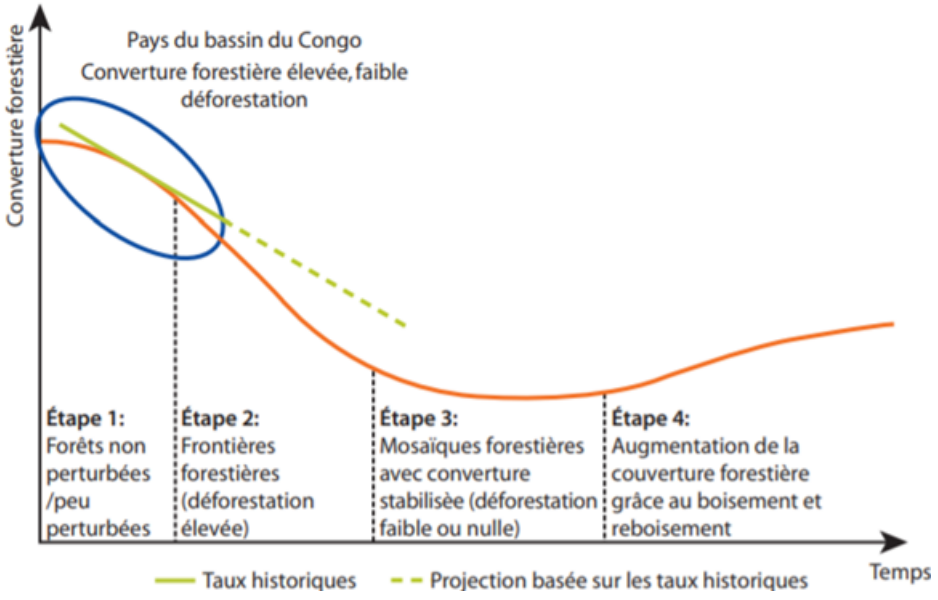

Figure 2 : *Theorical forest transition curve (Megevand and al., 2013)*

1.1.4 Forest typology in the Congo basin

In general, the typology of Central African forests varies greatly depending on the objective, scale or type of study. In order to overcome this problem, the Central African Forest Observatory (OFAC) has developed a standardized classification method that should allow a better understanding and cooperation between the different actors, both political and scientific. Appendix 2 shows the decision tree used by this new classification. The OFAC classification is hierarchical, going from the most general stratum (Forest/non-Forest) to more specific strata, such as at the stand level. Thus, to understand and use this new classification "One should no longer focus on the "label" (or name) given to the classes (each country has its own nomenclature) but rather on the methodology for constructing these classes, based on a rigorous definition of the basic elements and the relationships between these elements" (OFAC, 2022). Thus, some ecosystems that are geographically separated and have different endemic species can be included in the same class because their general physiognomy is quite similar. This method normally allows the user to refine the classification to the stand stratum as desired, without having to modify the entire OFAC classification (OFAC, 2022). This method differs greatly from the classical floristic method which focused on the fauna and flora found in forests (Namur, 1990; White, 1986). OFAC typologie can be visualize in Appendix 2.

1.1.5 Reduction of Emissions caused by Deforestation and Forest Degradation (REDD+)

REDD+ is an ambitious international mechanism encouraging developing countries to reduce the impact of global warming by reducing deforestation and forest degradation. Countries interested in this program must follow three phases to join the proposed programs and have their projects funded:

- Preparation: Establishment of plans, strategies, and capacity to meet the objectives.
- Implementation: Implementation of REDD+ activities and projects. Establishment of mechanisms to achieve the set objectives as well as the development of means to evaluate the results.
- Validation: Validation steps for the completed projects.

REDD+ projects are funded largely through bilateral agreements between developed and developing countries, particularly through the carbon credit system (Proforest, 2011). A 2018 meta-analysis attempted to assess the effectiveness of REDD+ (Duchelle and al., 2018). The conclusion is clear: in 2018 it was impossible to rigorously demonstrate the effects of REDD+ either on the well-being of populations or on climate change. Delays in project funding are also very common, even though those fundings were one of the keys to the REDD+ mechanism.

1.2 Remote sensing of tropical forest

Remote sensing is a relevant tool for monitoring and analysis of tropical forests (Boyd and Danson, 2005);(Moise Tsayem Demaze, 2011). Satellite detection of forest cover change at 30m resolution for all tropical forests has already been achieved by Vancutsem and al.(2021). 30 years of Landsat optical images were used. Many forest cover maps have also been produced using LANDSAT archives imagery (Figure 3).

1.2.1 Optical remote sensing limitation in tropical context

Although the results of Vancutsem et al. (2021) are unprecedented in their spatial and temporal magnitude and accuracy, the study cautions that only large poles of deforestation can be identified. However, small deforestation hubs are not negligible and therefore results may be underestimated (Hansen et al., 2013; Vancutsem and al., 2021).

Studies that consider the specific contexts of each region produce better results. For example, Souza and al., (2013) mapped deforested and degraded areas at the scale of the Amazon basin using Landsat imagery at 30m resolution. This study demonstrates the maturity of optical sensor remote sensing methods for change detection in tropical

environments at large scales and with high accuracy. However, the authors reported that many images (~30%) were not fully exploitable due to high cloud cover. Finally, small changes in land cover cannot be detected by this method (changes resulting from less than 25% canopy opening in 10 years are not considered). In conclusion, Landsat images, despite their high temporal resolution, cannot be used as the sole source of data for mapping the wettest and cloudiest regions of Central Africa.

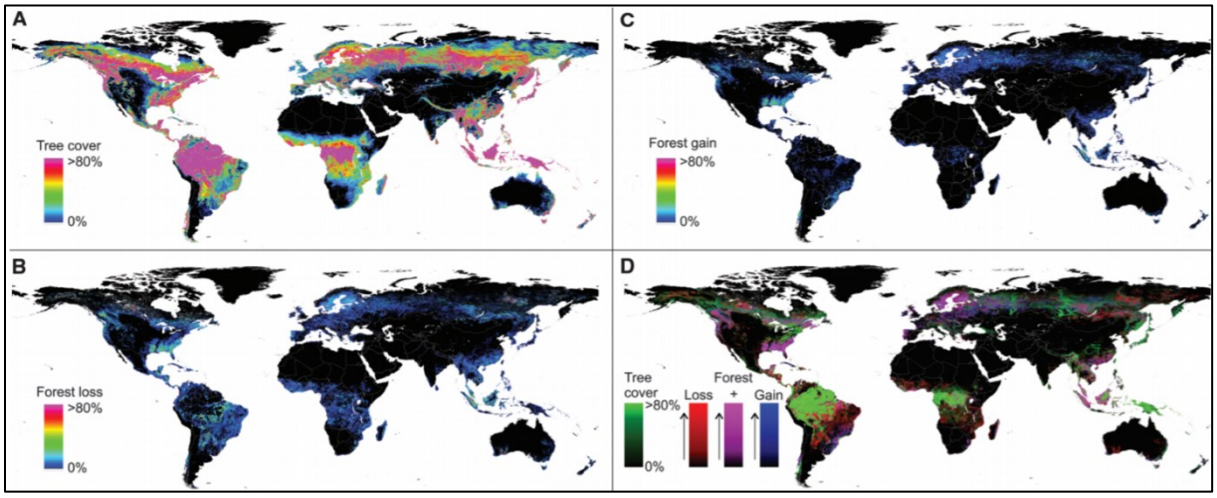

Figure 3 : *High-Resolution World Maps of 21st-Century Forest Cover Change (Hansen and al., 2013)*

To address the problems caused by cloud cover and rapid forest natural regeneration, researchers are increasingly coupling results from optical sensors with those from SAR sensors. However, the use of SAR data is hampered by inconsistent and unavailable databases in time and space. Prior to the Sentinel missions, SAR data often came from low scale scientific missions and were therefore often spatially and temporally inconsistent with any other studies. Thus, research in this area has been hampered primarily by the lack of an integrated radar data collection system. In general, the future of remote sensing will be the cross-use of data from multiple sources and spectral bands (Reiche et al., 2016). The arrival of the Sentinel-1 mission precisely addresses this need for quality radar data compatible with optical data and on an open access.

1.2.2 Sentinel-1 (S1)

The S1 mission is an initiative of the European Space Agency (ESA) in the framework of the Copernicus project. All the information in this section comes from the S1 mission user guide and technical guide (ESA, no date). The goal of this mission is to provide high resolution C-band radar coverage of the entire planet in an open access environment. To do this, ESA has established a constellation of two satellites S1A (launched in 2014) and S1B (launched in 2016) that share the same quasi-polar (98.18 °) and sun-synchronous (the local time constant to the descending orbit is 18h00) circular orbit. Both satellites share the same orbit with a phase difference of 180°. This orbit and inclination are not completely stable over time, to ensure a constant data collection the satellite is maintained in an imaginary cylinder of 100m diameter at about 693 km altitude. The satellites have an expected lifetime of 7 years and will be automatically replaced by S1-C and S1-D, thus guaranteeing the continuity of the program. Each satellite can cover the Earth's surface in a 12-day cycle with 175 orbits per cycle. Together, the two satellites can cover most of the globe in 6 days. However, Europe, Canada, and major sea routes can be covered in 1-3 days (Figure 4). The Republic of Congo region only benefits from the descending orbital coverage. For that reason, Sentinel-1 images are only collected every 12 days in this area. The collected data are transferred to the Copernicus service about one hour after acquisition.

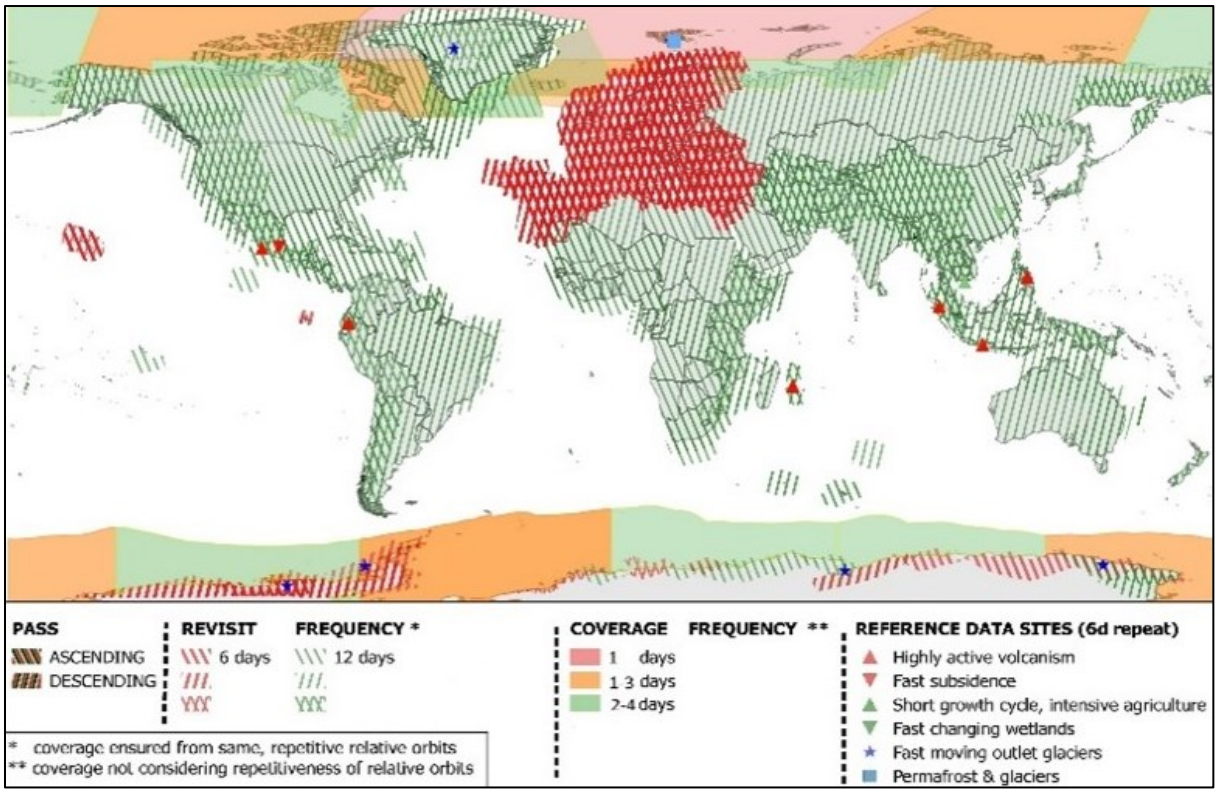

***Figure 4** : Sentinel-1 orbitals map (ESA, no date)*

There are 4 operational modes of S1 data acquisition (Figure 5):

- **Strip-Map Mode (SM)** Swath: 80 km, spatial resolution: 5 x 5 m (Polarization mode: HH+HV, VV+VH, HH and VV)
  This mode is composed of 6 beams of 80km width. Each beam has a different angle of incidence. This mode is mainly used to cover small islands and to provide emergency information.
- **Interferometric Wide Swath (IW)** Swath: 250 km, spatial resolution: 5 x 20 m (Polarization mode: HH+HV, VV+VH, HH and VV)
  Main mode of terrestrial data acquisition. Each 250 km wide swath is collected in 3 sub-swaths having all three a different angle of incidence and they themselves collected in multiple bursts. The different bursts overlap in part, which allow the complete large size image recreation in high resolution, thanks in particular to the TOPSAR technique, which electronically adjust each burst in order to avoid any compatibility problem between each burst. This mode is the one used for forest remote sensing.
- **Extra-Wide Swath Mode (EW)** Swath: 400 km, spatial resolution: 20x40 m (Polarization mode: HH+HV, VV+VH, HH and VV)
  Mainly used to cover polar, maritime and snowy areas, this mode can also be used in case of emergency to monitor the evolution of oil spills for example. This mode follows the same principle as the IW mode, only here the 400km swath is divided into 5 sub-swaths.
- **Wave-Mode (VW)** Swath: 20x20 km, spatial resolution: 5 x 5 m (Polarization mode: HH and VV)
  This mode collects data in the form of a small 20 km square thumbnail. A thumbnail is collected every 100 km along the orbit. One vignette out of two has an incidence angle of about 23°, while the other is 36°. This mode is used to cover the oceans but can also have the same role as the SM mode but with a much smaller volume of data.

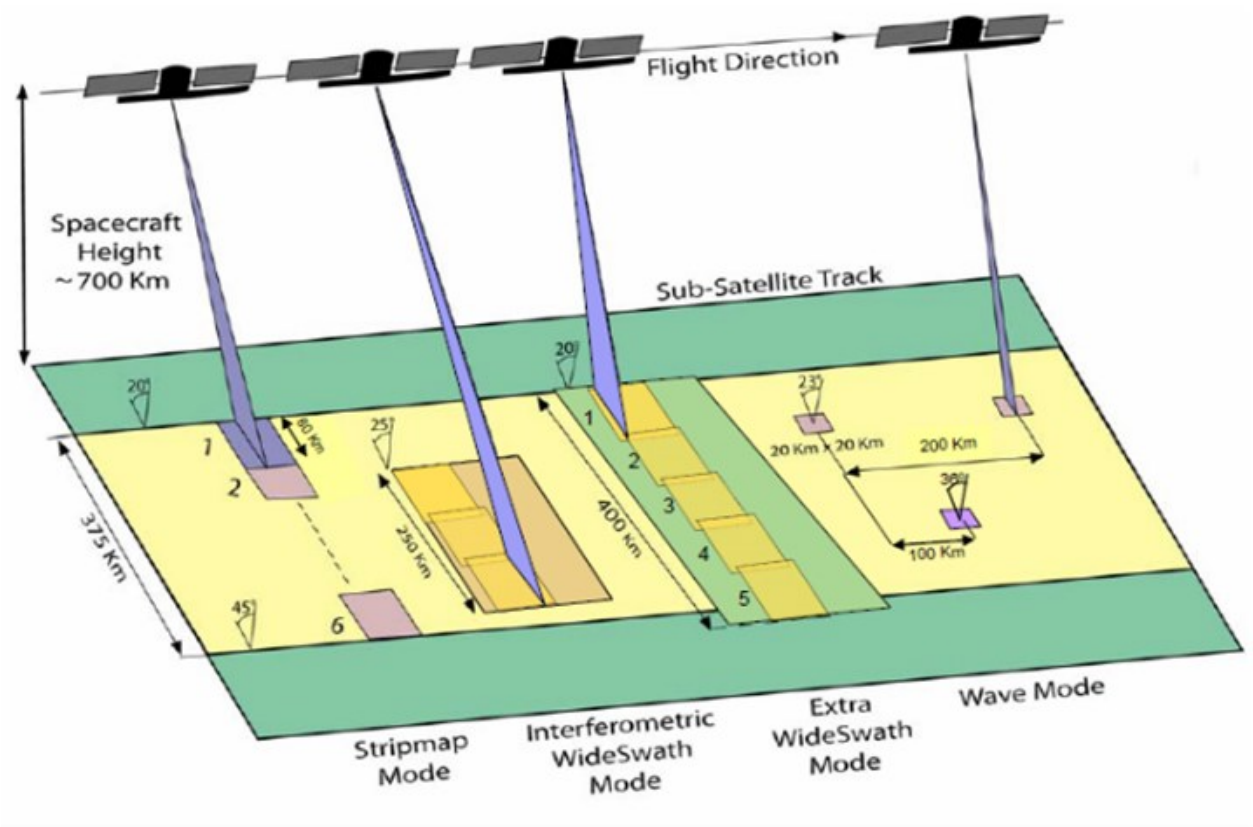

Figure 5 : *Schematic of the four acquisitions mode (ESA, no date)*

There are three levels of Sentinel-1 products, ranging from the rawest data to the most pre-processed and directly usable data:

- **Level 0**: Compressed data containing all information from the satellite instruments (SAR, instrument status, instrument position, ...). The SAR data are in full resolution
- **Level 1**: Decompressed data coming directly from level 0 containing all the information previously mentioned. The images are georeferenced using orbital and altimetric information for Single Look Complex data (SLC) (which retain their phase information) or by being projected onto an ellipsoid model for Ground Range Detected data (which lose their phase information). It is this level of product that is used for more advanced analysis. Only GRD data in SM mode are kept in full resolution. GRD data in IW and EW mode can be in high and medium resolution while VW mode is only available in medium resolution.
- **Level 2**: Data already highly pre-processed and are presented as environmental variables. They are of the same resolution and location as the level 1 data from which they are derived.

In addition to providing the data, ESA provides a series of "Toolboxes" containing algorithms, methods and tutorials on interferometry, polarimetry and interference management.

A recent anomaly event occurs in December 2021 on the Sentinel-1B satellite. The cause(s) of this anomaly are not yet clearly identified, but the satellite is unable to collect SAR data until recently (April 2022).

1.3 Sentinel-1 data

1.3.1 Pre-processing

Before relevant features can be extracted from Sentinel-1 GRD level 1 products, a series of pre-processing steps must be applied. Among the most common are speckle reduction, geocoding, ortho-rectification or resampling.

Speckle

The speckle phenomenon is caused by the coherent nature of the SAR signal which tends to cause interference. Although a homogeneous surface such as a wheat field has an average backscatter coefficient across the field, the coefficients can vary greatly from one object to another. Depending on the back scatterers encountered, the emitted signal causes constructive interference (signal amplification) or destructive interference (signal reduction). The radar image of the surface then obtained will be made of an alternation of very clear and very dark pixels. Thus, a surface that appears homogeneous on optical images will appear grainy on the radar images. This phenomenon caused photointerpretation and classification problems must therefore be removed. Speckle cannot be considered as "noise" in the data, but as a physical phenomenon for which models have been developed. These models are like filters that reduce the intensity of speckle by using the time series and the different polarizations of the SAR signal (Lee and al., 1991). One of the most widely used filters is the "Refined Sigma Lee filter" which preserves contours, textures and linear features and which continues to be improved since its creation in 1983 (Lee and al., 2009). Another method often used consist of a multi-temporal average of the image studied. This method can be used in addition to a filter.

Geocoding

In order to be able to set up most of the data analysis, it is essential to reference the data based on a common coordinate system, this process is called Geocoding. It is also important if we want to correct topographic deformations to use a radiometric terrain correction (Mercier and al., 2020), for example the Mapzen Digital Elevation Model (DEM) (Sentinel Hub, no date). A DEM combined with data acquisition conditions (angle of incidence, position of the satellite...) allows the application of an ortho-rectification on the data (Sentinel Hub, no date). Geocoding is also essential if we want to combine SAR data with other georeferenced data sources (C. Werner and al., 2002).

Resampling

To combine data of different resolutions or to avoid losing some information, it is possible to resample the data. A commonly used method consists in an interpolation followed by a resampling to keep an identical number of data. Spatial interpolation techniques are varied, we can cite the nearest neighbour technique, inverse distance or kriging for example (S. Kusano and al., 2011).

1.4 Classification process

Classification work with three main components: training data, validation data, an algorithm calibrated by those data. In order to use a model in an efficient way and specially to reduce over-fitting, it is essential to use resampling techniques on the training data. These techniques are mostly based on the ensemble learning (EL) theory (Sotiris Kotsiantis, 2011).

The objective of EL is to increase the efficiency of a classification by combining the predictions of several "weak learners" (weak classification tools if used alone). Each tool produces different predictions, and the average of their predictions is the final prediction. The basic assumption is that each classification model has weaknesses and strengths depending on the data encountered and algorithm used. By averaging the predictions, it is hoped that the strengths of some will compensate for the weaknesses of others. (S. Alim

and al.,2014) There are many resampling methods such as Rotation forest, Stacking or averaging but the most encountered EL methods are:

- **Bagging:** We create a multitude n' subset of a set n of training data (the ratio n/n' must be more or less 60%). The data composing the n' subsets are drawn at random with replacement in the n data. The n' subsets are then used to train the models. This method strongly reduces the variance of the predictions (Breiman, 1996).
- **AdaBoost:** This method works like Bagging except that after the first subset has been made, the n data in the trained model will be tested with the data from the created subset. We will then identify the data in n for which there were significant classification errors. When the next subset is created, the misclassified data will have a better chance of being selected and the process will continue for all the following subsets and models. This method greatly reduces model overfitting (Schapire, 2013).

These methods can be used separately or combined depending on the data encountered (Kotsiantis, 2011). EL methods can be used within classification algorithms (intra-operator variability) as for Bagging or between different algorithms (inter-operator variability) by combining for example SVM (support vector machine), Random forest or Logistic models (S. Alim et al., 2014) classification results.

The Random forest algorithm is a classical Bagging method applied to decision trees. Each decision tree is randomly generated according to a particular set of training data resampled via Bagging. The final prediction will be the average of the predictions made by all the decision trees (Breiman, 2001). Random forest is a supervised classification algorithm, so in order to train it, we must first define categorized training areas and introduce the desired number of classes. The popularity of Random forest is important (in competition with SVM) and its good performances in the remote sensing environment are not to be proven anymore (Sheykhmousa and al., 2020). The number of different types of metrics entering Random Forest is not theoretically limited. However, there is a limit at which it is no longer necessary to add metrics to refine the classification as demonstrate in Figure 6. This limit depends on the context but is inherent to the functioning of the algorithm which constantly balances between the diversity and the generality of the predictions made in order to avoid the phenomenon of over-fitting (Audreye and al., 2019).

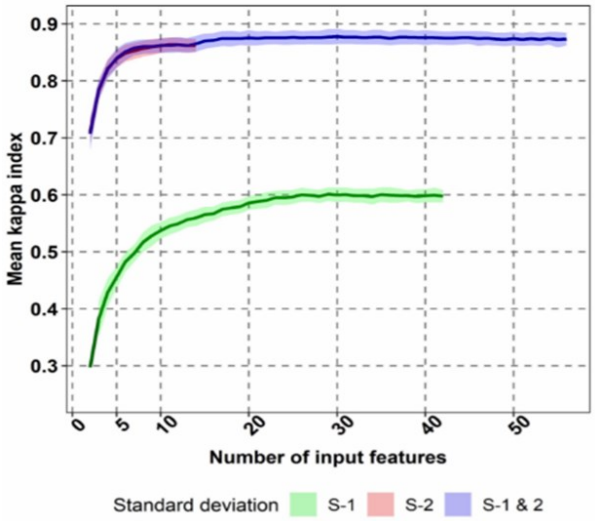

Figure 6 : *Evolution of a land cover classification performance with number of Sentinel-1 and Sentinel-2 features input. Sentinel-1 and 2 (Audreye and al. 2019).*

1.5 Sentinel-1 application

In most of the remote sensing applications, Sentinel-2 data gives better results than Sentinel-1. However, in areas where usable optical images are scarce, SAR data obtain better results. Finally, the combination of SAR and optical data consistently gives better results

than both separately (Hu and al., 2021). In this section are described a series of applications of the Sentinel-1 mission.

1.5.1 Land cover

Land cover can be mapped efficiently using S1 data. The best results are obtained using long time series. Coherence information discriminates better than intensity information, however, it is the combination of the two that provides the best results. For this application, the VV polarization provides better results than other polarizations (Jacob and al., 2020). Combining Sentinel-1 and Sentinel-2 data increase the accuracy of land cover type classification (Hu and al., 2021). Land cover can be mapped down to the local level for example to map small farms in developing countries (Kpienbaareh and al., 2021).

1.5.2 Deforestation

To measure deforestation, SAR data are used primarily in two different ways. First, the change in backscatter captured by the satellite can be measured for each pixel. In theory the intensity of the wave returned to the transmitter should change strongly over time if deforestation or degradation occurs. This method has proven itself and can detect deforested areas and degraded areas with high and low regeneration capacity. However, this method has its limits because the intensity of the backscatter is highly dependent on the nature and moisture of the soil. A calibration that considers the influence of seasons and soil type on the evolution of the backscatter intensity over time is therefore necessary. The edaphic characteristics of each region must be considered. It is therefore necessary to be very careful when this method is used over large areas (Joshi and al., 2015) .

The second method is to identify the occurrence of areas that the SAR can never reach, i.e., areas of zero backscatter. Depending on the orientation of the obstacle with respect to the satellite and according to the ascent or descent orbit of the satellite, a series of shadows will appear as illustrate is Figure 7. If these shadows appear and persist over time, then it is a deforested area. This method has the advantage of accurately detecting small changes in the middle of the forest or at the edge of large deforestation fronts. However, if the deforestation is sudden and large (such as for an oil palm plantation) then this technique is useless because the sensors will not have had time to observe shadows that persist over time, and thus only the fixed boundaries of the deforested area will be detected (Bouvet and al., 2018).

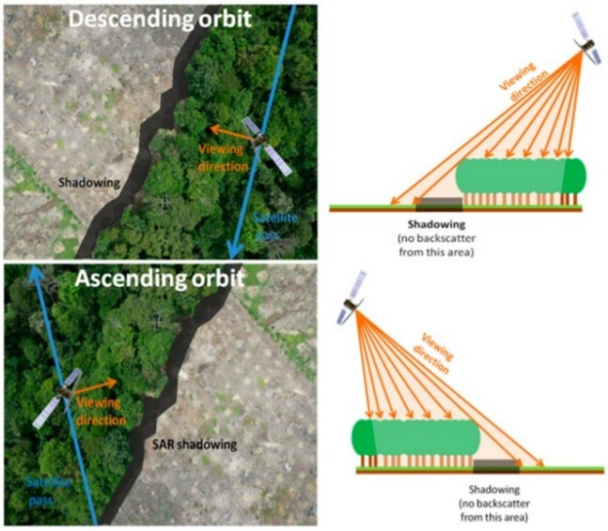

Figure 7 : *Illustration of SAR shadowing effect at the edges of a forest stand (A. Bouvet et al., 2018)*

1.5.3 Tropical Forest type

Even if Sentinel-1 data are less relevant than Sentinel-2 for forest type mapping, they can be essential in areas with few optical data availabilities. It was observed that L-band data are more suitable for forest type mapping because of its higher canopy penetration depth

(Mercier and al., 2020). Vegetation canopies are heterogeneous in shape, density and composition, which makes it difficult to be radiometrically described. Still the scatterers are leaves, branches and trunk. If we consider that the scatterers size decrease with increasing height, we can infer that the highest part of the canopy is composed of a high density of small scatterers. This density drastically decreases the signal penetration depth. SAR-C signals interact only with the first few meters of canopy primarily composed of small scatterers. SAR-L on the other hand penetrate more deeply into the canopy and interact also with trunks and big branches. SAR-P interact only with larger trunks and the ground scatterers (Woodhouse, 2006).

Objectives

The main objective of this master thesis is to develop an innovative SAR-based forest type mapping method applicable in the cloud-covered regions of the Congo Basin, to tackle the lack of optical data. Remote sensing capabilities of SAR multi-year time series is explored in the Congo Basin tropical forest. Building on the robust calibration and the limited atmospheric perturbations of SAR signals, several SAR-based vegetation features are developed and assessed in terms of discriminating power for the different tropical forest types and land cover in the surroundings of Pokola, Republic of the Congo.

A forest and land cover typology are established using only optical data photointerpretation, previous classification and the SAR-signal expected behaviours of each class. This typology aims to correspond to OFAC's standardize classification method and reinforce remote sensing potential in the African tropical forest.

This study mainly targets the evaluation of the potential of SAR-based data for the forest-cover changes monitoring during a 4-year-long period. The results are compared to optical based mapping.

Finally, the evaluation of three classification methodologies (pixel-based, object-based and textural-based) are conducted. Validation protocols and qualitative assessments would confirm their respective results, limitations, advantages and disadvantages.

Chapter 2: Study area

The region of interest (ROI) is located around the town of Pokola in the north of the Republic of Congo along the Camerounese border and cover an area of 4400km^2.The ROI is mainly occupied by two looging compagnies: the Congolaise Industrielle des bois (CIB) and Industrie Forestière de Ouésso (IFO) and is crossed by the Sangha river and its tributaries. The biggest city is Ouésso which is also the chief place of the Sangha province where the ROI is entirely located. Due to loging activities, main roads and paths cross the forest extent (Figure 8).

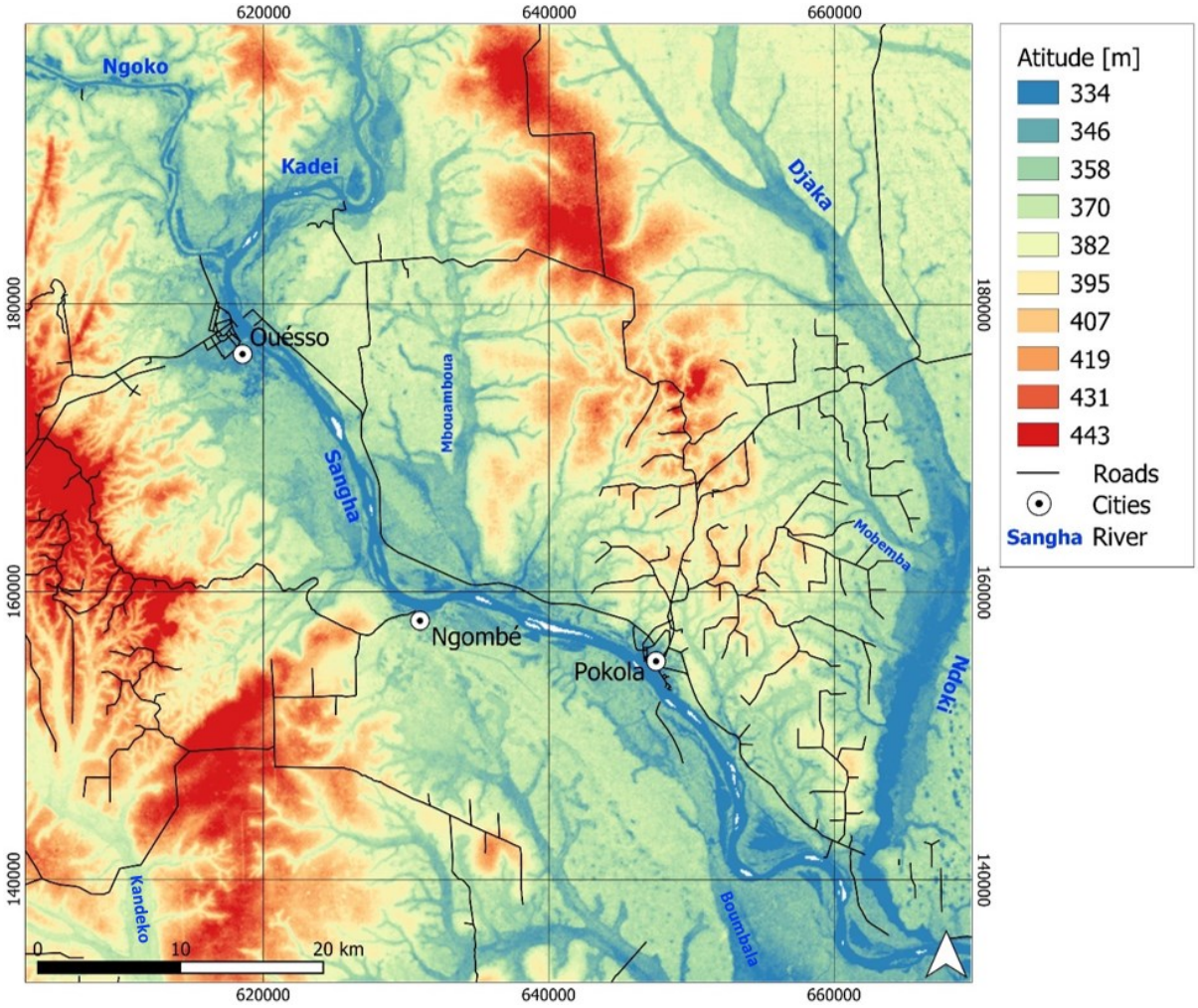

Figure 8 : *Topographic map of the ROI using SRTM data. Main roads, cities and main rivers are mentioned.*

The eastern part of the ROI is located in the Cuvette Centrale characterized by a high concentration of small rivers, wetlands and peatland. Those area are carbon-rich ecosystems and are still mainly preserved from forest degradation (G.Dargie and al., 2018). We can see in Figure 10 that main logging road and urban areas are avoiding wetlands. According to the newly updated Köppen-Geiger climate classification (Beck, H. E and al. , 2018) ROI is located at the edge of the Af Tropical Rain Forest Climate which means that the monthly average precipitation average is always superior to 60mm (Figure 9). In this condition, it is considered that Af area never encounter proper dry season like other tropical climate because precipitation are always high. However, precipitation variation can be observed throughout the year with a maximum reached between September and November and a minimum reached between December and February.

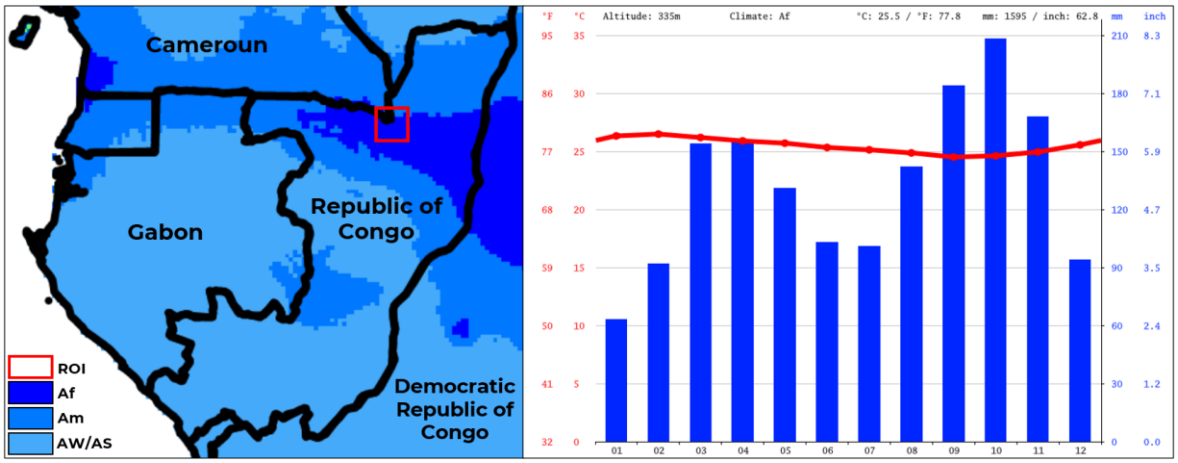

Figure 9 *: Köppen-Geiger climate classification (Beck, H. E and al. , 2018) and Pokola's ombrothermic diagram (Climate-data.org 2021)*

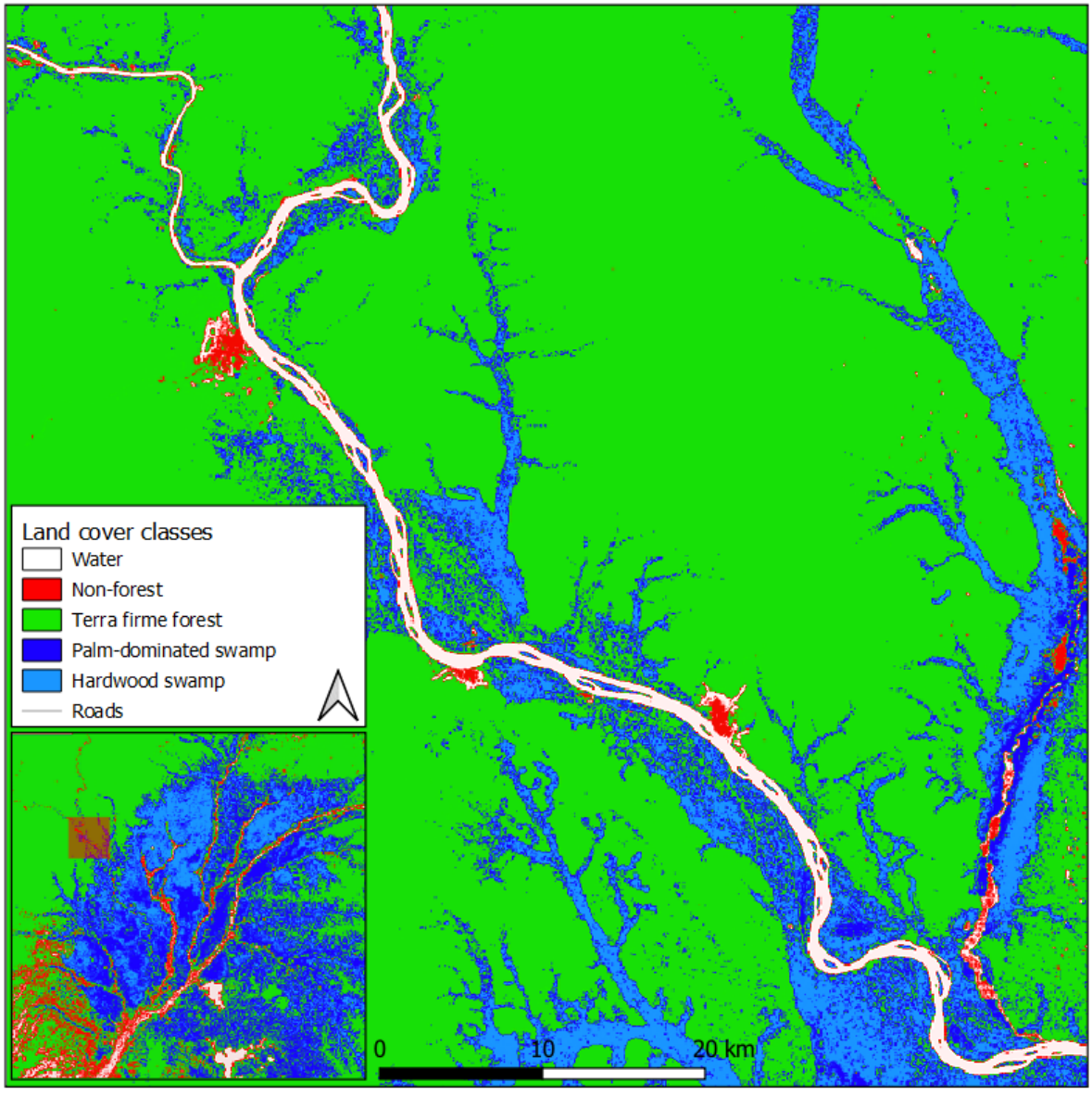

Figure 10 : *Pokola wetlands map. On the lower left the whole Cuvette centrale wetlands is represented using G.Dargie and al., (2018) classification based on SRTM, Landsat and ALOS PALSAR data.*

Chapter 3 : Materials and methods

3.1 Materials

3.1.1 SLC Sentinel_1 data

Figure 11 : *Orbital 7 (red) and ROI (Blue)*

Four years archives sentinel-1 Single Look Complex (SLC) images were collected in standard dual polarization (VV, VH and VV/VH) from 11 January 2017 to 28 December 2020. The image data acquisition mode is the Interferometric Wide Swath (IW). Data are collected data at a single look resolution of 5x20 meters on a 250km width swath has been selected. IW mode collects 3 partially overlapping sub-swath themselves subdivided into several bursts. The total amount of images collected and processed consist of 336 images. Data acquisition has been made on the relative orbital 7 and the whole area was covered by the first sub-swath (IW1). The incident angles at minimal orbit altitude are thought ranging from 30.87° to 36.59°. SLC products consist of georeferenced complex data containing both phase and amplitude information and sampled at the natural pixel spacing. For one acquisition step, 6 images are produced (3 sub-swaths with and 2 polarizations).

3.1.2 Pre-processing

Raw SLC data needs to be pre-processed to deliver analysis-ready data. The following steps have been applied on the whole study area for each period of time and each polarization using SNAP (Sentinel Application Platform) and OTB (Orfeo Toolbox tools) program.

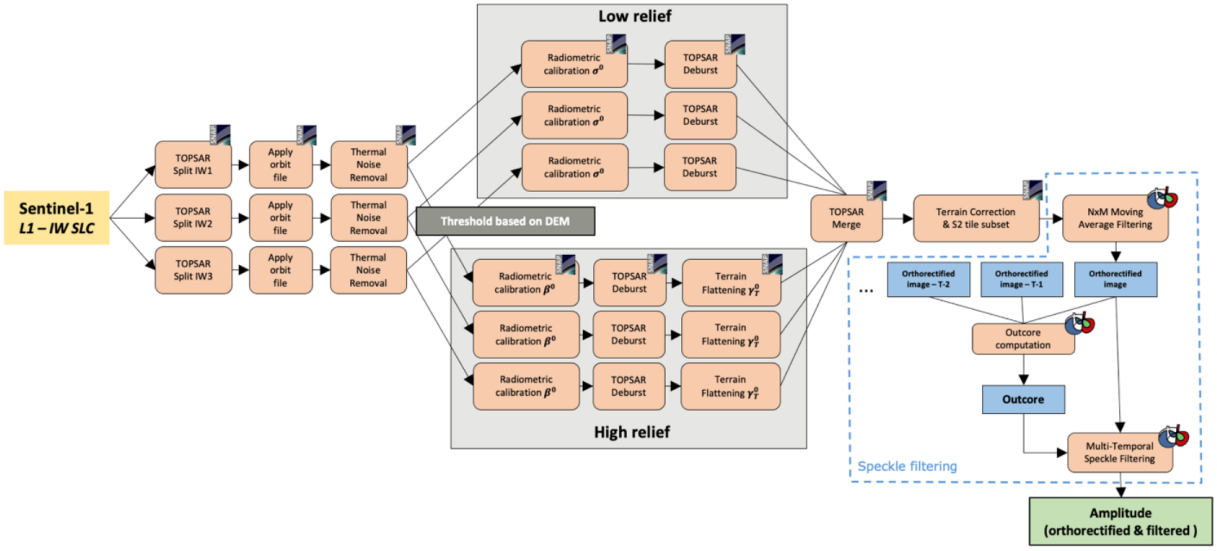

Figure 12 : *Diagram of the various pre-processing steps applied on the SLC data (ESA Sen4Stat, 2021).*

SNAP

SLC images were split in 3 different sub-swaths and each sub-swath in several bursts using the "TOPSAR split" tool (Terrain Observation with Progressive Scans SAR). Orbital state at acquisition time (satellite's position and speed) is also needed to improve processing efficiency. But the most accurate orbital state metadata are not available until 20 days after acquisition and is therefore not applied until then. Thermal noise is removed thanks to a thermal noise look-up-table (LUT) and all the phase information are lost in the process. To ensure quantitative use of images, the natural values are converted into sigma-calibrated naught (physical units) thanks to other dedicated LUT. Then all bursts from each sub-swath

are merged using “TOPSAR deburst” tool. Each deburst sub-swath are then merge into one image per polarization using “TOPSAR merge” tool. To avoid topographical distortion and get the correct geolocation of each pixel, a Range-Doppler approach is executed using satellite state and topographical information (Shuttle Radar Topography Mission). The final spatial resolution is set at 10 meters.

OTB
The speckle and distortion effect from SAR images were partially removed in 3 successive steps. First a horizontal convolutional average window (3X1) is applied to the images in order to mitigate the vertical aspect of the pixels (due to rectangular azimuthal resolution). Then for each image, an outcore is created which will compute and create a filter that identifies areas with slight variation over previous time period (Quegan speckle filters). Finally, the filters are applied on their respective image leading to a much higher quality product.

A square median filter with sides of five pixels is also applied to all features in order to mitigate the speckle even more.

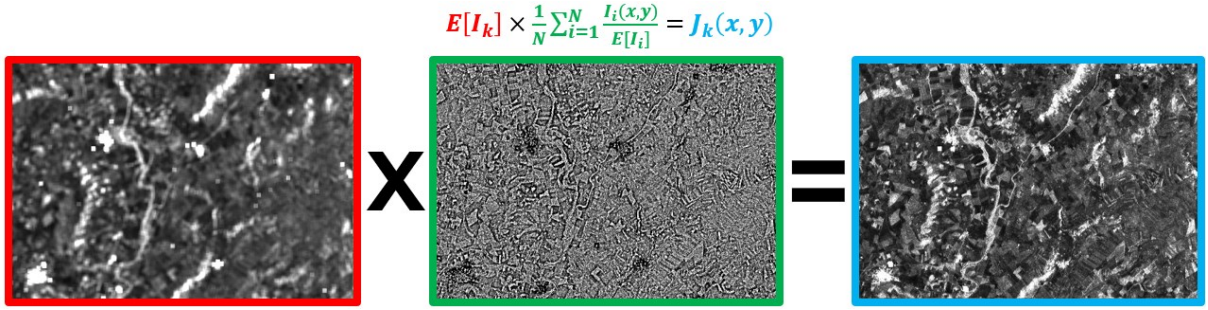

Figure 13 : *Illustration of the Quegan filter application. The base image is in red, the filter is in green, and the final filtered image is in blue (Nicolas Deffense and al. , 2020)*

3.1.3 Visualization sources

In addition to Sentinel-1 data, Planet and Google earth imagery were used for visualization purpose. Planet images are 4 band multi-spectral medium resolution (3-5 m) ortho-mosaic optical data. For the purpose of this study, trimestral scenes have been used from 2017 to 2020. Google earth images are made of a combination of data coming from various earth observation program including Maxar, CNES, Landsat and Copernicus.

3.1.4 Other information materials

Previous classifications of the study area were used as complementary information for both training and validation sampling. The first one was made by del Marmol, (2019) using Sentinel-2 images and achieved a 10 classes classification. The second one was made by Herincks, (2019) using both Sentinel-1 and SRTM data achieving a 10 classes classification. The third source was not especially made for Pokola area but cover the entire Congo basin. It was made by Dalimier and al., (2022) on behalf of OFAC using various dataset including Sentinel-1 and Sentinel-2. This classification can be visualise in Appendix 3. For the Pokola area a 10 classes classification was made.

The last source is the “Long-term (1990–2019) monitoring of forest cover changes in the humid tropic” achieved by Vancutsem and al. (2021) and was mainly used to map Tropical Moist Forest (JRC_TMF) at 30m resolution using Landsat 4,5,7 and 8 multispectral optical images. The forest-mask produced by Vancutsem and al. can be visualise in Appendix 4.

Finally, the complete description of forest type that was made for a part of the Pokola area in GILLET (2013) doctoral thesis helped identify more precisely forest types and tropical forest ecosystems.

3.2 Methods

3.2.1 Sentinel-1 features computation

Even with previous pre-processing, SAR data are characterized by speckle that leads to high temporal backscattering variations. Those are due to time inconsistent interferences of coherent echoes coming from the shape and composition of detected object smaller than a pixel (10-meter resolution). To mitigate this effect of randomness in the data the mean and standard deviation of pixels on a long time series were computed. All features described below will be 4-years long time series.

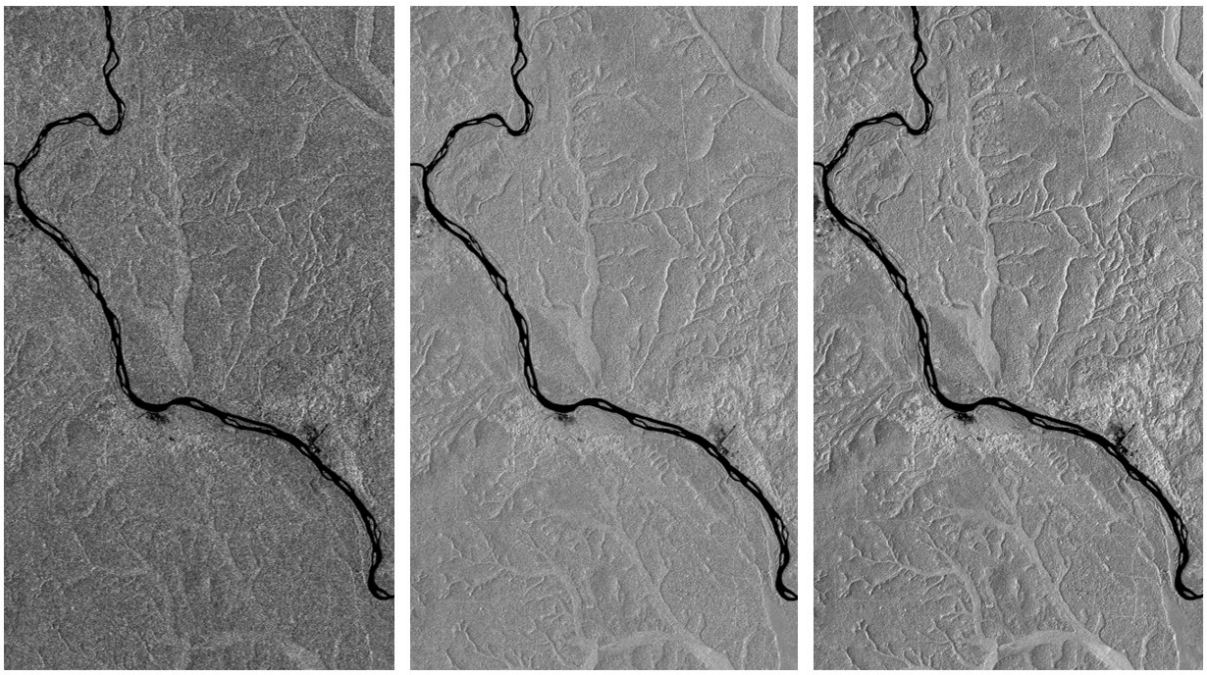

Figure 14 : *Comparison between a one day (left) one year (middle) and 4-year (right) long time series from the Mean VH polarization value.*

3.2.2 Index computation

Long time series allows the extraction of meaningful information by computing indices. For this purpose, Radar Vegetation Index (RVI) and the Coefficient of variation (CV) were computed.

CV

The CV also known as Relative Standard Deviation (RSD) provides information about dispersion and main backscattering values tendencies over time. In Pokola's context CV highlight anthropic areas in comparison with forest and water area.

$$CV_{VH} = \left(\frac{STD_{\sigma_{VH}^0}}{\bar{\sigma}_{VH}^0}\right)$$

RVI

The RVI was created in order to provide an alternative to the NDVI with Sentinel-1 available data RVI tends to be closer to 0 for bare soil and other smooth surfaces and closer to 1 with increasing vegetation density. This index was proven useful in monitoring crop evolution in tropical context but is rarely used in tropical forest remote sensing (Dipankar and al., 2020).

$$RVI = \frac{4.\bar{\sigma}_{VH}^0}{\left(\bar{\sigma}_{VH}^0 + \bar{\sigma}_{VV}^0\right)}$$

SARAd (SAR adjusted features)

With SAR data comes also double bound effect (DBE) at some forest stand's boundaries. This effect is characterized by a parasite enhanced backscattering either in VV and VH polarization leading to misclassification. This enhanced signal propagates to composite features like standard deviation and CV. To mitigate this effect the features values were divided by ($Mean_{VV}$ + $Mean_{VH}$). The features that are divided by ($Mean_{VV}$ + $Mean_{VH}$) have the prefix SARAd added to the original name a few as illustrated in the equations below.

$$SARad\ CV_{VH} = \frac{CV_{VH}}{(\bar{\sigma}_{VH}^{0} + \bar{\sigma}_{VV}^{0})}$$

$$SARad\ (Mean_{VV} - Mean_{VH}) = \frac{(\bar{\sigma}_{VV}^{0} - \bar{\sigma}_{VV}^{0})}{(\bar{\sigma}_{VH}^{0} + \bar{\sigma}_{VV}^{0})}$$

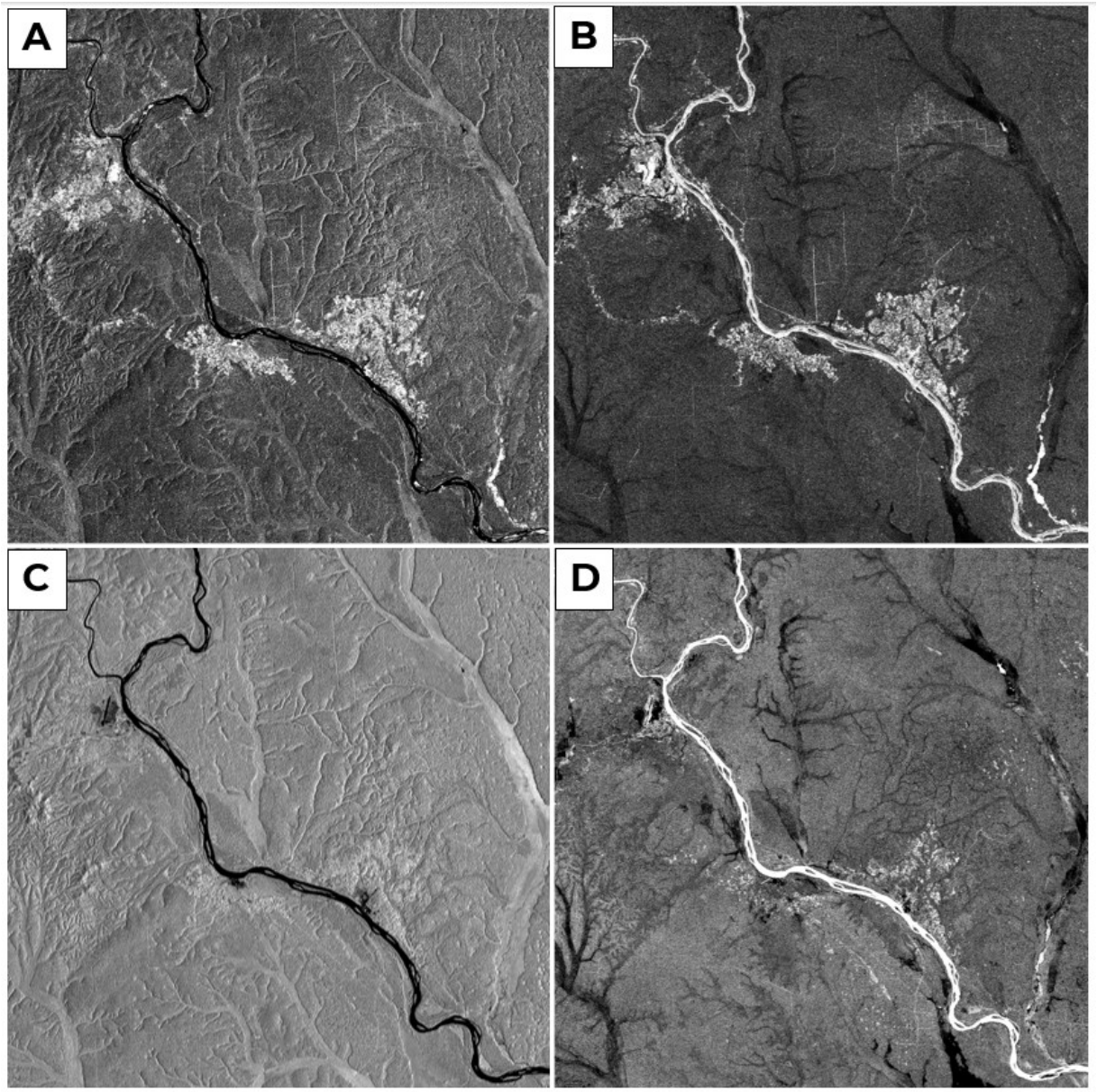

Figure 15 : *Illustration of the effect of the SARad transformation on A) CV_{VH} and C) MeanVH into respectively B) SARad CV_{VH} and D) RVI.*

SARad transformation provide flattening data and significantly removes the DBE (Figure 16). One counter effect is the fact that water's extremely low signal backscattering intensity are much more heterogeneous than before which can lead to misclassification with other low backscattering areas like bare soil. Another consequence is the inversion of amplitude values.

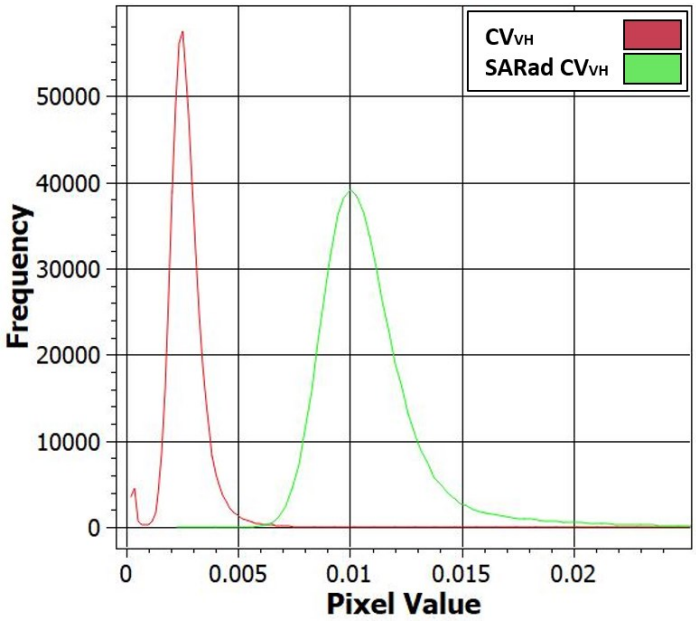

Figure 16 : *Pixel value distribution from CVVH and SARad CVVH*

To ensure that SARad features are not conilear and thus provide different informations to the model, a corralation analisys has been made between SARad features and their respective composite features. A strong correlation is not a guarantied of colinearity. On the other hand, a weak corralation indicates a non colinearity and thus SARad features can be considered as new a index.

As illustrated in Figure 17, the new SARad features are weakely corralated with their non modified origin features and thus can be considered as new index providing new informations to potential classification.

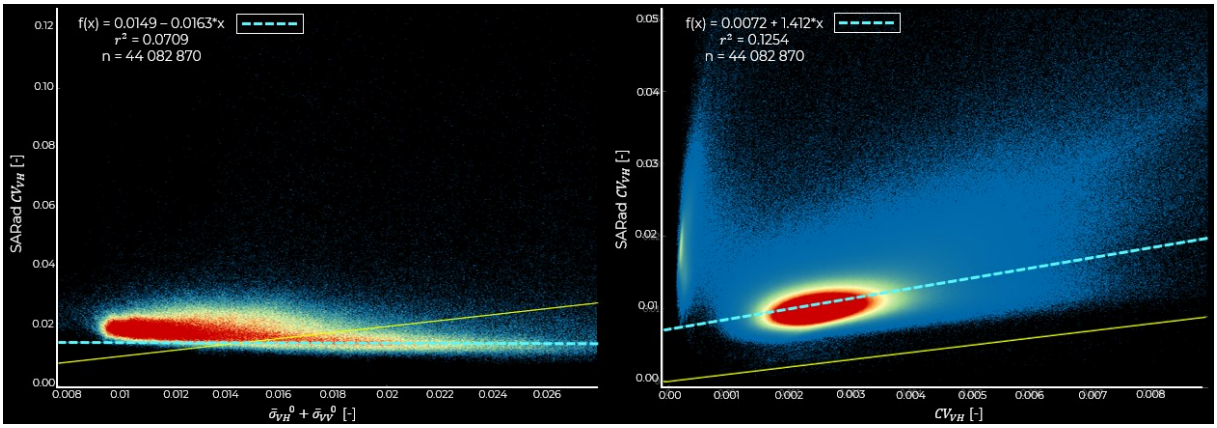

Figure 17 : *Plot of the correlation between SARad CVVH and his respective component : MeanVH +MeanVV (left) and CVVH (right).*

3.2.3 Colour composite images

Good data visualization in remote sensing is especially useful to collect training and validation samples especially where ground collected training data are not available. One of the most promising visualizations found during the process of features selection is the false colour presented in Figure 18 images helping discriminate many forests type and land cover.

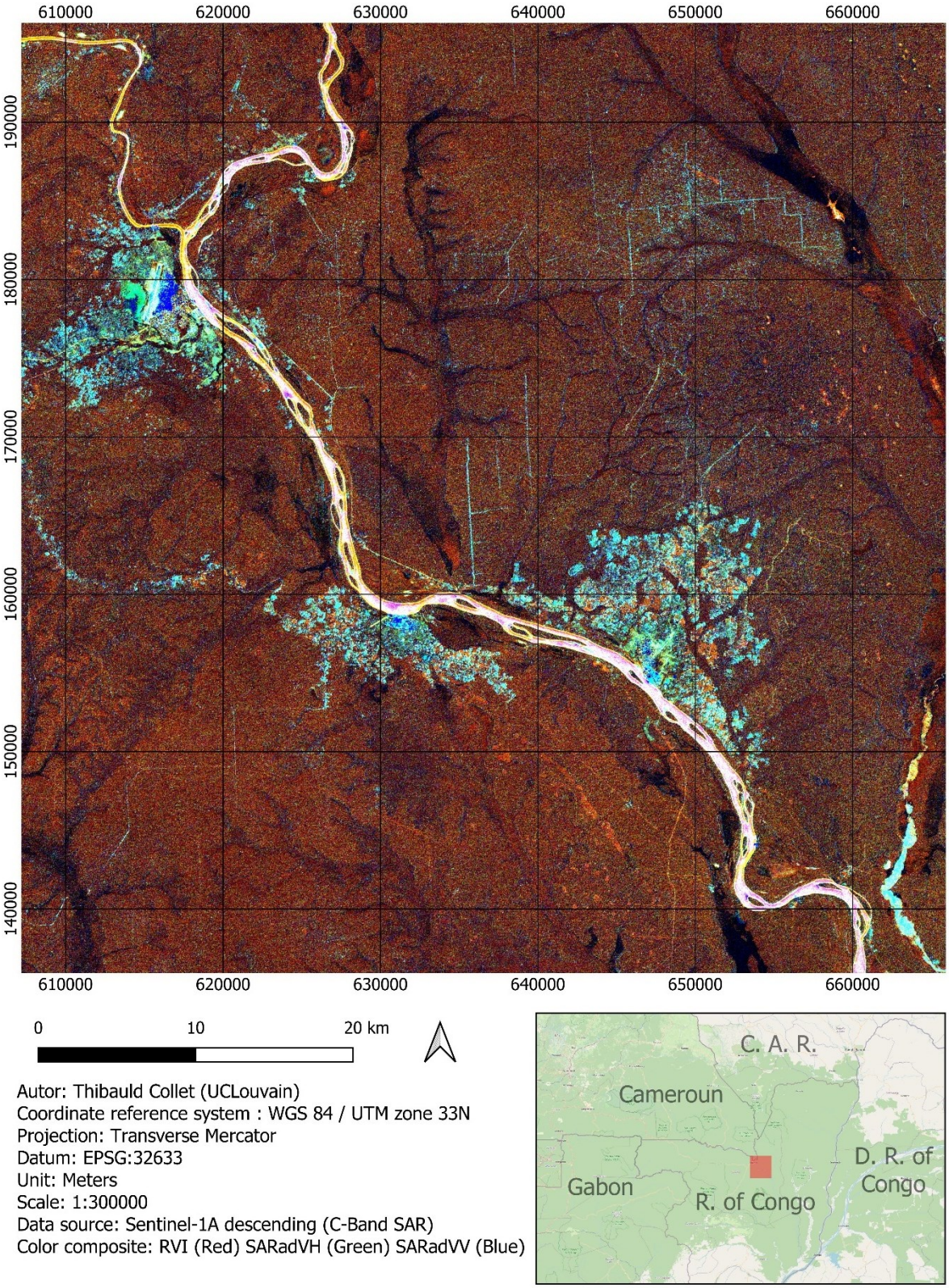

Figure 18 : *Colour composite image of the Pokola area used for photointerpretation.*

3.2.4 Textural features

Given the remaining speckle and the high structural heterogeneity of forest stands it seems to be impossible to classify rightfully each individual pixel regardless of his context. Two approaches have been followed to take this context into account. The first one consists of an Object-based Image Analysis (OBIA) and will be discussed in a further section. The second one (that can be combined with OBAI) consist in of the extraction of the textural environment of each pixel. Those textural features were formalized by Haralick and al., (1973) and were proven to be useful in land cover remote sensing (Dengsheng Lu and al., 2014). Those features are based on a Grey Level Co-occurrence Matrix (GLCM). This square matrix compiles the number of occurrences of each pixel values combination for a given context window. Those combinations can be detected in 4 direction (vertical, horizontal and two diagonal directions). The obtained values are then normalized, and relation probability matrix are also computed. Based on this GLCM, 14 features can be computed for each pixel of interest, each features describing a particular aspect of the textural context of those pixels.

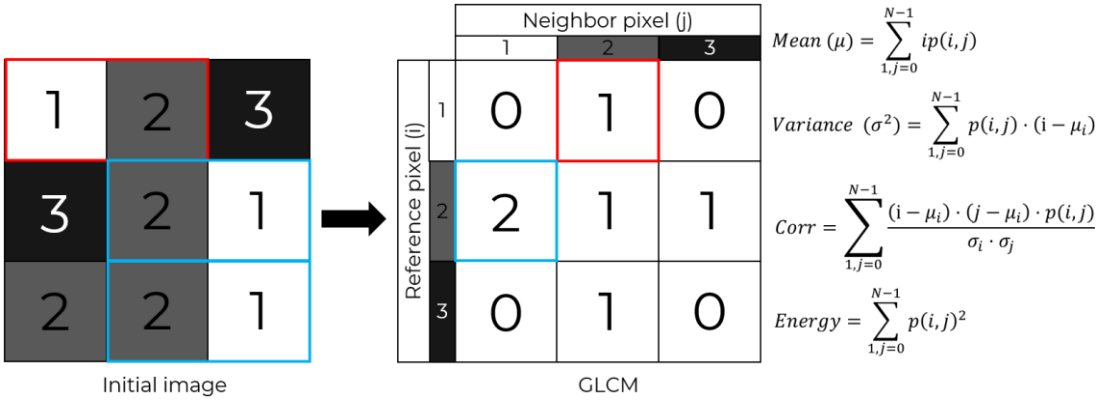

Figure 19 : *Schematic of the GLCM computation. The initial 3x3 image is centred on the pixel of interest. GLCM is build in the horizontal direction. For 9 pixels of 3 shade of grey (N) we end up with a NxN matrix filled with 6-pixel combination. On the right are presented 4 of the 14 computable features.*

In this study various window sizes were evaluated and the GLCM were computed in all the directions making the GLCM and thus the computed features direction invariant. The 10 advanced textural features were computed (Mean, Variance, Dissimilarity, Sum Average, Sum Variance, Sum Entropy, Difference of Entropies, Difference of Variances, Information Measures of Correlation 1, and Information Measures of Correlation 2(IMC1 and IMC2)). The features were computed using *HaralickTextureExtraction* tool from OTB that input a grey-scaled image and output a multi-band image were each of the 10 bands represent a feature. Multi-band images are then split using the *SplitImage* tool from OTB in order to select and use each band as a feature in classifications.

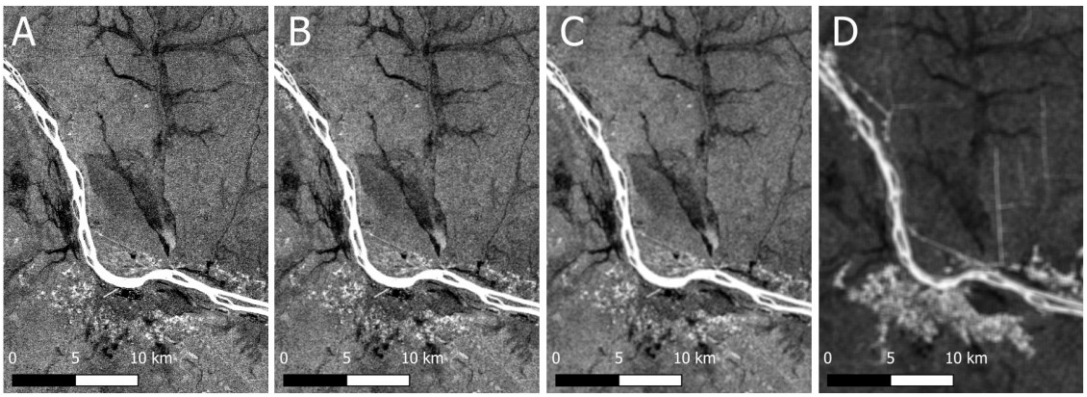

Figure 20 : *Comparison of various window size on the GLCM "Mean" textural feature of RVI feature (A = 5x5, B = 11x11, C = 21x21 and D = 41x41)*

3.2.5 Forest and land cover typology

In order to ensure comparison with other recent classification it was chosen to use land cover OFAC classification as classes definition base. However, some changes have been applied to best fit with Sentinel-1 detection capabilities. In total 16 classes were identified and regroup in 9 super-classes. Field data are not available in this area thus multiple raster data were chosen to identify and collect training and validation samples. Classes were described regarding of the forest stands and land cover backscattering behaviours.

3.2.5.1. Anthropized area

Anthropized areas are devided into 3 differents super classes regarding their radiometric signatures and relative artificialisation level. Those classes ranges from artificialized area to high density low vegetation.

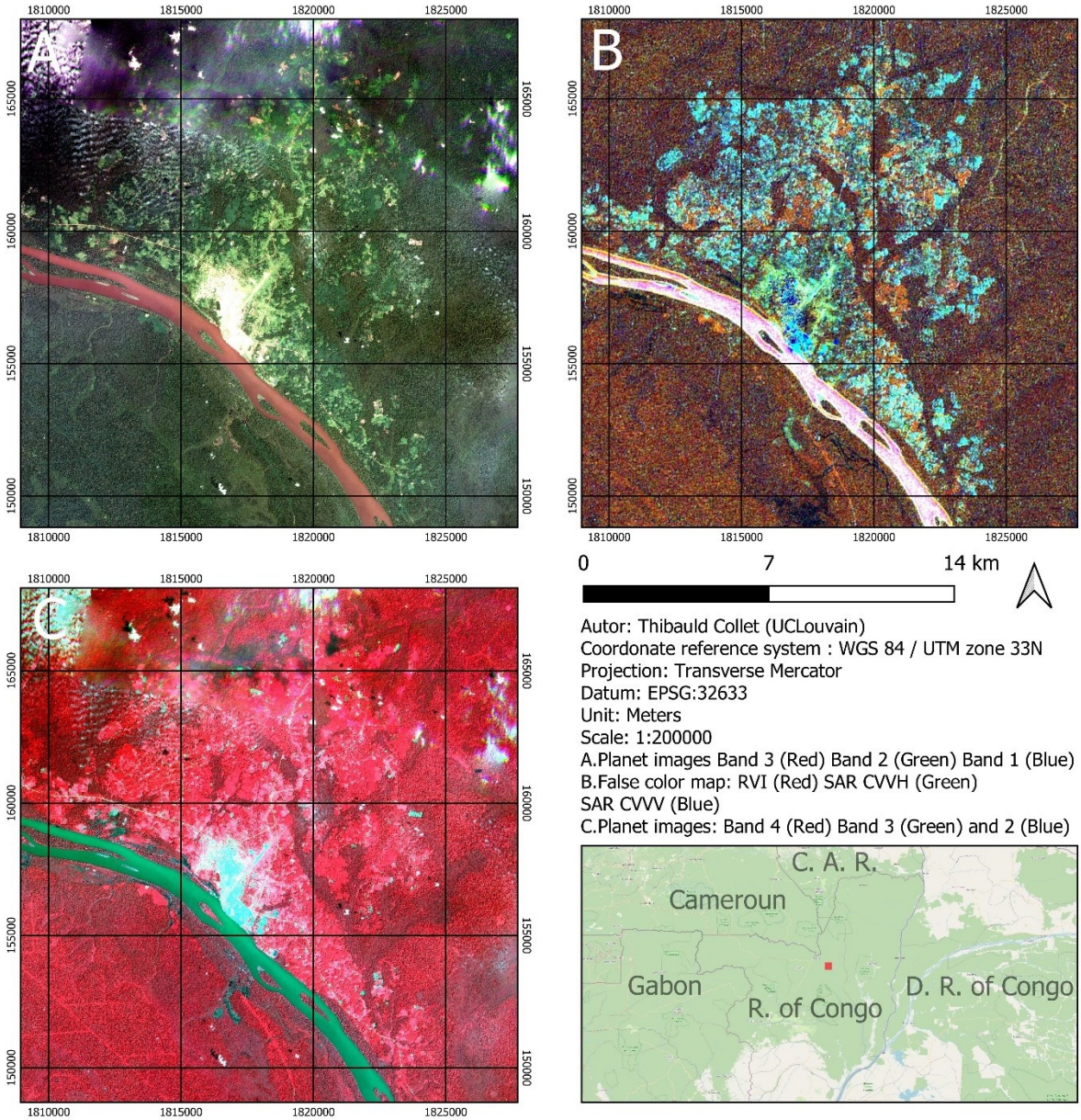

Figure 21 : *Comparison of 3 different visualization from Pokola and its surroundings. Colour composite is made combining 4 years long time series. Planet images were collected for the year 2020.*

Artificial area (Figure 22)

The first class is called as **high urban density** and is characterized by full urban density, low tree cover, a bare soil area and heavily used roads. Those characteristics leads to an alternation between high return signal intensity caused by double bounce effect next to buildings, and low return signal intensity due to specular reflection caused by bare soil and roads.

The second class is called as **low urban density** and is characterized by urban area with a higher tree cover and multiple little bare soil areas but less predominant than in the first class giving up place to grass, bushes and little garden. Double bounce effect is less predominant and left gradually the place to more volume backscattering. Those areas are still punctuated by areas with high specular reflection effect.

The third class is called **bare soil** and is characterized by big, open, and flat bare soil or artificialized open areas. It usually contains airfields, marketplaces, or open-air tree trunk storages. Lack of vegetation and the openness terrain leads to an acute specular reflection somehow comparable with the one occurring on water body. There is not a clear distinction between those three classes and those could be seen more as a gradient of urbanization than as separate classes and thus are resembled into one super-class called “Urbanized area” and are characterized acute level of artificialization areas

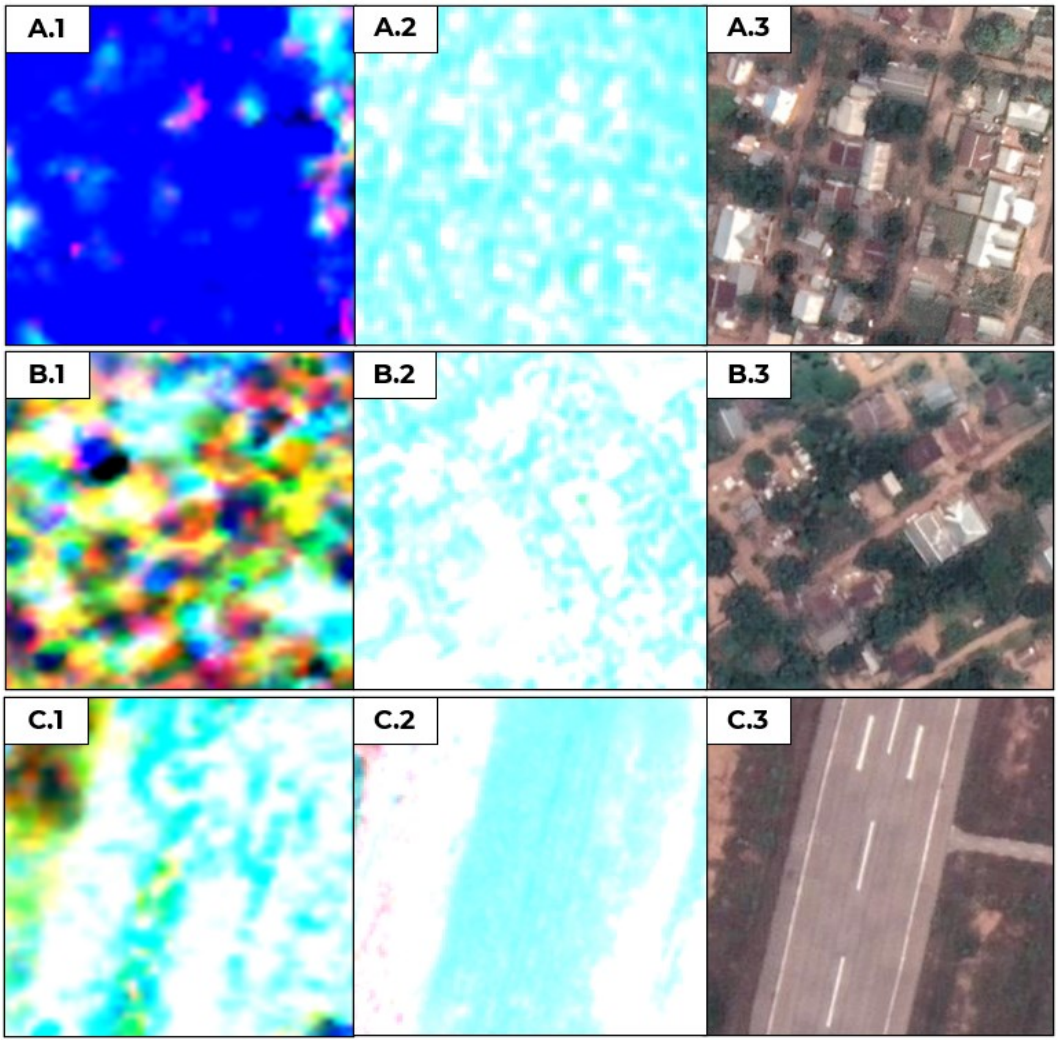

Figure 22 : *A) Ouésso city centre. B) Ouésso suburbs. C) Ouésso landing strip. 1) Colour composite [RVI, SARadCVVH, SARadCVVV]. 2) Planet images [Band 4 (Red), Band 3 (Green) and Band 2 (Blue)]. 3) Maxar images (Google earth, 2022).*

High density low vegetation (Figure 23)

Those areas are primarily composed of various Marantaceae species covering almost all the shrub layer and can reach a 3-meter height. This almost exclusive monospecific covering allows some parasol tree to grow but the superior layer canopies never exceed 10-15%. This vegetal formation occurs either naturally around forest clearing (after a storm or a sudden change in local water regime) or artificially after a brief but intense episode of deforestation. This class can be found mostly around cities but can also be found in the middle of the forest always around body of water or clearings. This class also designes all types of long lasting dense low vegetation areas regardless of the species even if Marantacea are usualy dominant.

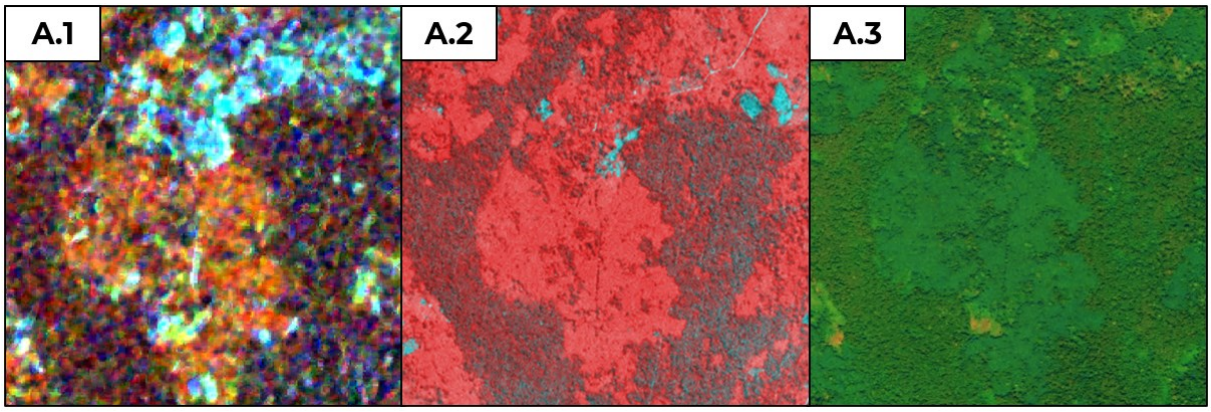

Figure 23 : *A) Low density low vegetation area near Pokola. 1) Colour composite [RVI, SARadCVVH, SARadCVVV]. 2) Planet images [Band 4 (Red), Band 3 (Green) and Band 2 (Blue)]. 3) Planet images [Band 3 (Red), Band 2 (Green) and Band 1 (Blue)].*

Low density low vegetation (Figure 24)

This super class is divided into three sub-classes regarding of their respective tree cover and land use. It defers from the previous classes by their dense low vegetation cover in comparison with artificial areas.

The first class is labelled as **sparse vegetation**. It contains deforested areas used intensively over an extended period. It is mainly found around city centre or along roads, but it might also be crops with short fallow period or recent burned vegetation areas. Due to low vegetation density and height, specular reflection effect is strong but significantly weaker than for long duration bare soil areas thanks to the fast vegetation regrowth occurring after the disturbance.

The second class is labelled as **crops and low vegetation**. It is characterized by an extremely low tree cover and is mainly composed of crops in rotation with early regrown forest. This class also contains recent deforested areas covered by early vegetation regrowth and permanently low vegetation. In those areas specular reflection is high, and backscattering is low.

The third class is labelled as **mixed agricultural landscape** and consists of crops and low vegetation areas dotted with parasol groves and arboriculture practices areas. Those characteristics lead to some backscattering similarities with forest areas. The volume backscattering is low due to average low tree cover but still higher than in the two previously mentioned classes.

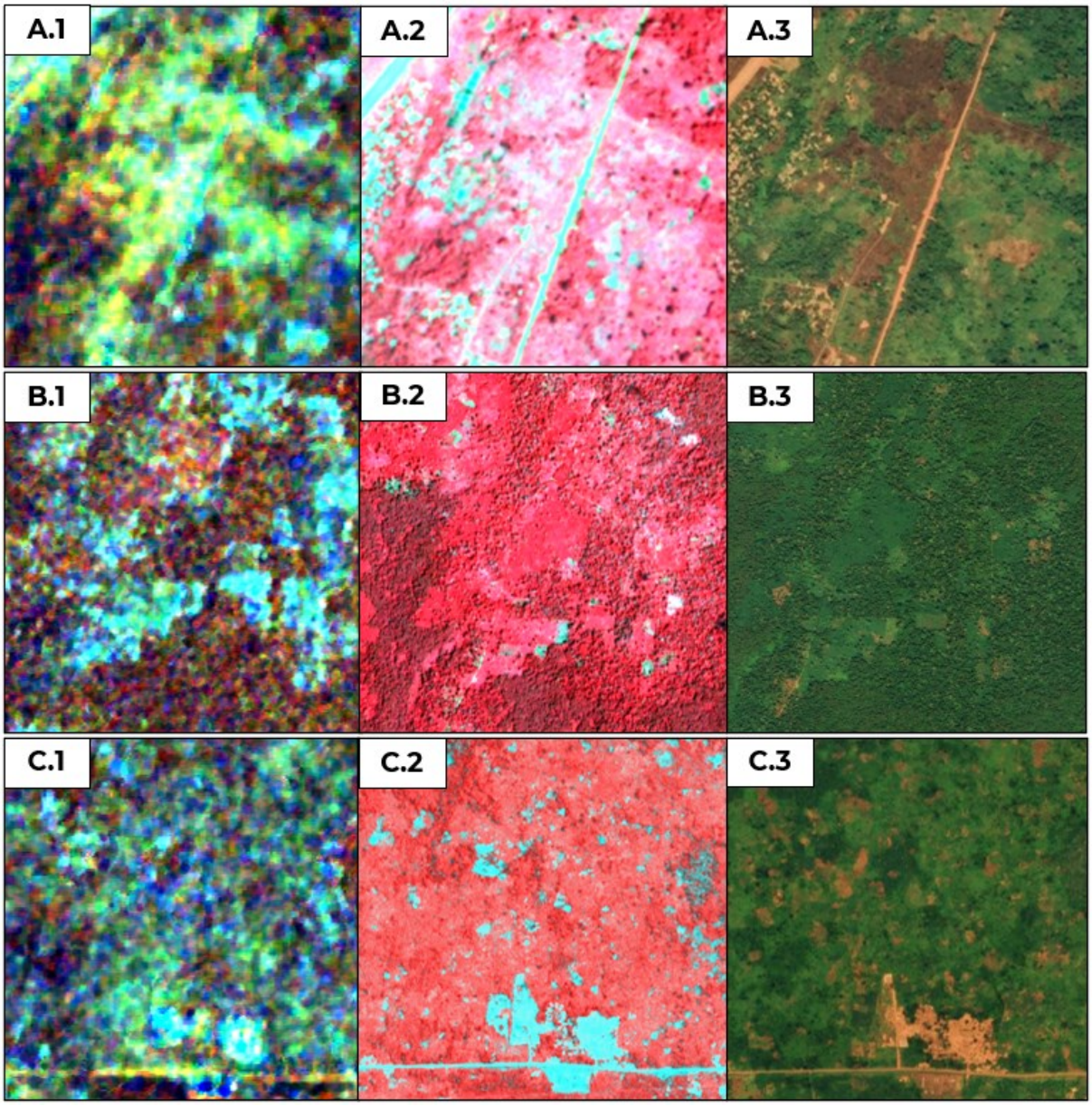

Figure 24 : *A) Sparse vegetation surrounding a road in Pokola suburbs B) Crops near Pokola. C) Mixed agricultural landscape near Ouésso. 1) Colour composite [RVI, SARadCVVH, SARadCVVV]. 2) Planet images [Band 4 (Red), Band 3 (Green) and Band 2 (Blue)]. 3) Planet images [Band 3 (Red), Band 2 (Green) and Band 1 (Blue)].*

3.2.3.3. Flooded non-forest area

Free Water (Figure 25)

This class contains all types of streams and water bodies. Its radiometric signature is characterized by an acute specular reflection.

Aquatic grass land (Figure 25)

Aquatic grass land are characterized by a sparse vegetation flooded more than 4 month a year. The signal behaviour is close from the water ones but is diminished by few volumes backscattering coming from vegetation. This class can be found around shallow river and on river island.

Floodable grass land (Figure 25)

This class contains all the grass land and bare soil that are flooded less than a few months a year. It is characterized by periodic alternations between shallow flooded terrain and bare soil. The radiometric behaviours consist of a variable high specular reflection effect over time.

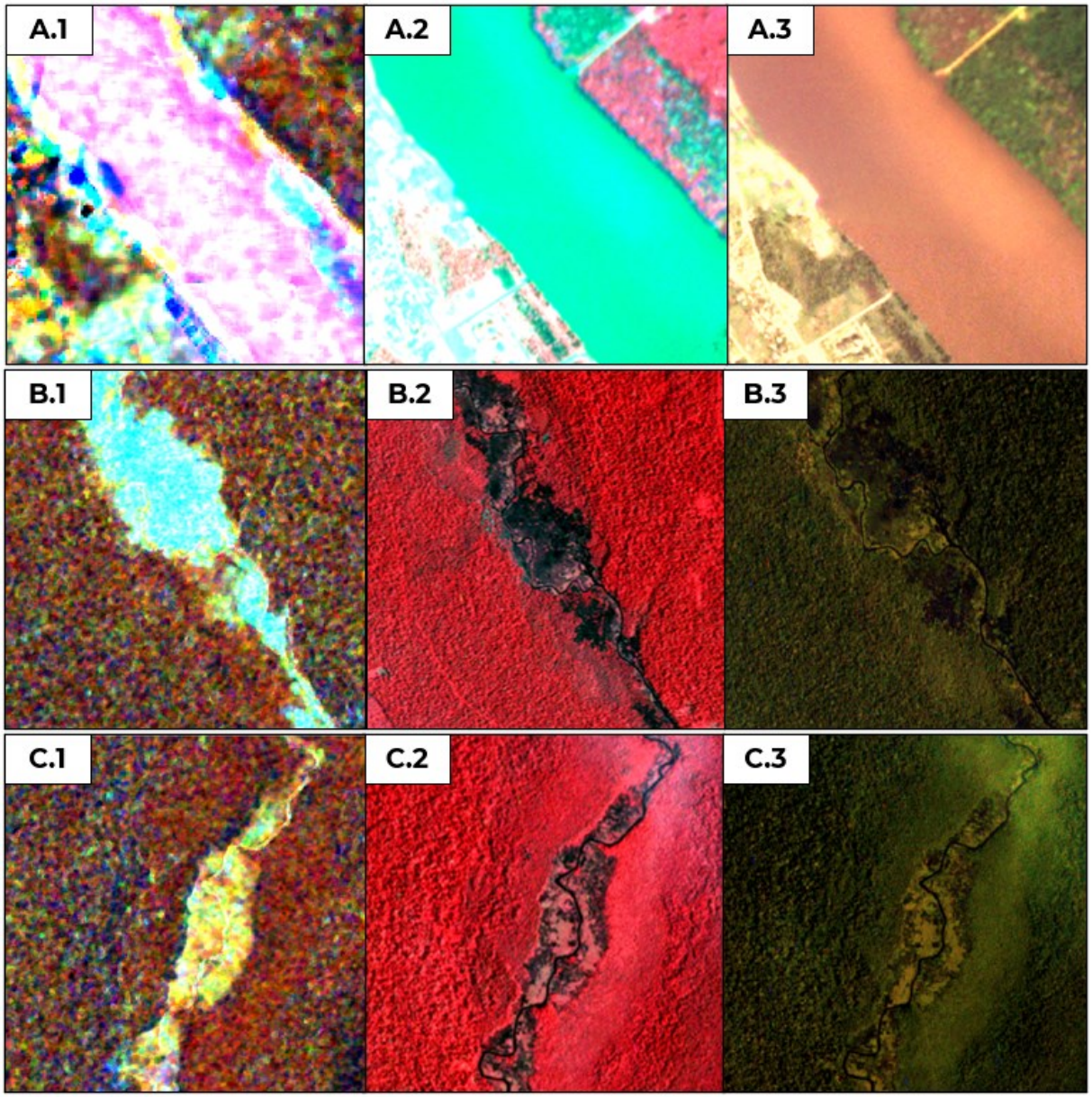

Figure 25 : *A) Portion of the Sangha River near Ouésso. B) Aquatic grass land on the Ndoki river. C) Floodable grass land on the Ndoki rive. 1) Colour composite [RVI, SARadCVVH, SARadCVVV]. 2) Planet images [Band 4 (Red), Band 3 (Green) and Band 2 (Blue)]. 3) Planet images [Band 3 (Red), Band 2 (Green) and Band 1 (Blue)].*

3.2.5.2 Forest area

Tropical moist forest types are harder to identifies and visually discriminate from each other than anthropic areas using only Sentinel-1 data sources. Tropical forest stands are complex entities that do not have clear boundaries. They are usually heterogenous in terms of species, canopy composition and ground water content. However, a meticulous image analysis made possible a visual discrimination of 6 forest classes. Due to spatial and temporal speckle in SAR data, it is almost impossible to identify specific forest types at pixel scale. Thus context, surroundings and forest stand's average signal values were used to identify forest stands. Due to low SAR-C canopy penetration depth it is not possible to discriminate lots of various dense forest. Because of their specific architecture induced by hydric condition flooded forest are easily identifiable in comparison with non flooded forest or Limbalis stands.

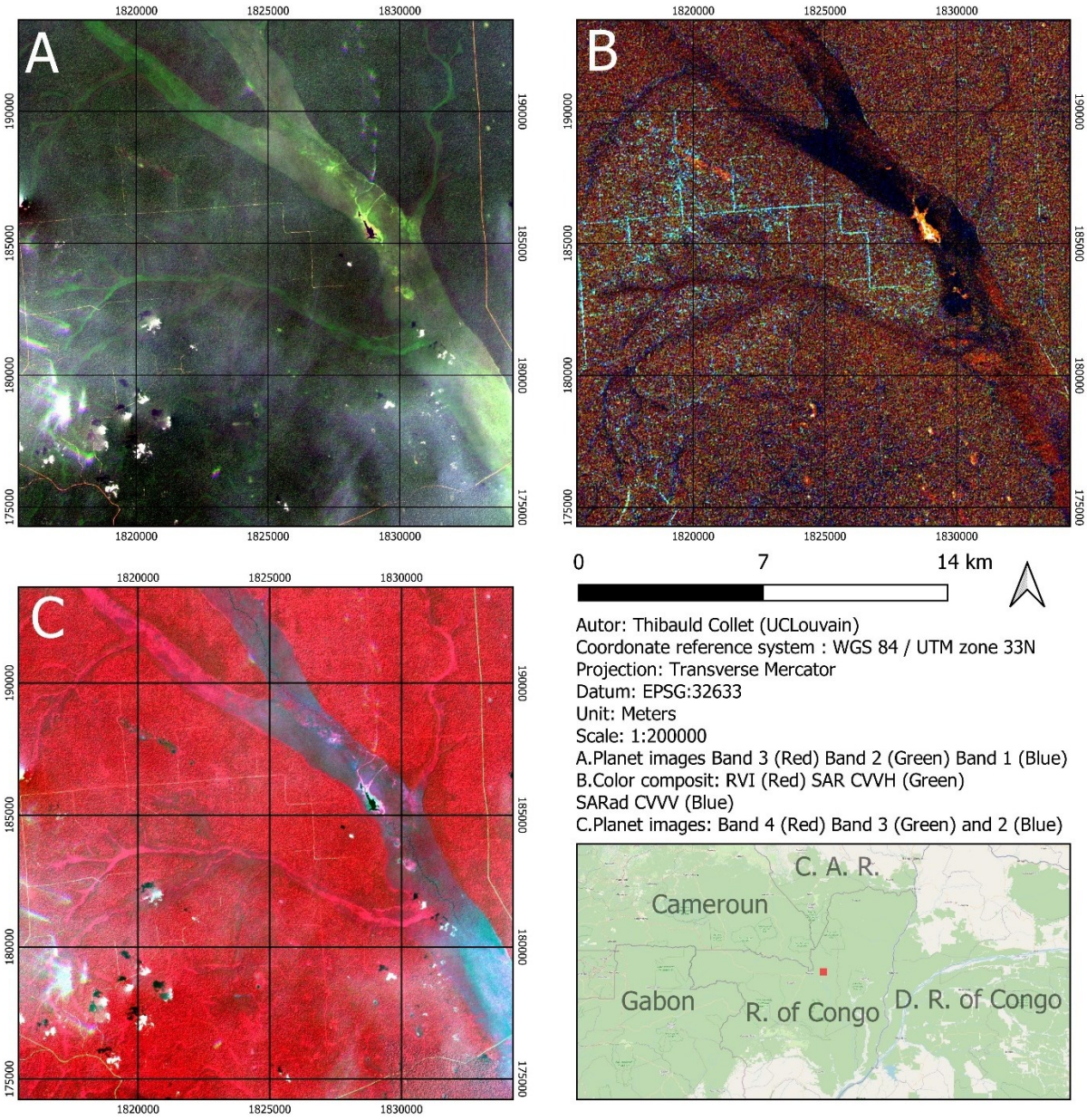

Figure 26 : *Comparison of 3 different visualization from a portion of Djaka river. Colour composite is made combining 4 years long time series. Planet images were collected for the year 2020. In the middle of the river, we can see the Raphia stands along with the other flooded forest. Limbalis forest can be seen on the river edges surrounded by semi-deciduous forest.*

Raphias forest (Figure 27)

Due to specific forest stands architecture, Raphia forest their can be radiometrically isolated from the other flooded forest. For the same reason palm tree plantations have almost the same radiometric behaviours as Raphia forest. This class is characterized by a moderate vegetation density on a permanently flooded terrain next a river and with a clear dominance of Raphia trees. This moderate cover density allows the signal to penetrate deeply into the canopy and provide a moderate to high deep volume backscattering. All those reasons allow a clear identification of Raphia stands from various data sources but tends to include all the palm trees stands.

Open flooded forest (Figure 27)

Those forest are in permanently flooded terrain. This class is characterized by low density and discontinuous canopy allowing low floodable vegetation to grow between the small forest stands. Radiometrically speaking, canopy volume backscattering is lower than for Raphia forest and it adds up with the volume backscattering and specular reflection of floodable grass. Furthermore, temporal signal variability is high due to seasonal changes in hydrographic regime.

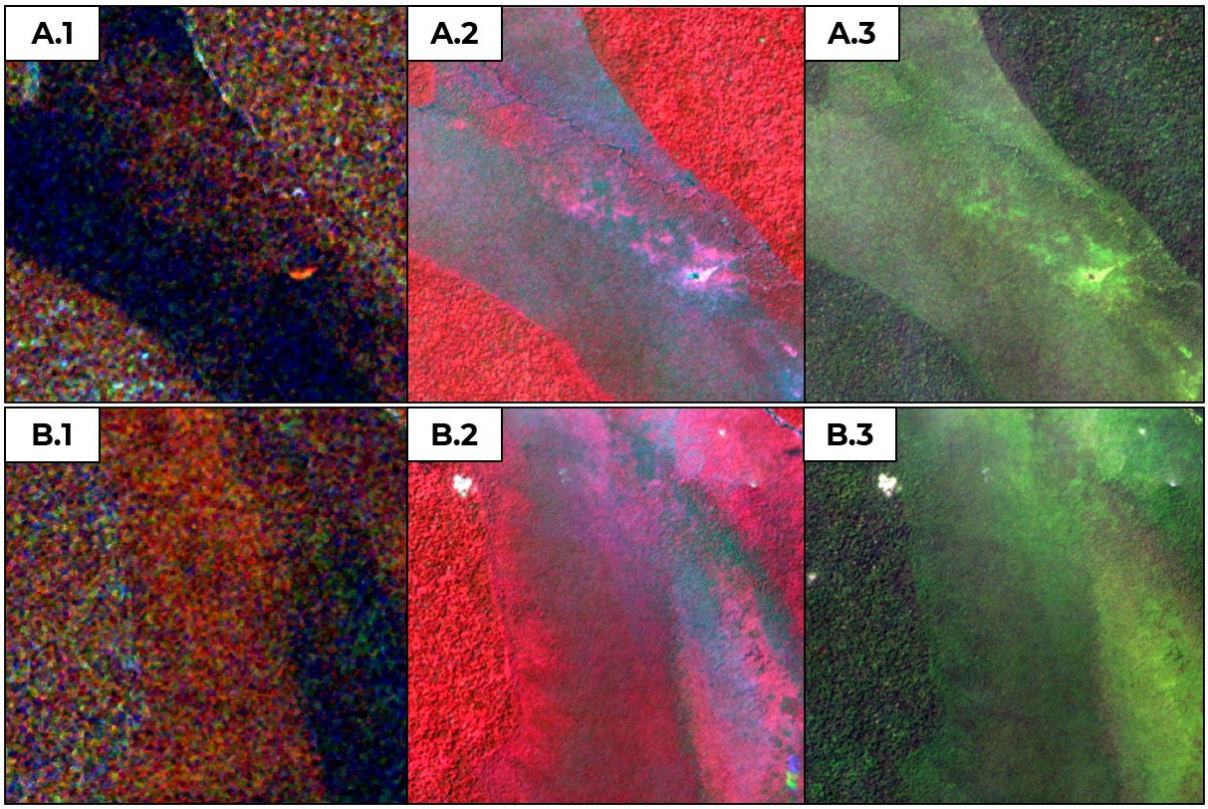

Figure 27 : *A) Raphia and B) Open flooded forest along the Djaka river. 1) Colour composite [RVI, SARadCVVH, SARadCVVV]. 2) Planet images [Band 4 (Red), Band 3 (Green) and Band 2 (Blue)]. 3) Planet images [Band 3 (Red), Band 2 (Green) and Band 1 (Blue)].*

Flooded forests with mixed vegetation (Figure 28)

Flooded forests with mixed vegetation are dense flooded forests where there is no clear dominance either from Raphia or other forest type. Their radiometric behaviour is a combination of the two previously described forest type.

Bubinga swamp forest (Figure 28)

Bubinga forest are in non-permanently flooded terrain and are exceedingly rare in the Pokola area. They specific radiometric behaviour allowed a clear visual discrimination with other classes.

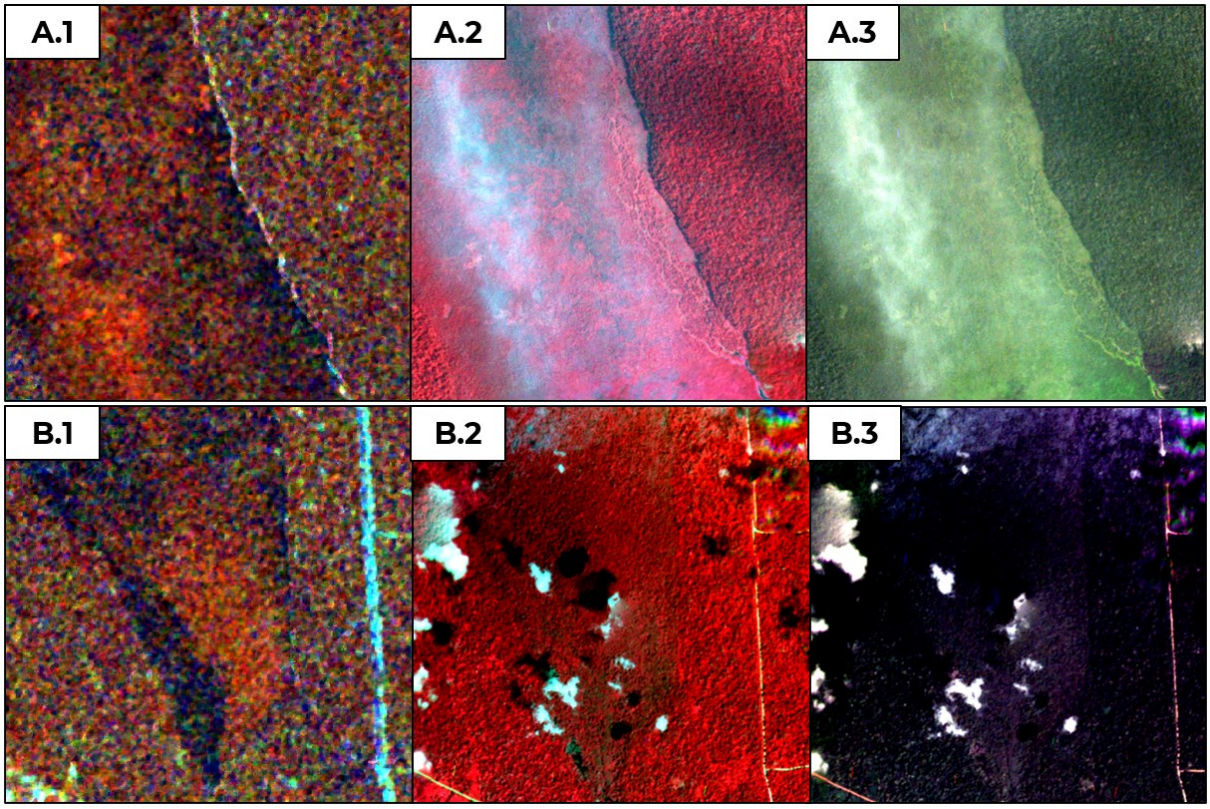

Figure 28 : *A) Flooded forests with mixed vegetation along the Djaka river. B) Bubinga swamp forest along the Mbouamboua river. 1) Colour composite [RVI, SARadCVVH, SARadCVVV]. 2) Planet images [Band 4 (Red), Band 3 (Green) and Band 2 (Blue)]. 3) Planet images [Band 3 (Red), Band 2 (Green) and Band 1 (Blue)].*

Monodominant forest (Figure 29)

This class represent the dense evergreen monospecific forest. In the Pokola's area, the main species from this class from the *G. dewevrei* family and are also called "Limbalis." Those species are gregarious and shade tolerant and have the capabilities of having their main regeneration happening under their own canopy. Limbalis stands can be found in both flooded and non flooded terrain and differs greatly in terms of under cover vegetation. This class is characterized by a high-volume backscattering happing at the edges of the canopy. The very dense cover does not allow the signal to penetrate furthermore into the canopy. In regards with these radiometric behaviours, it is not possible to distinguish the flooded Limbalis from the non-flooded one using only Sentinel-1 images.

Non-flooded forest with mixed vegetation (Figure 29)

This class gathers all the other dense semi-deciduous forest regardless of their tree species composition and architectures. Those forest have unequally suffered of various degradation which explains partially their heterogenous space and temporal radiometric behaviours. For all those reasons and because of the low penetration depth of Sar-C signal, Sentinel-1 data do not enable an easy photointerpretation of the various non flooded forest type.

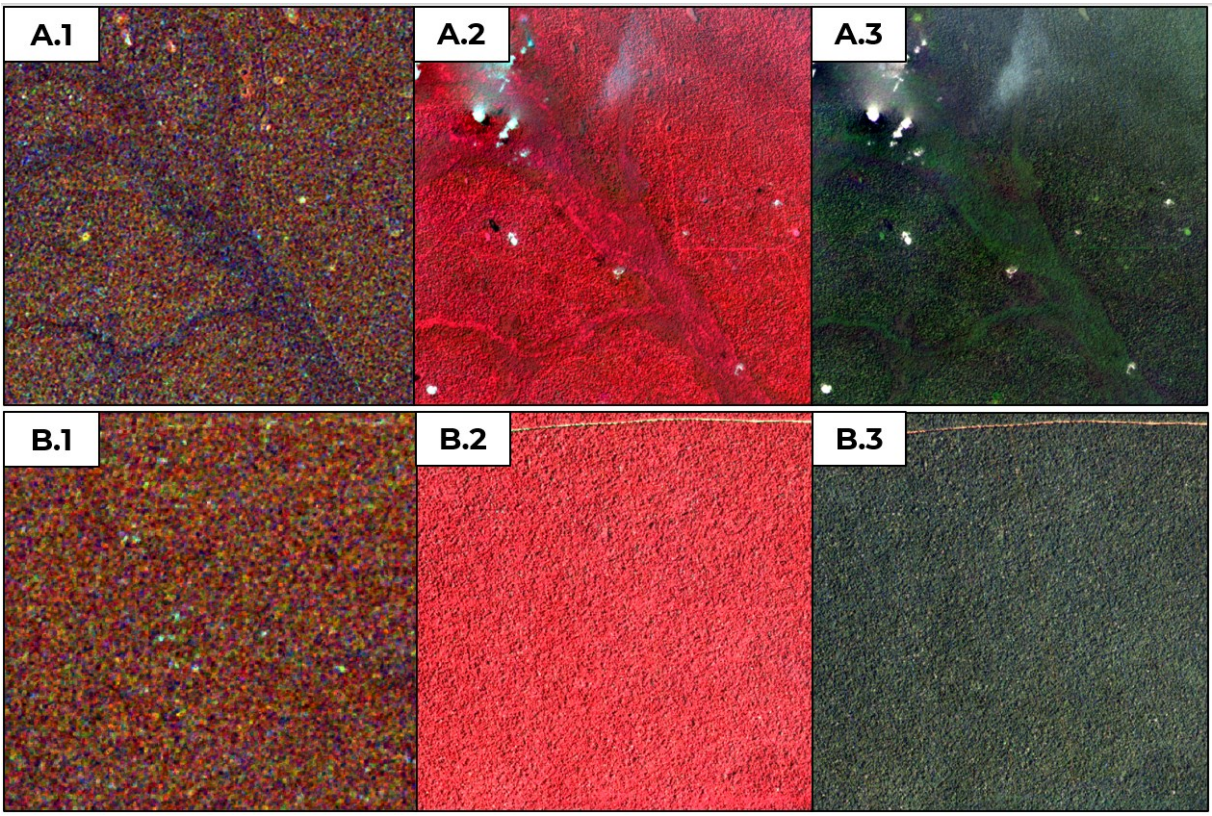

Figure 29 : *A) Limbalis forest along the Mbouamboua river. B) Semi-deciduous forest near a small road on the western side of the Sangha River. 1) Colour composite [RVI, SARadCVVH, SARadCVVV]. 2) Planet images [Band 4 (Red), Band 3 (Green) and Band 2 (Blue)]. 3) Planet images [Band 3 (Red), Band 2 (Green) and Band 1 (Blue)].*

3.2.5.3 Summary

In Figure 18 is represented the various class level and their respective mother and children's classes. It ranges from 2 classes (forest and non forest) to 9 classes and finally to 16 classes.

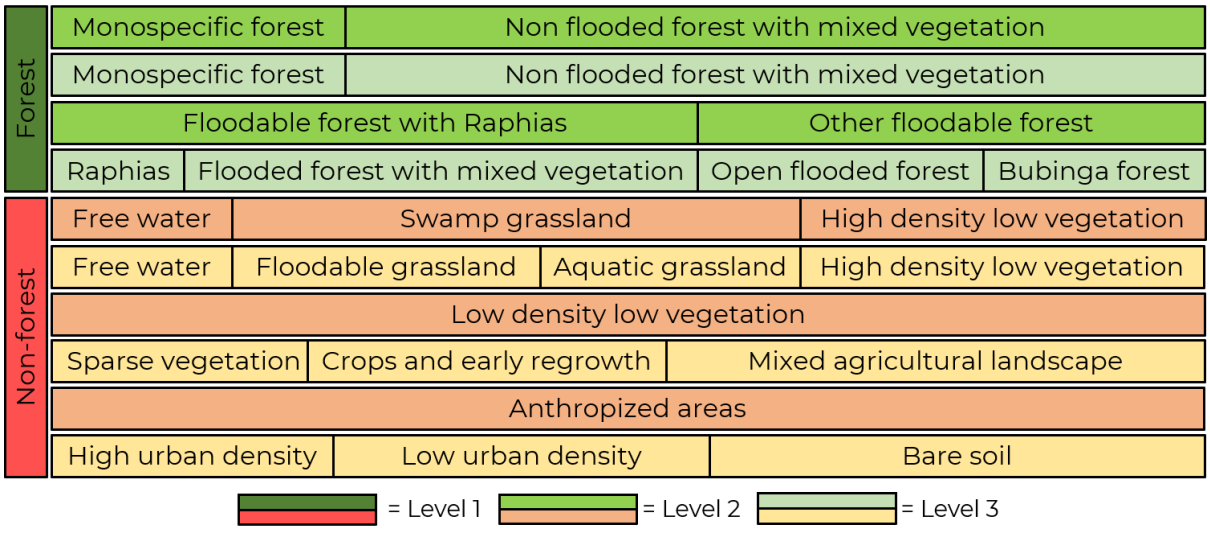

Figure 30 : *Schematic of the various class levels. Level 1 = 2 classes, Level 2 = 9 classes and Level 3 = 16 classes.*

Because of the limited SAR-C detection capabilities, the OFAC class definition was not entirely followed. The Figure 31 shows the classes that were used in the classification with their respective relations with the OFAC typology.

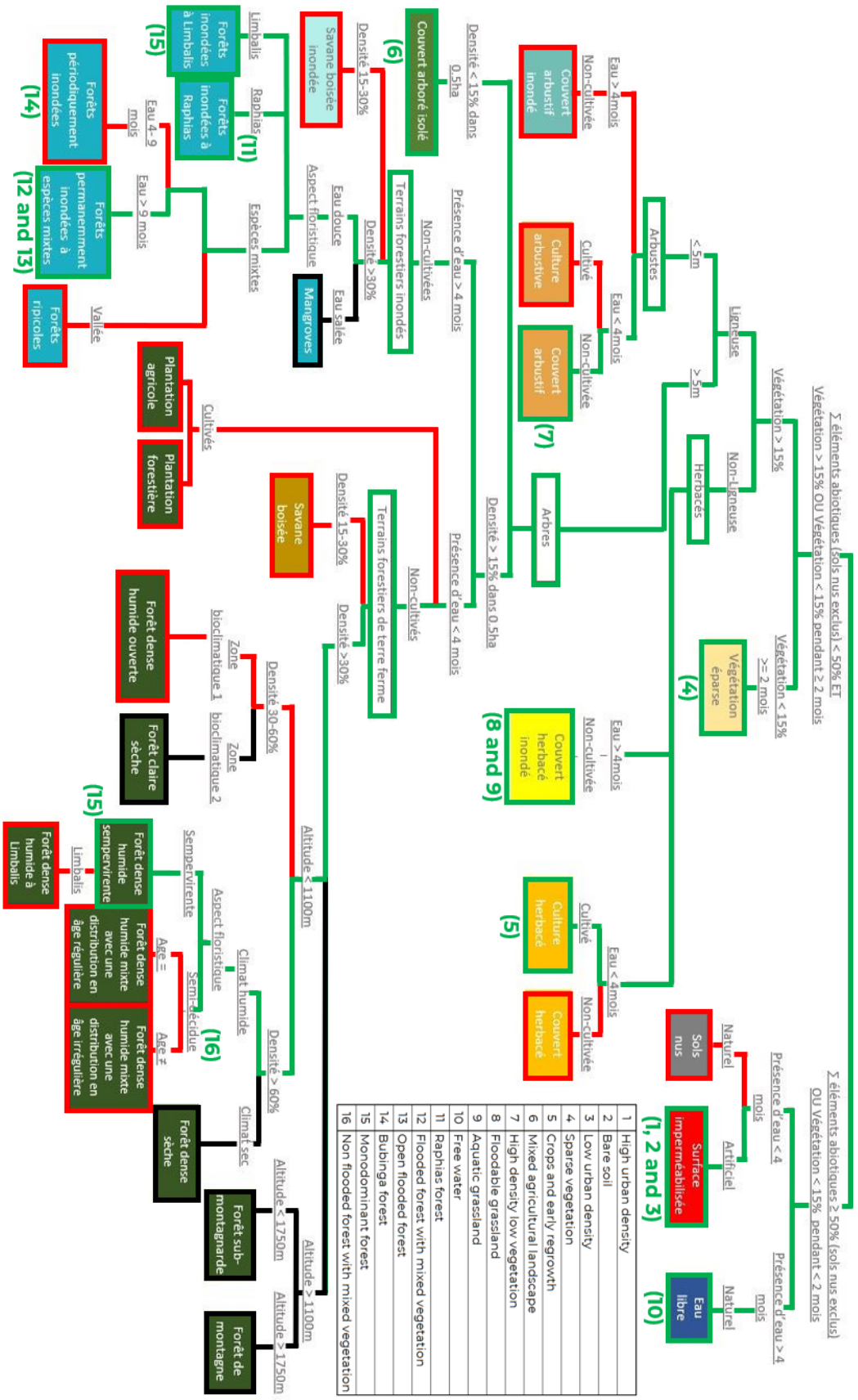

Figure 31 : *Schema of the relation between OFAC typology (OFAC, 2022) and the classes defined in this study. (Green) Part of the decision tree that were followed. (Red) Part of the decision tree that was not followed. (Black) Part of the decision tree that contain classes that can not be present in the ROI due to topographical and climatic condition.*

3.2.6 Collection of training data

3.2.6.1 Data sources

Training data were collected by photointerpretation using Planet and Sentinel-1 images. In addition to that, Dalimier (2021) classification and Maxar images (Google Earth) were used as confirmation sources. Most of the samples were collected using only optical source and previously mentioned classification at the exception of flooded forest. Those classes were not distinguishable on Planet images.

Based on forest type and land cover typology described previously, 400 points were collected as reference samples (Figure 32). Several rules were followed during this sampling to prevent overfitting and having more then one classes per polygon sample in the OBIA. Training data were collected proportionally to the assumed occupation rate of each class in the ROI. Samples were separate from at least 15 pixels (150m) from each other. If possible, sampling is done in all the ROI without oversampling a specific area. Samples were only selected in non-ambiguous area where all references agreed on each other. Sample were collected in the centre of assumed forest stands to prevent border misclassification. To ensure fair comparison between pixel based and object-based classification, the same training points were used for both calibrations. Training points were then labelled in all classification levels.

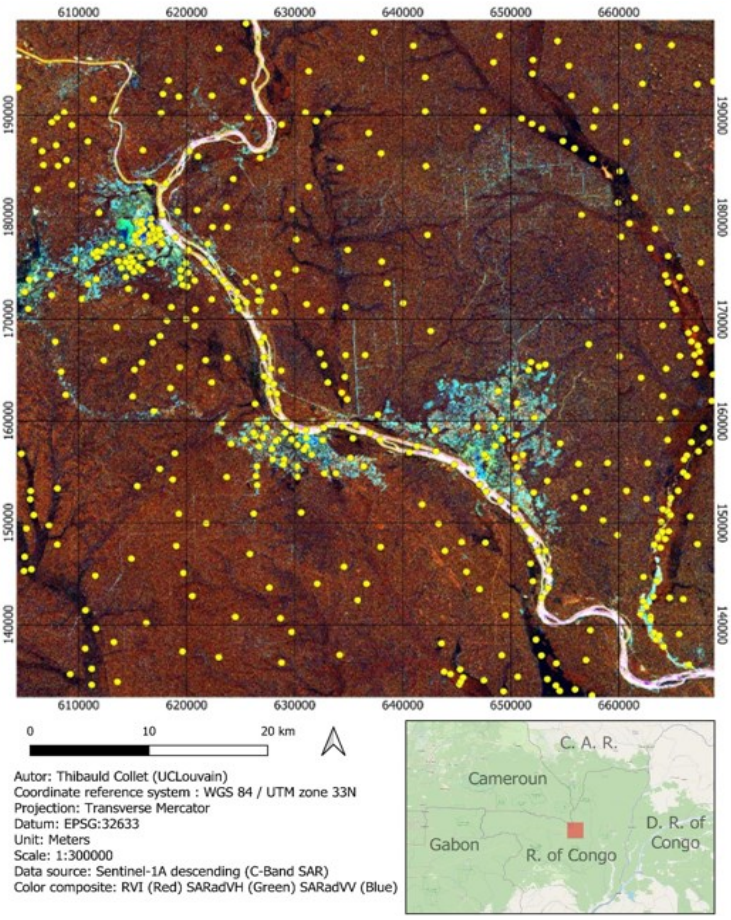

Figure 32 : *Color composite image from the ROI. The yellow points are the 400 training samples.*

3.2.6.2 Object based sampling

To perform an OBIA classification, samples must be polygons. In order to do that ROI was first segmented creating polygons. Then polygons were labelled regarding of their overlapping pixel samples. This pixel-to-polygon method has two main advantages. First, it is easier and faster to collect points and transform then into polygons than directly drawing all polygons. Then by first segmenting the area in various forest stands, the forest stands boundaries and complexities are preserved in the samples.

3.2.6.3 Pixel based sampling

To perform a by pixel classification, samples must be pixels. In contrary with an object-based approaches, polygons must be small and numerous to avoid overfitting. However, a negative buffer of 30 meters was applied around the samples points to catch the number of pixels needed for a pixel-based approach (around 25-30 pixels per polygon). A general overlook of the training data has been conducted to controlled if the new buffered point did not overlap with other classes. Then the polygons were rasterized.

3.2.7 Unsupervised multiresolution segmentation algorithm (MRS)

The initial phase of OBIA consists of image segmentation. This crucial step divide images into homogeneous image object. The degree of homogeneity and shape of the created objects are defined by hyperparameters. Image segmentation is especially important and can have massive impact on classification results (Liu, D. and Xia, F. ,2010)

3.2.7.1 Algorithm description

MRS is an iterative bottom-up multidimensional segmentation algorithm that locally optimize spatial and spectral homogeneity. MRS is a bottom-up approach because it creates objects by beginning with a single-pixel object that grows to increasingly large object. It is iterative because the object will grow up by merging multiple times with the neighbouring objects that maximize the mutual multidimensional homogeneity if the hyperparameters conditions are fulfilled. It is multidimensional because the homogeneity optimization can be done with multiple spectral layers. The optimization is spectral and spatial because the object size and shape can be optimized as well as the spectral homogeneity. The process in which objects are merged is called Local Mutual Best Fitting rule (LMBF) (Martin BAATZ and Arno SCHÄPE, no date). This process ensures that an object or a pixel merge with the surrounding pixel that minimize the mutual heterogeneity (Δh_{XY}) as show in Figure 33.

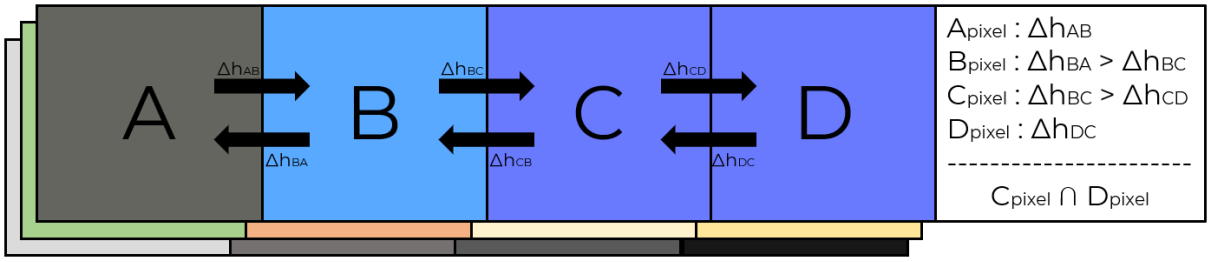

Figure 33 : *Simple example of multidimensional LMBF process pixel. C will merge with pixel D.*

The segmentation can be optimized using 3 hyperparameter: scales, shape and compactness. The different spectral layer can also be weighted regarding of their assumed segmentation importance (Aly M. El-naggar, 2018). For this study it was assumed that all the layers have the same segmentation importance. The scales parameters define the level of homogeneity wanted within the object. The smaller the scale parameter, the more homogenous the object will be. In general, small-scale parameter means also smaller objects but small objects can remain at high scale parameter value if they have a particularly rare spectral composition compared to the surrounding objects. The impact of scale parameter is illustrate in Figure 34.

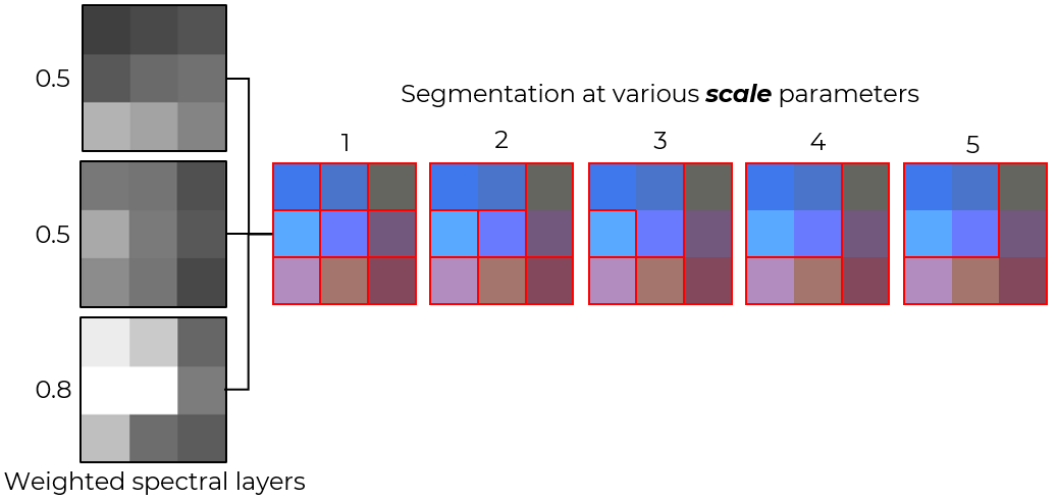

Figure 34 : *Schematic of the segmentation process at various scale values for three features. From top to bottom RVI, SARad CV$_{VH}$ and SARadCV$_{VV}$.*

The shapes parameter ranges from 0 to 0.9 and indicates how important the shape of the object will be in comparison to spectral composition. It is usually preferable having a small shape parameter if spectral composition matters (which is the case in this study) and if shape is not a crucial characteristic. A high shape parameter is useful in very high resolution where precise object with predictable shape like houses or cars can be detected, which is not the case with Sentinel-1 data in tropical context. The compactness parameters described the balance between smoothness (border length/borders) and compactness (border length/object area) in the segmentation. These parameters range from 0 to 0.9 and directly depends on the scale parameters for its relative importance in regards with spectral composition. The higher the parameter, the higher the compactness of the object will be. A high compactness value means fewer edges and a more square-like shaped objects. There is no universal best hyperparameters combination and every data set has its specific set of optimal hyperparameters. In this study, the MRS algorithm was provided by eCognition software.

3.2.7.2 Segmentation optimization

Various existing optimization method relied on already existing segment from cadastral records for example) which were not available for the ROI. The only way to optimize parameters is thus the trial-and-error method combined with theoretical consideration. First the shape parameters must be small to enhance the spectral aspects of the segmentation. Then, in regard with the irregular forest stands pixel value composition due to speckle and natural forest stands heterogeneity, it is better to have a high compactness value to prevent unrealistic object shapes. Finally, the scale parameter can be adjusted in regards with the wanted relative classification precision with the upper bound value defined as the value before which multiple training or validation samples are contained into one object (a situation to absolutely avoid). Figure 35 shows how drastically segmentation and thus classification can be changed by modifying hyperparameters.

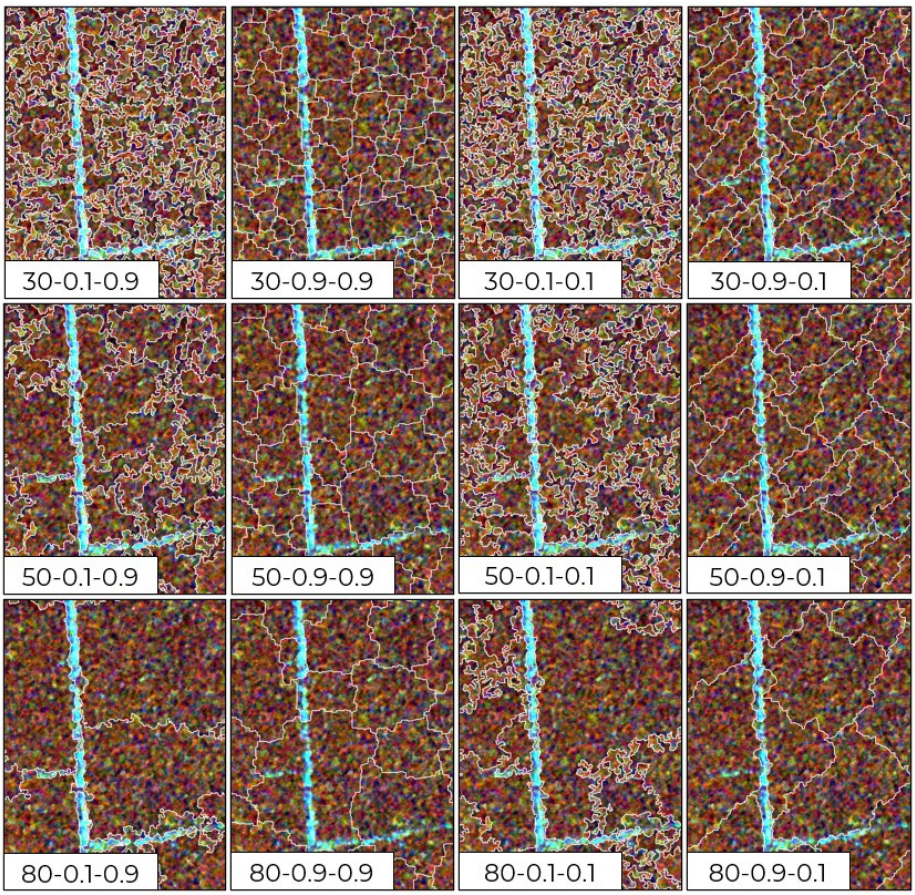

Figure 35 : *Various segmentations on a colour composite (RVI, SARadCV$_{VH}$ and SARadCV$_{VV}$). The hyperparameters are respectively scale, shape, and compactness.*

3.2.8 Classification

There is three ways to improve classification: by developing and optimizing classification algorithms, by improving the training samples and by improving input data quality and number. In this study the main effort consist in the optimization of dataset input. The classification algorithm for both PBIA and OBIA approach was Random Forest. The MRS "Shape" and "Compactness" hyperparameters were optimize for each dataset using the trial-and-error method. The following sections described the different classification scenarios computed.

3.2.8.1 Non textural Dataset collection

Five different non-textural datasets were used as classification input. Each scenario differs in terms of dataset input or classification approach. The dataset composition can be seen in the Figure 36. The first data set called "Basic" is composed of twenty SAR features including standard deviation, mean, CV and median for each polarization and both for long time series coherence and amplitude data. The second dataset called "SARad" consist in 16 "B" derived features that have all been divided by (MeanVV + MeanVH). The third dataset is called "A" and is the merging of the first and the second dataset. The fourth dataset called "Best features" contains the six features that have the best explicative power during the first classification. Finally, the fifth dataset called "S" the three selected features used for sampling (RVI and SARadCV for both polarization).

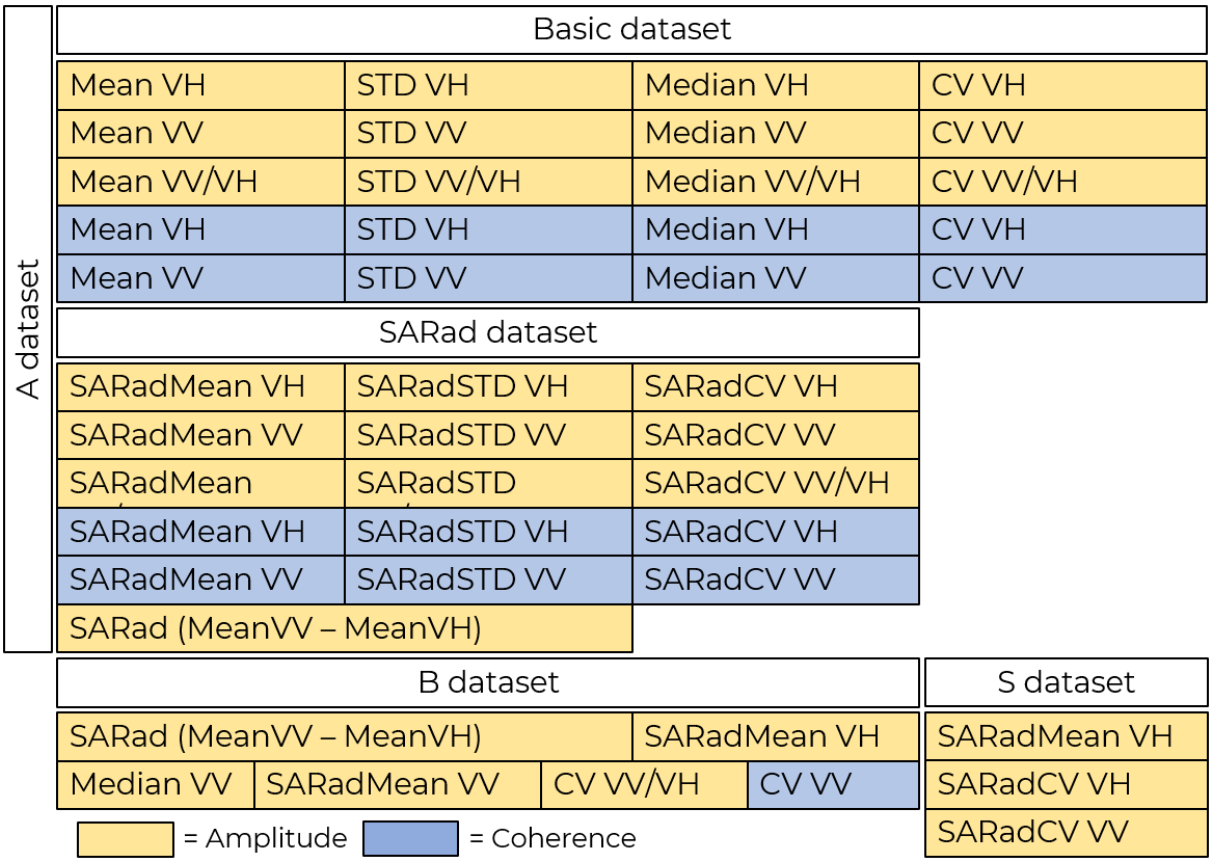

Figure 36 : *Composition of the five non-textural features dataset. "Mean VH" equals to mean values of VH polarization during a 4-year long time period", same signification for the other features.*

3.2.8.2 Textural dataset collection

Based on the S dataset, different datasets were built for each window size (radius of 2,5,10 and 20). Four datasets have been made for each radius values consisting of three features and containing only the mean textural features for each S features. The same have been done for all ten advanced textural features. The third dataset contains all the advanced textural features for all the S features and the four radius values. Each scenario differs in terms of dataset input or classification approach. The dataset composition can be seen in

the Figure 37. Finally, the biggest dataset contains all the textural and non-textural features and consist thus in 156 unique features.

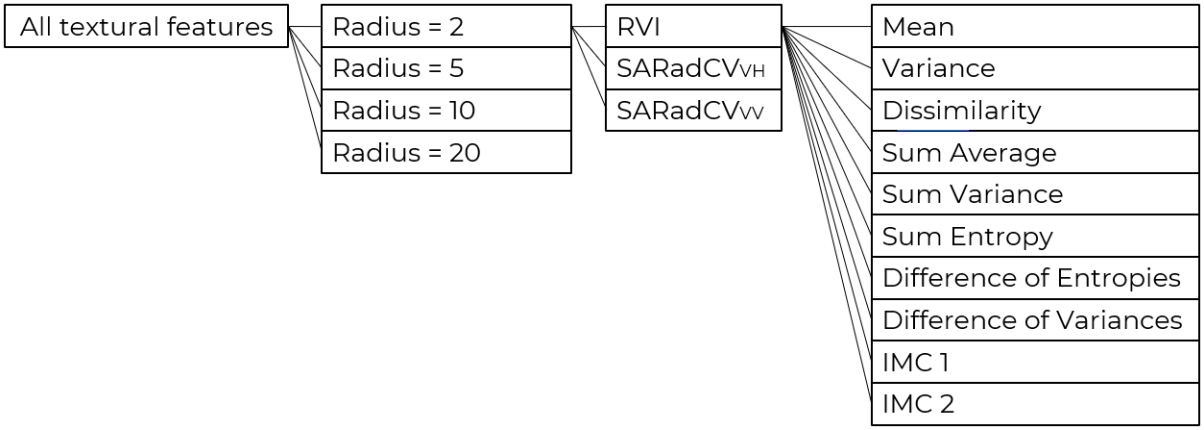

Figure 37 : *Description of the various textural features dataset*

3.2.8.3 Pixel based approach
To analyse the impact of input dataset on classification, various scenarios were computed with different dataset combinations ranging from 3 to a 156 inputs features. In addition to that, a majority filter was applied on each scenario to compare its effects in comparison with nonfiltered results. Textural features were only extracted for the non-textural features that were the best at segmenting the ROI in the OBAI approach. In addition to a comparison between 1 and 10 textural features per non-textural input features it was also chosen to analyse the results when textural features with various window sizes are used in the same classification.

The Random Forest algorithm was parametrized with the default parameter of the RandomForestClassifier algorithm from the scikit-learn library, except for the number of trees that was set at 150 and the maximum number of levels in each decision tree set at 30.

3.2.8.4 OBIA approach
Because each dataset has its optimal set of segmentation hyperparameter, it was considered a to much time-consuming approach to optimize hyperparameter for all the datasets. So only two datasets were optimized and compared with trial-and-error method. It is the S dataset and its non-modified twins from the Basic dataset (MeanVH and CV for VH and VH polarization). For the classification input data, it was chosen to use the best input dataset from the pixel-based approach. The set of hyperparameter for S and Basic segmentation dataset were respectively 70 and 50 for scale, 0.2 and 0.3 for shape and finally 0.8 and 0.9 for compactness. Various scale parameters were evaluated (30, 40, 50, 70, 90 and 110) to analyse the effect of segmentation hyperparameters on the classification accuracy. The ten advanced textural features were computed for each object and for each input features in all of the OBAI scenarios.

The Random Forest algorithm was parametrized with the default parameter from *eCognition* software excepted for the number of trees that was set at 150 and the maximum number of levels in each decision tree set at 30.

3.2.8.5 Scenario summary
A total of twenty-eight scenarios were evaluated. The two main criterium used to distinguish each scenario are input dataset and classification approach. Each scenario was built in regards with the results of the previous one, beginning with the PA scenario (all non-textural features as input for a pixel-based classification) and ending with the various object-based scenarios. The main goal was to brush an overall set of data combinations and classification approach to identify the strength and weaknesses of each approach. Scenarios are named and described in Figure 38.

Pixel based non-textural features	n	Pixel based textural features	n	Object based	n
PBASIC	20	PT20_Mean	3	OS_S_SEG30 + T	36
PBASIC_M	20	PT10_Mean	3	OS_S_SEG40 + T	36
PSARad	16	PT5_Mean	3	OS_S_SEG50 + T	36
PSARad_M	16	PT2_Mean	3	OS_S_SEG70 + T	36
PS	4	PT5_All	30	OS_S_SEG90 + T	36
PS_M	4	PTC(2,5,10,20)_Mean	12	OS_S_SEG110 + T	36
PA	36	PTC(2,5,10,20)_Mea_M	12	OA_S_SEG50 + T	360
PA_M	36	PTC(2,5,10,20)_All	120	OA_N_SEG100 + T	360
PB	6	PTC(2,5,10,20)_All + A	156		
PB_M	6	PTC(2,5,10)_All + A	126		

P = Pixel based approach
O = Oject based opproach
A = All computed non-textural features (36)
B = The 6 features with the highest explicative power from the A dataset (6)
S = Selected features for vizualisation [RVI, SARad CVVH, SARad CVVV] (3)
M = Majority filter
SARad = Modified features (16)
BASIC = Basic features (20)
T = Textural features for S datset
Txx = Context windows size (**x** = radius)
Mean = Mean textural feature (1)
C(x,x,x,x) = Use of multiple window sizes in one classification (**x** = radius)
All = All Haralick features (10)
n = Number of input features
SEGx = Segmenation using a **x** Scale parameter
S_SEGx = Segmentation using S features
N_SEGx = Segmentation using [VH, CV_{VH}, CV_{VV}] features

Figure 38 : *Summary of the different scenarios. The legend below the table described the abbreviation contained in each scenario's name.*

Due to the time consuming and highly subjective evaluation of the MRS performance, it was chosen not to evaluate lots of different dataset for the segmentation step. The scale parameter was stile optimized by photointerpretation. Because the MRS algorithm aims to provide a segmentation close to the one made by visual interpretation, it was chosen to use the combination of features that offers the best photointerpretation potential (dataset S = RVI, SARad CV_{VH} and SARad CV_{VV}).

3.2.9 Accuracy assessment

Due to a lack of terrain validation data the accuracy assessment can not be considered as a classic map accuracy measurement. All the results are thus related with non fully reliable validation data and must be consequently analysed. However, by comparing various scenarios, the relative accuracy of various classification method can be measured. In summary, this accuracy assessment is about asserting which methodology and which dataset provides the best classification.

To ensure faire comparison the same accuracy assessment has been conducted for both pixel based and object-based approach. Accuracy assessments have been done for each level of classification and each scenario. As for training data, field validation samples were not available, so the accuracy assessment relies only on photointerpretation. The two hundred training samples were carefully selected using Planet images and previously mentioned classification. To avoid biased overall accuracies, samples were collected respecting a parity rule for all classes in each classification level (for instance there is one hundred samples of forest samples and 100 from non-forest). The used metrics are the

recall, precision, and F-score to evaluate class accuracy and the overall accuracy to evaluate an entire classification.

recall represents the proportion of well predicted samples from a class over the total number of samples from this class. Precision is the proportion of well predicted samples from a class over the total number of samples that have been predicted as being this class. F-score is the harmonic mean of recall and precision where and the. F-score can be considered as a single metric that evaluate the model performance for each class.

The overall accuracy is obtained by computing a confusion matrix. This matrix confronts the predicted classes of samples with their true respective classes. The overall accuracy is the ratio of the well classified samples (sum of matrix diagonal values) over the total number of samples. This ratio is then weighted by the proportion of samples from each class.

Chapter 4: Results and discution

This section presents the various classification results and discussions. All the scenarios will be compared and analysed, and the best methodology founded will be described in detail.

4.1 Classification results and model saturation

In Figure 26 are presented the classification results from the various scenarios described in section 3.2.8.1. All the features used in each scenario are Sentinel-1 data related and all the classification are trained and validated using the same four hundred training samples (11104 pixels) and 200 validation samples (2430 pixels).

		Pixel based classification			
	Scenarios	LEVEL 1	LEVEL 2	LEVEL 3	n
Non-textural features	PBASIC	94,3	67,7	60,0	20
	PBASIC_M	95,0	72,7	64,2	20
	PSARad	95,1	67,2	60,9	16
	PSARad_M	96,1	71,8	64,8	16
	PS	93,8	58,9	54,3	4
	PS_M	96,2	65,5	60,5	4
	PA	94,7	69,6	62,6	36
	PA_M	95,5	73,5	66,9	36
	PB	91,2	62,1	57,9	6
	PB_M	93,0	67,6	63,6	6
Textural features	PT20_Mean	95,6	54,8	50,0	3
	PT10_Mean	98,5	74,9	69,5	3
	PT5_Mean	98,2	74.12	71,5	3
	PT2_Mean	96,4	67,9	64,5	3
	PT5_All	96,4	74,3	71,9	30
	PTC(2,5,10,20)_Mean	98,2	82,6	80,0	12
	PTC(2,5,10,20)_Mean_M	98,0	79,9	77,8	12
	PTC(2,5,10,20)_All	98,5	83,7	80,9	120
	PTC(2,5,10,20)_All + A	98,5	85,0	81,9	156
	PTC(2,5,10)_All + A	98,4	85,2	81,6	126

	Object based classification			
Scenarios	LEVEL 1	LEVEL 2	LEVEL 3	n
OS_S_SEG30 + T	97,1	82,1	76,8	36
OS_S_SEG40 + T	97,5	83,9	78,2	36
OS_S_SEG50 + T	98,5	88,9	78,3	36
OS_S_SEG70 + T	98,4	88,9	81,3	36
OS_S_SEG90 + T	98,1	83,1	71,0	36
OS_S_SEG110 + T	98,0	81,6	71,6	36
OA_S_SEG50 + T	97,8	86,5	77,6	360
OA_N_SEG100 + T	96,6	83,7	70,4	360

First relative best result per methodology
Second relative best result per methodology
Third relative best result per methodology

P = Pixel based approach
O = Oject based opproach
A = All computed non-textural features (36)
B = The 6 features with the highest explicative power from A (6)
S = Selected features for vizualisation [RVI, SARad CVVH, SARad CVVV] (4)
M = Majority filter
SARad = SARad features (16)
BASIC = Basic features (20)
T = Textural features for RVI, SARadCV for VH and VV
Txx = xx are the context windows size
Mean = Mean textural feature (1)
C(x,x,x,x) = Use of multiple window sizes in one classification (x = radius)
All = All Haralick features (10)
n = Number of input features
SEGx = Segmenation using a x Scale parameter
S_SEGx = Segmentation using RVI, SARadCV for VH and VV features
N_SEGx = Segmentation using VH, CV for VH and VV features

Figure 39 : *Recapitulative table of the overall accuracy from all the scenarios computed. The acronyms used are described in the bottom right corner.*

We can see that the increasing number of input features increase the OA to a certain point. However, as demonstrate by Audreye and al. (2019) when reaching a certain number of input features, the OA do not increase with the number of input feature anymore.

In fact, if a feature is already the best to discriminate a class from another in a decision tree, adding more feature from lower explicative power for that class will not change the classification. This has two consequences. First if the number of features is large enough, there cannot be misleading features. Then there is a number of input features from which it is not necessary to add more features to the model. The caricatural example is illustrated by comparing the PTC(2,5,10,20) 12 features scenario with the PTC(2,5,10,20)_All+A 156 scenario. The addition of 144 features did not significantly change the classification results.

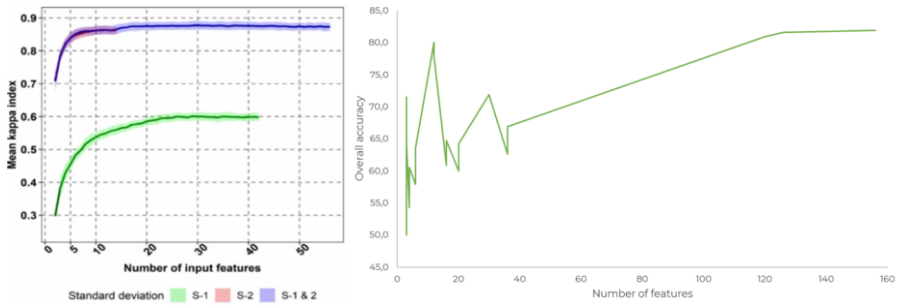

Figure 40 : *Illustration of the model saturation by Audreye and al. (2019) study on the left and from this study on the right.*

4.2 Forest-mask and comparison with optical classification

The LEVEL 1 which consists in a forest-mask classification discriminates efficiently forest and non forest in regards with the overall accuracy obtained which ranges from 90% for the PBM scenario to 98.5% for the OS_S_SEG70+T and the PTC(2,5,10,20)_All+A scenario. It was showed that adding textural features increase the OA of a forest=mask in tropical area (Pulella .al, 2020). This conclusion is confirmed in this study where the OA increase by 2 or 3% when adding textural features to the classification. A more detailed analyse of the respective F-score reveals that all the forest where well predicted (recall = 1) but some non-forest areas were classified as forest (Precision = 0.97). Those promising results must be carefully analysed regarding of the small number and quality of the validation data. In Figure 41 we can see that even with comparable OA the look each classification method is strongly different. We can conclude that the Level 1 classification can be well achieved almost evenly regardeless of the input dataset.

To ensure a stronger validation, both OBIA and PBIA best classifications were compared with the deforestation map coming from (Vancustem .al, 2020) and the one from (J. Dalimier, 2022). We can see on Figure 41 the comparison between four scenarios and the two classifications previously mentioned. An OA analysis was conducted taking the JRC_TMF classification as validation data. The OA from all the classification evaluated were around 94%. However, with a recall of 75% and a precision of 65%, we can conclude that the model tends to overestimate the non-forest area even if most of the actual non-forest area is well predicted. The misclassified forest areas are small roads and logging path. The overestimation of non-forest areas can be caused by several reasons. Firstly, the higher resolution of Sentinel-1 in comparison with Landsat imagery allows the detection of numerous smaller non-forest areas. Secondly the use of textural features in PBIA create buffer around classes which tends to let the non-forest areas appear bigger than they truly are. That explains why roads, river and deforested areas are bigger in PBIA than in the JRC_TMF classification. Thirdly in OBIA there is no buffer effect but the trade of between maximizing the heterogeneity between the classes and maximizing the homogeneity within class lead to a choice of scale parameter value that is good for forest type classification but that is not intended to keep deforested object small as it should be but in contrary tends to increase the size of those objects and thus making them bigger than they are. The best scenario using JRC_TMF as validation data is the PT5_Mean scenario.

Another forest-mask evaluation was conducted by comparing the recent deforestation occurring between 2017 and 2020 for both JRC_TMF and the best forest masks computed in this study. The forest-mask with the highest OA, precision and recall cam from the PT5_Mean scenario. To do that, all the non-forest areas detected by JRC_TMF classification in 2016 were removed from both 2020 forest-mask classification. The OA analysis using the recent JRC_TFM deforestation detection as validation data reveals an OA of 96%. The recall and the precision for the deforestation class are respectively 76% and 26% and for the forest class it was 97% and 98%. We can conclude again that the classification produced in this study tends to overestimate deforested areas even if a lot of actual deforested areas are well predicted. Part of the misclassification can also be imputed to input data which are only optical for JRC_TMF and only radar for this study. In Figure 42 we can see the differences between JRC_TMF and PT5_Mean classification scenario for various deforestation hotspots. JRC_TMF data detected a net deforestation of 1.825% in a 4-year period when PT5_mean detected a net deforestation of 4.075%.

Even with speckle, SAR-C backscattering signal are purely defined by the remote sensed entity physical properties. But by including textural features to the classification process, we start to shift away from a pure physical classification. In fact, the buffer effect and the loss of resolution induced by PBIA textural features can transform the classification into a middle resolution deforestation-hotspot map. When it comes to forest-mask it is thus difficult to select the best forest-mask based on OA and F-score analysis. However, the classification with the best non-forest class precision and recall when compared to JRC_TMF classification was the scenario PT5_Mean for both forest-mask and recent deforestation maps.

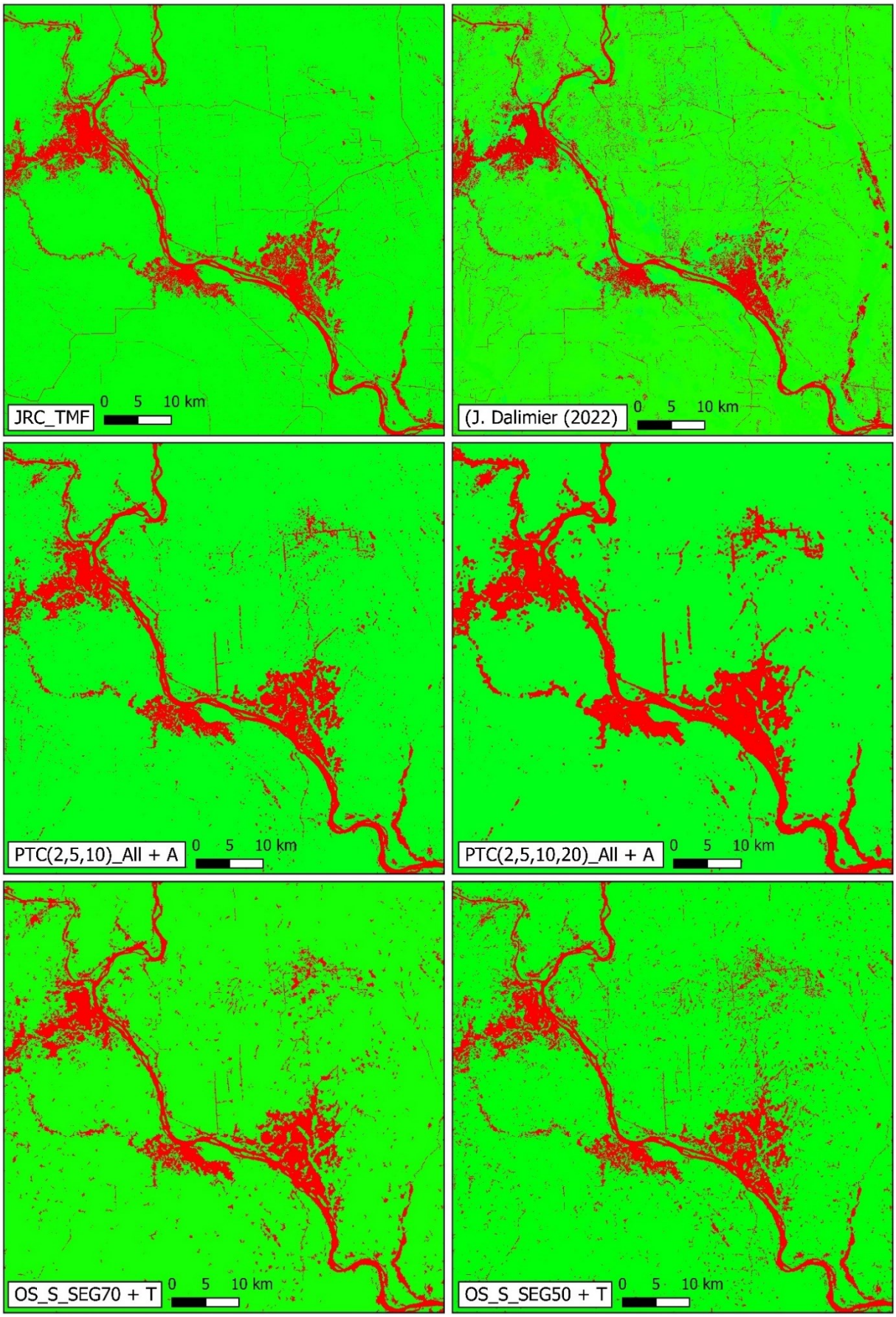

Figure 41 : *Comparison between JRC_TMF, (J. Dalimier, 2022) classification and the best produced forest-mask. The forest areas are in green and the non-forest areas are in red.*

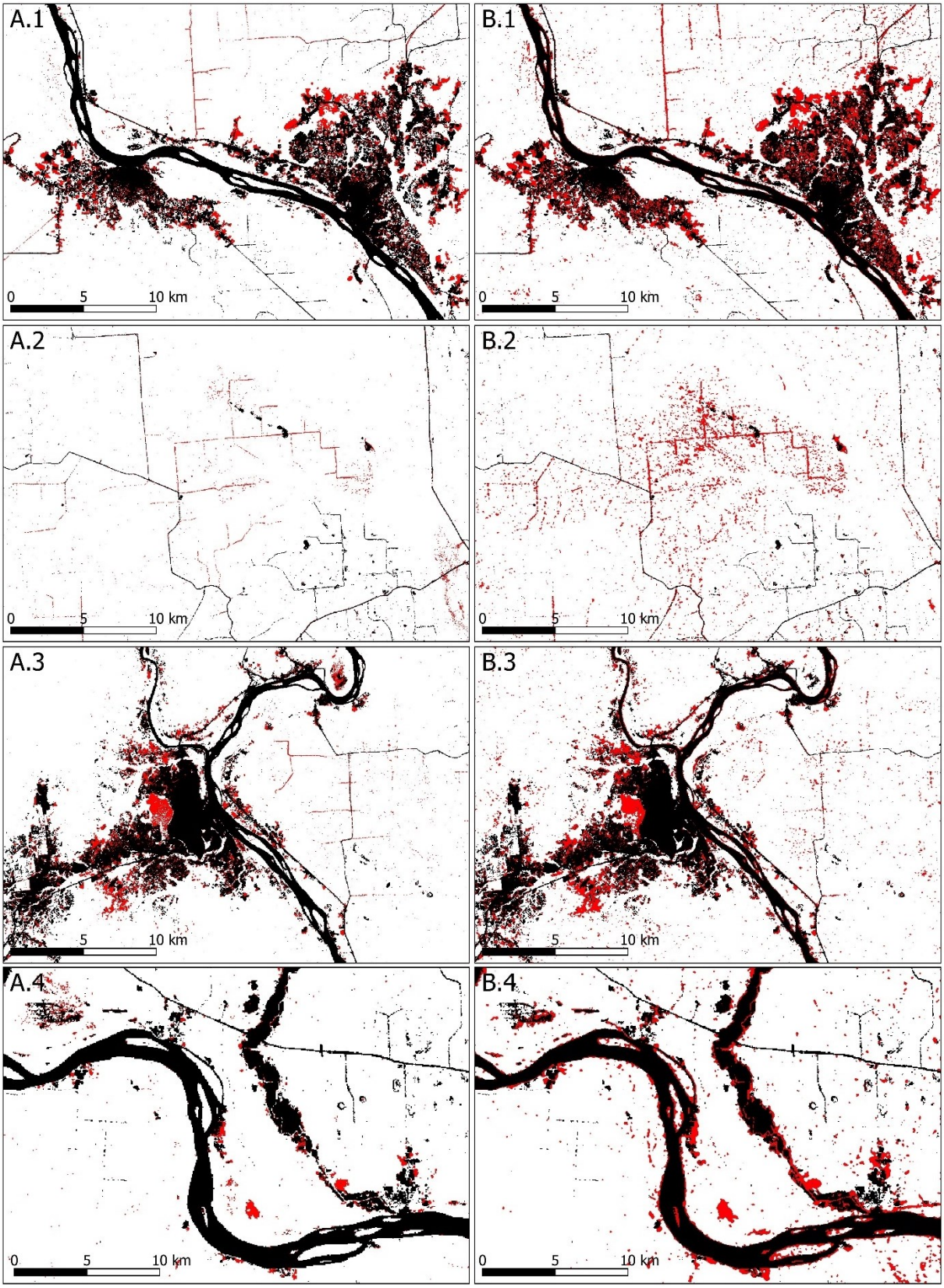

Figure 42 : *Comparison of the deforestation that happened between 2017 and 2020 (red) for A) JRC_TMF classification and B) PT5_Mean scenario classification. Non-forest areas before 2017 (black) and forest areas (white). 1. Pokola and its surroundings. 2. An area that encountered a brief deforestation event during the year 2018. 3. Ouésso and its surroundings. 4. Junction between the Sangha and the Ndoki river south of Pokola.*

4.3 Forest type and land cover classification (Level 3)

The classification consists in a complete forest type (6 classes) and land cover (10 classes) classification.

	LEVEL 3 best scenario F-score [%]					
Land cover and forest type classes	PA	PAM	PT5_Maen	PTC(2,5,10,20)_Mean	PTC(2,5,10,20)_All + A	OS_S_SEG70 + T
High urban density	94	94	82	80	67	90
Bare soil	59	65	61	68	68	55
Low urban density	79	82	51	70	89	74
Sparse vegetation	72	80	98	98	91	96
Crops and early regrowth	71	72	65	82	62	81
Mixed agricultural landscape	73	85	75	74	93	91
High density low vegetation	95	97	98	98	96	100
Floodable grassland	36	50	0	40	98	100
Aquatic grassland	44	49	38	25	65	82
Free water	97	98	89	91	94	97
Raphias forest	77	88	87	84	89	86
Flooded forest with mixed vegetation	33	36	61	64	72	64
Open flooded forest	29	32	49	78	77	74
Bubinga forest	0	0	58	72	72	72
Monodominant forest	27	18	62	81	82	70
Non flooded forest with mixed vegetation	53	57	70	83	85	84
Overall accuracy	62,6	66,9	71,5	80,0	81,9	81,3

Figure 43 : *F-score and OA comparison between the best scenario from each classification categories. (Level 3 = 16 classes)*

4.3.1 Non-textural PBIA approach

If we look at the non textural dataset on Figure 39 we can see that the use of both B and S dataset produce almost the same results and that the addition of the two dataset produces the best results at Level 3 classification. Nevertheless using only the 6 features from the B dataset produces results close to the one from B and S dataset which probably means that a certain number of features from the A dataset don't have a lot of explicative power or that they have the same explicative power. For this categorie of scenario, the application of a majority filter increasses the overall accuracy from 4 to 6 %. In general with only non textural input features, all the forest classes are poorly classified as shown in Figure 43 with the exception of Raphias forest. Contrarely non-forest classes tends to be wel classified with the exception of floodable and aquatic grass land. If we take a closer look at the classification in Figure 43 we can see that the algorithm failed to differentiate forest type probably because of the high amplitude backscattering heterogeneity within each forest class. However those scenarios helped iddentifie the best non textural dataset which is the A dataset. It will be used for the textural PBIA classification.

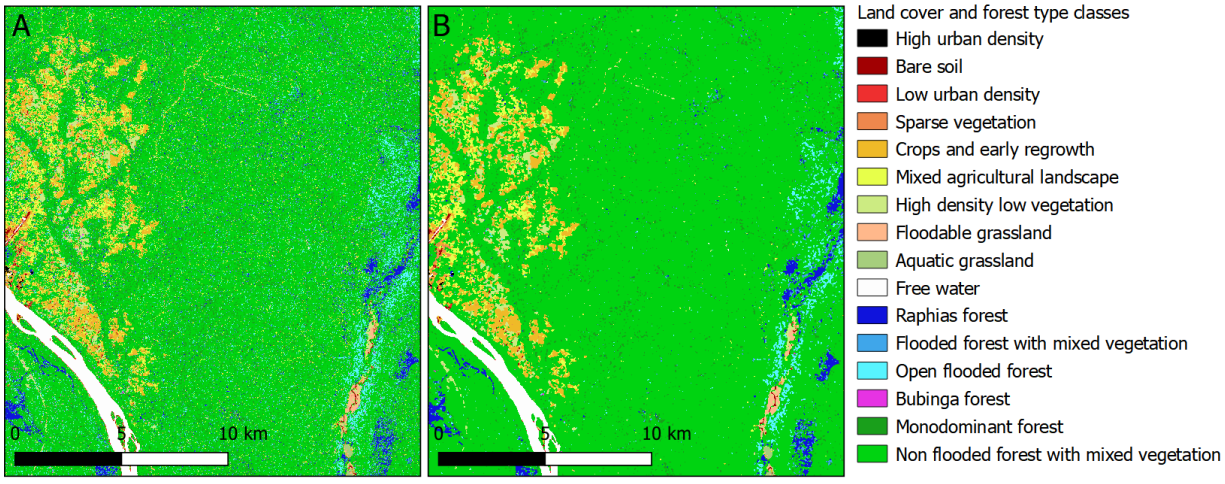

Figure 44 : *A comparison between A) PA and B) PAM classification that illustrate the effect of the majority filter on the classification rendering.*

4.3.2 OBIA approach

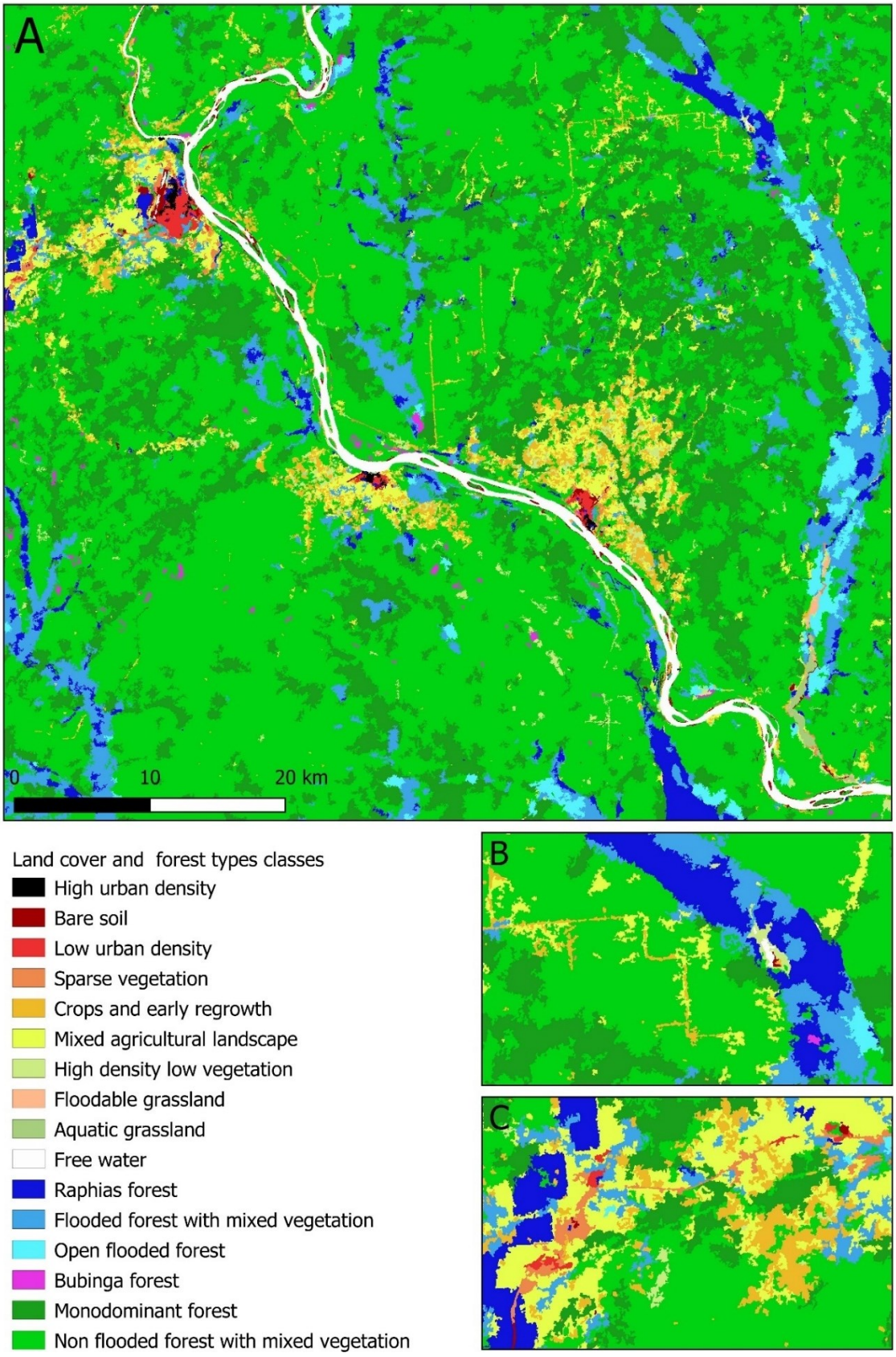

Figure 45 : *A) OS_S_SEG70 + T classification map of all ROI. B) Zoom on an old logging area close to flooded forest stands. C) Zoom on a heavy deforested area west of Ouésso.*

On Figure 39 we can see that the optimal scale parameters for the S dataset is 70 and the overall accuracy tends to decrease with the change of scale parameters. We can also see that using the A dataset produces poorer results than using the S dataset which is surprising given the results obtained in the pixel based approches. We can also see that using the Basic dataset in the segmentation process lower drastically the overall acurracy. The best OBIA results wich is also the best from all the scenarios was obtained in the scenario OS_S_SEG70+T which only use 3 non-textural and 30 textural features for an overall accuracy of 80% at Level3 and 89% at level2. This classification can be visualized in xxxxx.

Even if the OBIA approache produces the best results, this method is not without limitation. First, the fact that the segmentation must be vizualy optimized reduce the reproductability of the results even with a slightly different input dataset. In fact including in a classification process a step involving to solve visualy a multi-dimentional problem might be to difficult, subjective and hazardous to produce reproductible results. Some supervised optimisation segmentation technic exist but involved the MRS model to be trained with object the are representative of the general object shape we want create (Belgiu and al., 2014). However, those segmentation samples might be to hard to draw for a heteregenous terrain like tropical moist forest which means that a supervised segmentation is probably not possible. MRS algorithm aims to produce homogenous continuous object in very-high resolution (Belgiu and al., 2014). At 10 meter resolution and at the forest stand scale such object don't really exist which also explain why MRS fail to correctly segmented the ROI.

With OBIA come also acute loss of resolution aspecilly with high scale value (coming from a 44 000 000 pixel classification to a 17 000 object one). In this study the validation data were colected in the center of forest stands allowing the OBIA method to well classify them. However, visual analysis shows that object shapes and size don't match with the attended forest satnds and land cover rendering.

In conclusion, OBIA add more limitation and subjectivity than usefull and reproductible rendering results in Pokola's tropical moist forest context. For that reason and even if it produces the best OA results, it can not be considered as proper usefull and reproductible classification.

4.3.3 Textural PBIA approach

PBIA results tends to increas with the use of textural features. The best results using only one radius value and 3 textural features was obtained with the PT5_Mean dataset. The results tends to quickly decrease with the changes of radius values. The addition of more different textural features increases slightly the results. Combining various radius value dataset drastically increase the overall accuracy by almost 9%. Adding the non-textural features to the classification slightly increase the results. We can see that adding majority filter decrease significantely the results if we use textural dataset. The best scenario from this category which is also the best pixel based classification is the PTC(2,5,10,20)_All+A and combined all the 156 computed features. However, even if the PTC(2,5,10,20)_All+A is the best in terms of OA and F-score, it seemes that the rendering of the PTC(2,5,10)_All+A (which has almost the same accuracy metric values) is better.

4.3.4 Analysis of the best classification

Choosing wich classification is the best requier to relie not only on numerical accuracy assement. In fact in regards with the low number and low quality of validation dataset, the OA results can not be the only criterium to evaluate the classification produced in this study. In addition to that, photointerpretation was used at every class definition, sampling and segmentation steps wich allow the results to also be photointerpretable. In order to ensure a proper visual accuracy assessment, tree criterium were visualy evaluted. First the overall shape of the detected forest stands. Then the vizual proximities between the classification and the optical sources used for training and validation samples. Finally, the vizual proximities with previous classification mainly from Dalimier (2022) and Vancutsem and al., (2021).

The conclusion from the overall acurracy analysis shows that object based approchae produces the best results at Level 3 even if they are close from the best PBIA scenario. However in terms of rendering, PTC(2,5,10)_All+A classification is beter than the OBIA.

The PTC(2,5,10)_All + A scenario confusion matrix, OA and F-score are detailed in Figure 46. The normalized overall accuracy is 79%.

	1.0	2.0	3.0	4.0	5.0	6.0	7.0	8.0	9.0	10.0	11.0	12.0	13.0	14.0	15.0	16.0	Recall
1.0	78	0	8	0	24	25	0	0	0	14	0	0	0	0	0	0	52
2.0	0	95	0	0	44	0	0	0	0	8	0	0	0	0	0	0	65
3.0	0	0	132	0	8	0	9	0	0	0	0	0	0	0	0	0	89
4.0	0	12	0	116	14	0	0	0	0	0	0	0	0	0	0	0	82
5.0	0	0	0	0	149	0	0	0	0	0	0	0	0	0	24	12	81
6.0	0	0	0	0	25	123	0	0	0	0	0	0	0	0	0	0	83
7.0	0	0	0	0	0	0	145	0	0	0	0	0	0	0	0	0	100
8.0	0	0	0	0	0	0	0	25	0	0	0	0	0	0	0	0	100
9.0	0	0	0	0	13	0	0	0	12	0	0	0	0	0	0	0	48
10.0	0	0	0	0	0	0	0	0	0	145	0	0	0	0	0	0	100
11.0	0	0	0	0	0	0	0	0	0	0	145	9	0	0	0	0	94
12.0	0	0	0	0	0	0	0	0	0	0	23	95	0	0	26	0	66
13.0	0	0	0	0	0	0	0	0	0	0	0	21	100	0	0	23	69
14.0	0	0	0	0	0	0	0	0	0	0	0	0	10	13	0	0	57
15.0	0	0	0	0	0	0	0	0	0	0	0	0	0	0	253	82	76
16.0	0	0	0	0	0	0	0	0	0	0	0	0	0	0	12	358	97
Precision	100	89	94	100	54	83	94	100	100	87	86	76	91	100	80	75	Overall accuracy
F-score	69	75	91	90	65	83	97	100	65	93	90	71	79	72	78	85	82

High urban density	1.0
Bare soil	2.0
Low urban density	3.0
Sparse vegetation	4.0
Crops and early regrowth	5.0
Mixed agricultural landscape	6.0
High density low vegetation	7.0
Floodable grassland	8.0
Aquatic grassland	9.0
Free water	10.0
Raphias forest	11.0
Flooded forest with mixed vegetation	12.0
Open flooded forest	13.0
Bubinga forest	14.0
Monodominant forest	15.0
Non flooded forest with mixed vegetation	16.0

Figure 46 : *Recapitulative table of the Precision, Recall, Overall accuracy, and F-score for the PTC52,5,10)_All+A scenario.*

The following pages described in detail the classification achievements and limitation by zooming on specific areas.

4.3.5.1 Flooded forest

With a general F-score of 79, a recall of 72 and a precision of 88, we can consider that flooded forests were well classified. With no surprise, the main misclassifications happen between the several types of flooded forest because of high proximity in terms of forest architectures and species composition. Still some misclassifications happen between flooded forest and non flooded forest at the river edges but also in the semi-deciduous forest. In fact, we can see in Figure 47 that small patches of flooded forest remain in the centre of semi-deciduous stands and sometimes on the high grounds where it is very unlikely to find flooded forest. The backscattering proximity between Flooded Forest with mixed vegetation and the monodominant forest might be caused by the fact that some of those monodominant forests are also floodable and thus are submitted to the same seasonal hydric regimes. In Figure 47 we can see that palm oil plantations are classified as Raphia forest highlighting the low canopy penetration depth of SAR-C signal who is no able to detect the surface water beneath the canopy. The bubinga forest class tends to be overestimate even if its F-score is 72. This good F-score is due to the lack of available validation data which do not offer a proper representative analysis. This class tend to visually confuse with the High-density low vegetation class.

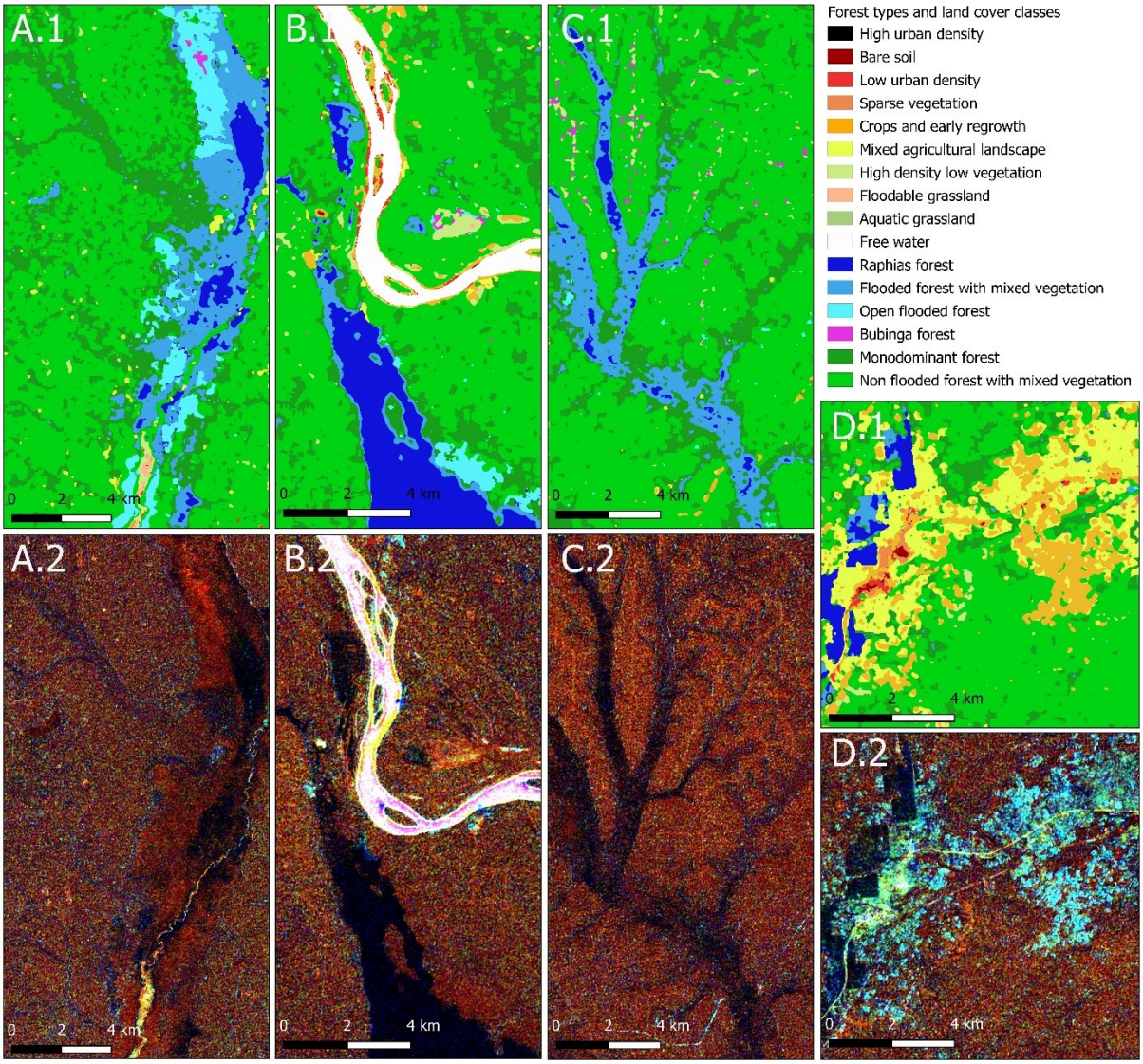

Figure 47 : *Example of predicted flooded forest. A) Around the Ndoki river. B) Big Raphia forest along the Boumbala river. C) Around the Kandeko river. D) Palm oil plantation west of Ouésso. 1. PTC(2,5,10)_All + A classification. 2. Colour composite [RVI, SARad CVVH, SARad CVVV].*

4.3.5.2 Monodominant forest

With a general F-score of 78, a recall of 76 and a precision of 80, we can consider that monodominant forests were well classified. Figure 48 shows that Monodominant Forest can be found in various hydric conditions along river, in wetland, in high grounds or near cities. In addition to the buffer effect previously mentioned, Figure 48 highlight another PBIA textural effect. This effect tends to create square-like forest stands shapes at large scale. That effect is due to the square GLCM computation window and the lack of transition class. The main misclassifications confusion happens with the Semi-deciduous forest class because of the previously mentioned effect and their backscattering proximity.

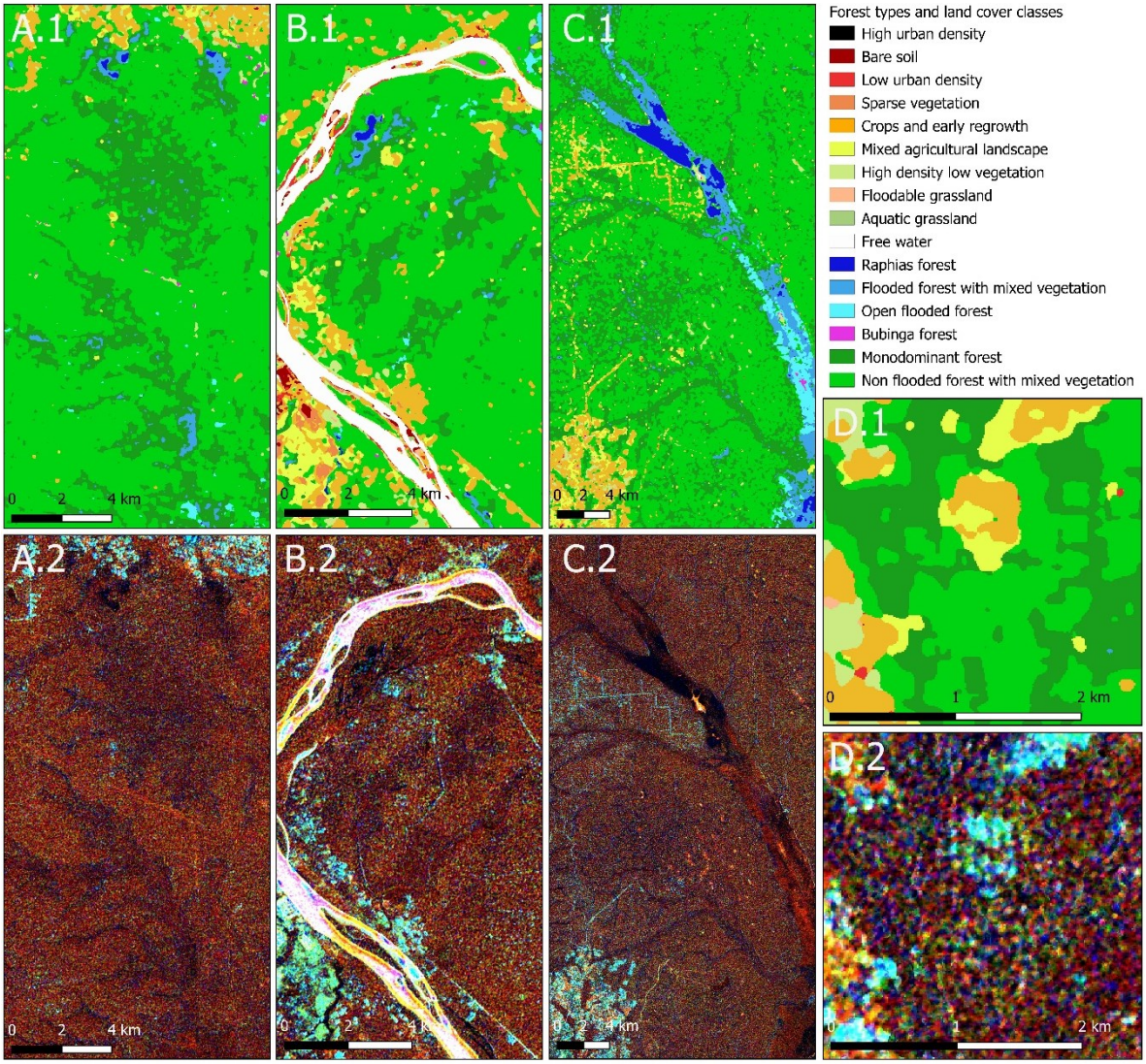

Figure 48 : *Example of predicted monodominant forest. A) around Boumbala river. B) On a high ground near Sangha River east of Ouésso. C) Around the Djaka river tributaries. D) Square shape forest stands caused using textural features. 1. PTC(2,5,10)_All + A classification. 2. Colour composite [RVI, SARad CVVH, SARad CVVV].*

4.3.5.3 Non-flooded non forest areas

With a general F-score of 89, a recall of 83 and a precision of 96, we can consider that non-flooded non forest areas were well classified. However, in Figure 49 we can see some misclassification. First the river sides are mostly misclassified with artificial areas. Those classification errors are due to the high specular reflection of both land cover. On the opposite, some urban areas are for the same reason classified into water. In Figure 49 we can see an obvious case of the negative buffer effect happening around a body of water. The model predicts well most of the classes surrounding the water but when it tries to classify pixels that are in the transition between Marantacea and Raphia stands, it classifies them into the closest class which is semi-deciduous forest instead of another transition class which do not exist.

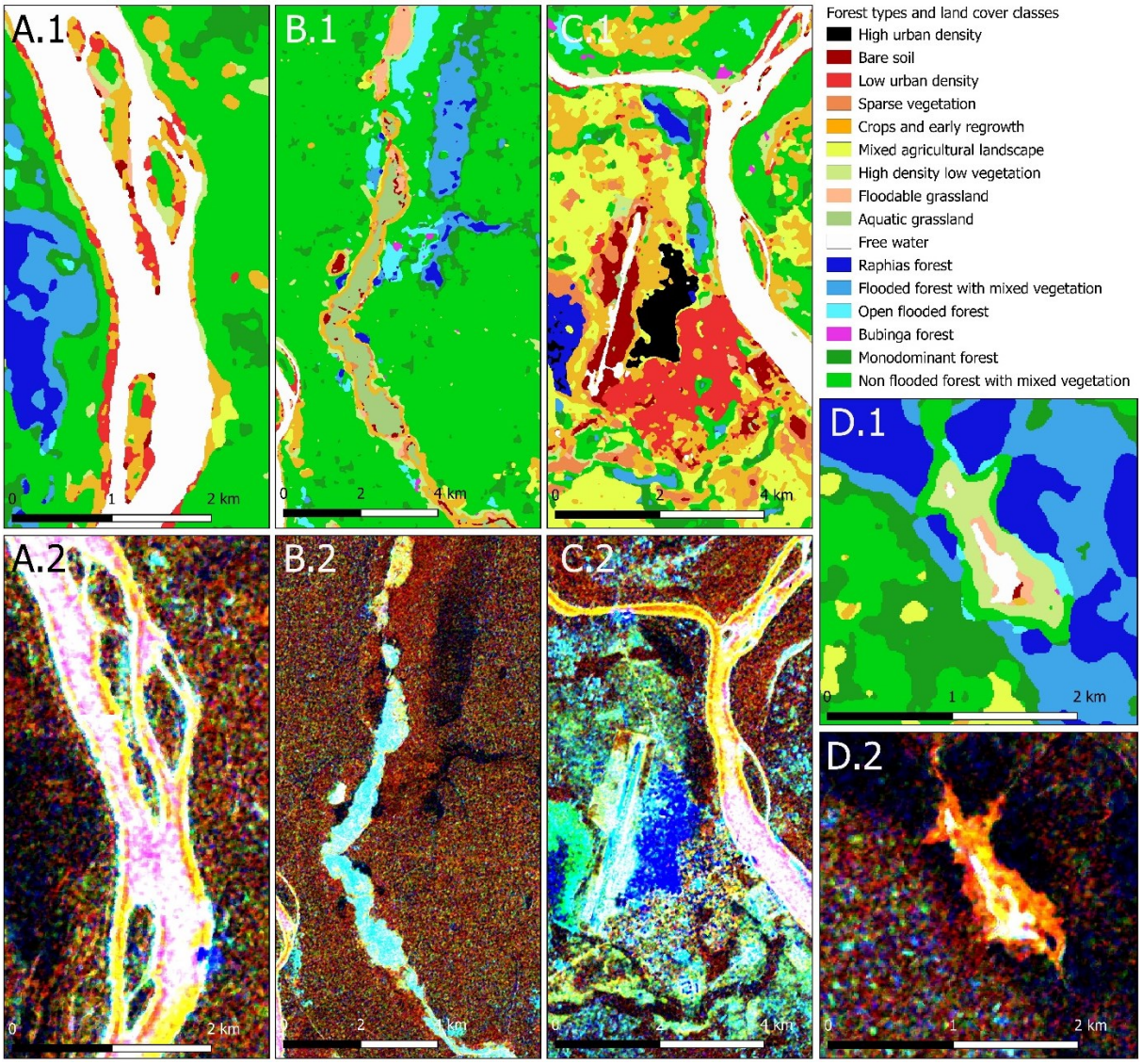

Figure 49 : *Example of predicted non-flooded non-forest area. A) River island and sandbank on the Sangha River. B) Aquatic grassland on the Ndoki river. C) Misclassification of the Ouésso's airfield. D) Typical case of misclassification at the class borders. In this case around a water body on the Djaka Rive. 1. PTC(2,5,10)_All + A classification. 2. Colour composite [RVI, SARad CVVH, SARad CVVV].*

4.3.5 Class boundaries

The object boundaries tend to be more sharp and less compact in OBIA and smoother in PBIA. This difference is caused by the tendencies of OBIA low shape parameter that create long and colour-homogenous entities which might be a wrong approach in highly heterogenous terrain like tropical forest. Textural PBIA in the other hand take the environment of each pixel into account which tends to smooth the predicted entities boundaries and produces more natural rendering forest stand edges, but it also lowers the overall classification resolution. In fact, we can see in Figure 50 that roads and other non-forest areas are disproportionately predict in regards with their true sizes. As said before this phenomenon is caused by using large windows textural feature (10 and 20 radius values) that function as a buffer around de deforested areas. Therefore, the F-score analyse shows that OBIA better predict non-forest type which are characterized by homogenous backscattering values and tends to have sharper edges. In contrary PBIA classified better forest type, those areas are characterized by higher backscattering heterogeneity and tends to have more blurred boundaries which best fits with a convolutional textural approach. Those reasons also explained why non-textural PBIA failed to rightfully predict forest classes, this method combines both weaknesses from the previously mentioned methods which are a lack of capabilities to classified object with high heterogeneity in terms of pixel value distribution and lack of capabilities to take the individual context of each pixel into account.

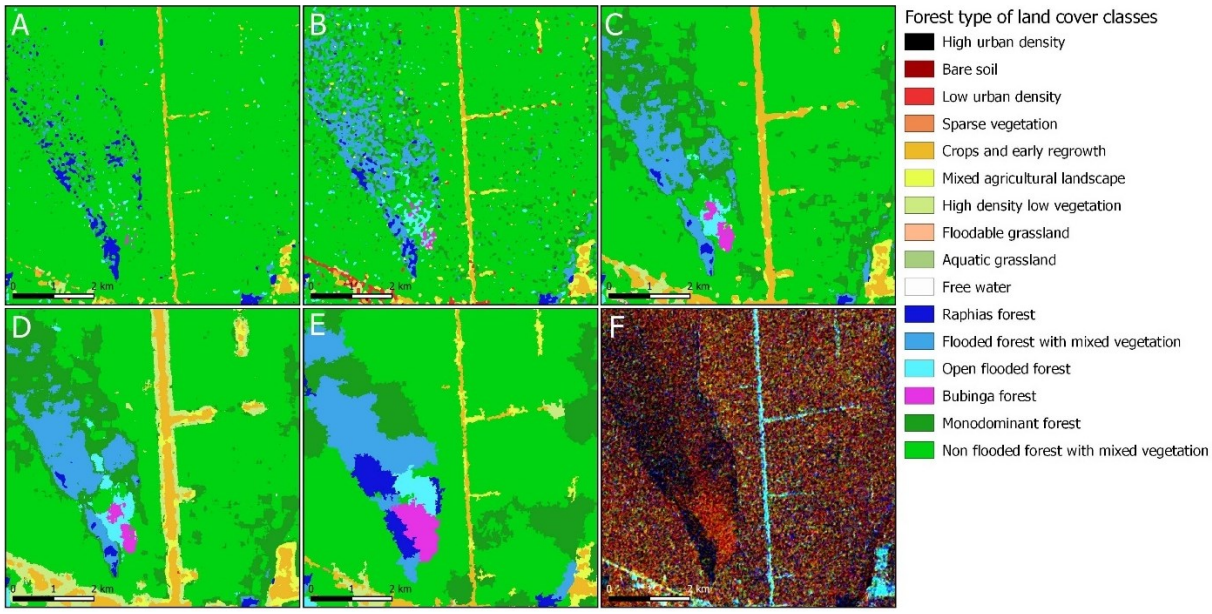

Figure 50 : *Illustration of the road size and shape for different scenarios. A) PAM. B) PT2_Mean. C) PTC(2,5,10)_All + A. D) PTC(2,5,10,20)_All + A. E) OS_S_SEG70+T. F) Color composite [RVI, SARad CV$_{VH}$, SARad CV$_{VV}$].*

The succession between permanently flooded forest and non floodable forest is a gradual process in tropical area. This transition is better represented in PBIA than in OBAI as showed in Figure 51. In fact, in PBIA we can see the succession from pure Raphia stand to mixed flooded forest and finally to flooded forest without Raphia which is more realistic than in OBIA classification where big pure Raphia stands touch big semi-deciduous forest without any transition. However, this more realistic classification is no more based on only physical backscattering properties but is due to the effect of textural features that create artificial buffer around certain classes if a transition class exist.

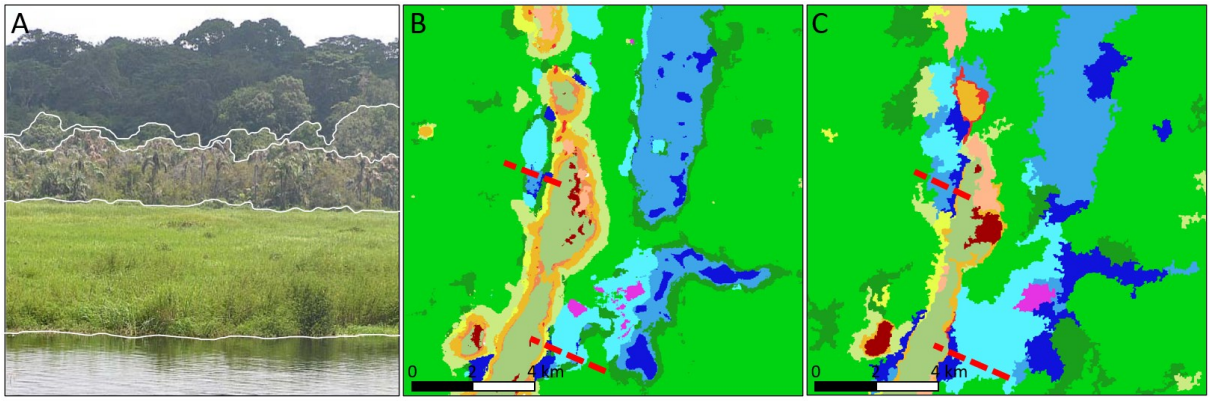

Figure 51 : *Comparison between a forest succession view and the classification around the same river. A) Plant succession photography on a bank of the Ndoki River (from bottom to up respectively the aquatic grassland, the Raphia forest with R. hookeri, H. ciliata open swamp forest and dense moist semi-deciduous forest) by Gillet (2013). B) PTC(2,5,10)_All+A classification. C) OS_S_SEG70+T classification.*

In theory those specific buffered non-forest classes areas must not occurred because all classes have their proper textural characteristics and thus their proper buffer. This abnormal situation highlights the fact that some transition classes are missing. In fact, due to lack of terrain training data and the impossibility to detect it from the various data sources, the transition classes were never defined and use in the classification. This explains why the buffer between forest and non-forest is unrealistically large. For example, when the algorithm has to chose between a pure dense forest and a non-forest area, it has no intermediate class to put the “Degraded forest” into a forest class and choose to classify it into the closest alternative which is usually “Mixed agricultural landscape” class probably due to the high tree cover of those areas which texturally speaking are a mix between dense forest and agricultural land.

4.3.6 Prediction probability map

The Radom Foret algorithm can be considered as a democratic classifier in its classification process. In fact each trees “vote” for each classes idependently from the others depending of its particular bagging output. For a given pixel, the class that received the highest number of votes becomes the predicted class. The higher the number of classes and backscattering proximity between them, the higher the votes are likely to be distpersed. The RandomForest algorithm from *scikit-learn* library offers the possibility to compute a multidimentional probability matrix that provides for a given pixel the proportion of trees that voted for each classes. By taking the higgest probabilities for all individual pixels we can produce a predict-class probability map which give the proportion of trees that actually voted for the predicted class. This map provides thus informations about the level of uncertainety of the model fore each predicted pixel and can be vizualised on Figure 53. A probalily of 1 means that all tress voted for the predicted class. A probability of 0.33 means that one third of the tress voted for the predicted class. The probability map value distribution indicates a mean certainty value of 81% which means that the model predict most of the classes with a high level of certainety.

A deep analysis of those uncertainties in Figure 52 highlit the fact that the model is particularely certain when it classify the Raphias forests (86%), water (94%) and semi-deciduous forest stands (89%). The model is also certain when it classify the center of the monodominant and the flooded forest (68%). In the other hands the model is highly uncertain at the classes borders where most of the misclassification are also located. Those uncertainteses are particularely present in the non-forest classes . This can be explained by the high degree of proximities between those classes both in terms of mean and variability of backscattering values. By vizual interpretation, the model uncertainties seems to be caused by the textural effects previously described. This map can be used as a tool for

further classification using textural features. It can be used to feed a post textural-based-classification decision tools to classified some areas based on their class predicted probabilites. By highlighting the boundaries of the forest stands as uncertain areas, this map can show where new classes are needed. It also highlight the fact that more training samples must be collected at the edges of the forest stands and land cover types to allow the model to not misclassifies those areas.

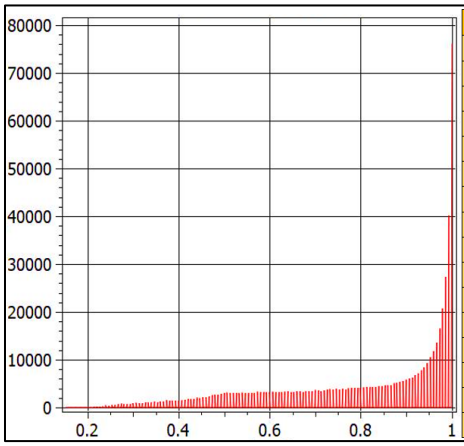

Class	Proportion of votes	Cover	F-score
High urban density	0,66	0,05%	69
Bare soil	0,49	0,13%	75
Low urban density	0,48	0,34%	91
Sparse vegetation	0,48	0,13%	90
Crops and early regrowth	0,55	4,00%	65
Mixed agricultural landscape	0,57	2,38%	83
High density low vegetation	0,54	1,47%	97
Floodable grassland	0,50	0,09%	100
Aquatic grassland	0,77	0,08%	65
Free water	0,94	1,75%	93
Raphias forest	0,86	1,17%	90
Flooded forest with mixed vegetation	0,67	3,50%	71
Open flooded forest	0,62	0,98%	79
Bubinga forest	0,49	0,17%	72
Monodominant forest	0,68	16,01%	78
Non flooded forest with mixed vegetation	0,89	67,73%	85

Figure 52 : *Pixel distribution for each level of model certainty (left). Comparison between the model certainty, percentage of land covering and the F-score for each class (right).*

The model provides results with a high certainety level. If we combine this observation with the fact that for a classification with high OA, the amount of SAR-C related features needed to achive those results are irrelevant when reaching a certain number, we can infer that adding new SAR-C related features will not drasticaly increase the results. In conclusion, the model prediction produce stable results for the given classes and features sources. Which means that in this study, the full potential of SAR-C related features have been reached and that no more relevant additional varability can be extract from SAR-C data to feed the weakclassifiers.

However, this model can be considered as a weak classifier in an inter-operator-classification that combines features from very different sources like optical or SAR-L data. This inter-operator-classification have to keep the same original classes, but can add more subclasses and new classes. That way, we can keep the full potential of SAR-C detection and combine it with the dection capabilities of other data sources.

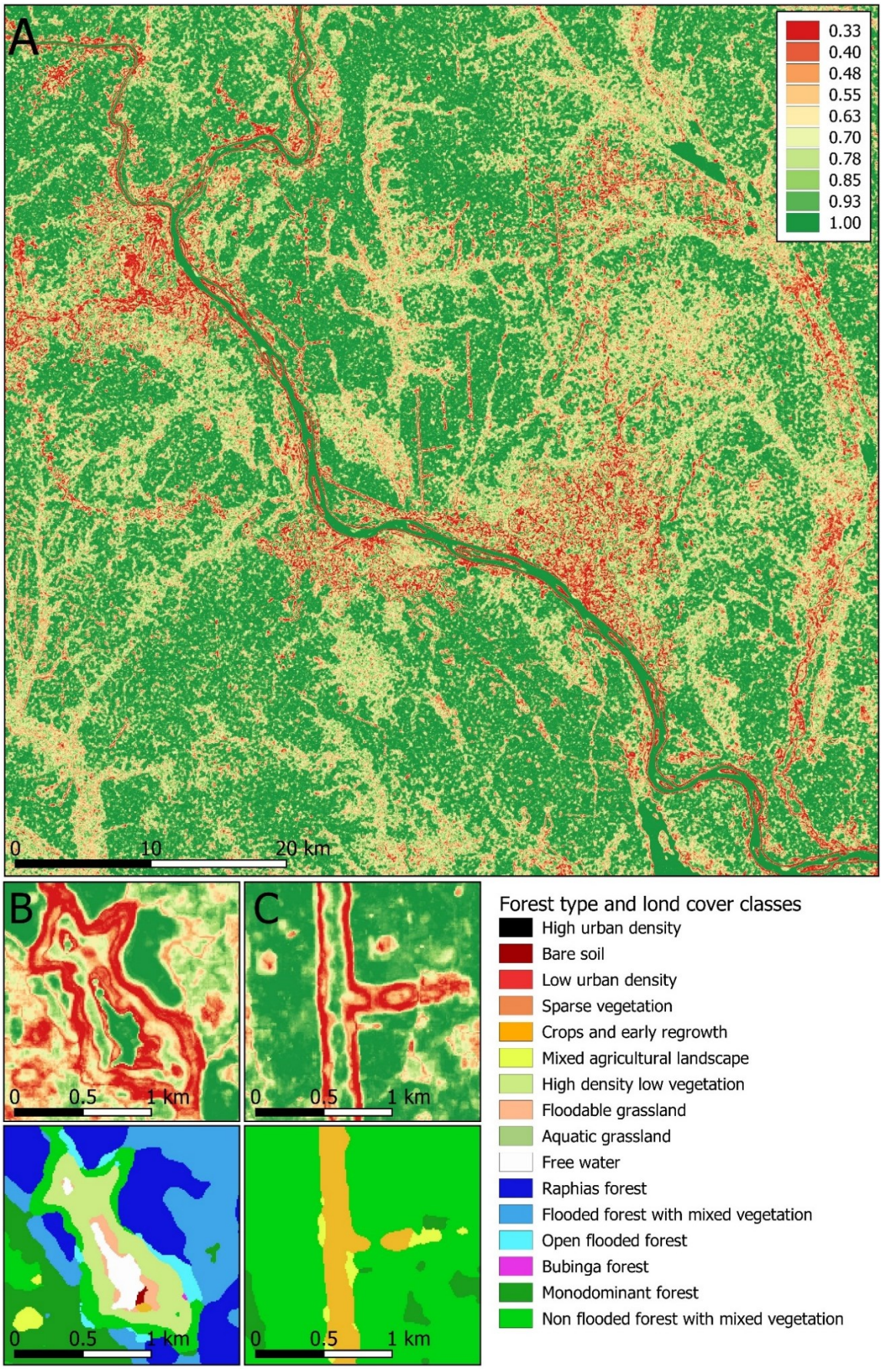

Figure 53 : *A) Probability map of the whole ROI. B) A body of water along the Djaka river. C) Recently made road west of Pokola.*

4.3.7 Complete land cover map

A complete land cover map has been produced. It contains six artificialized classes, four classes of non forest and six forest type classes. The overall accuracy is 82%.

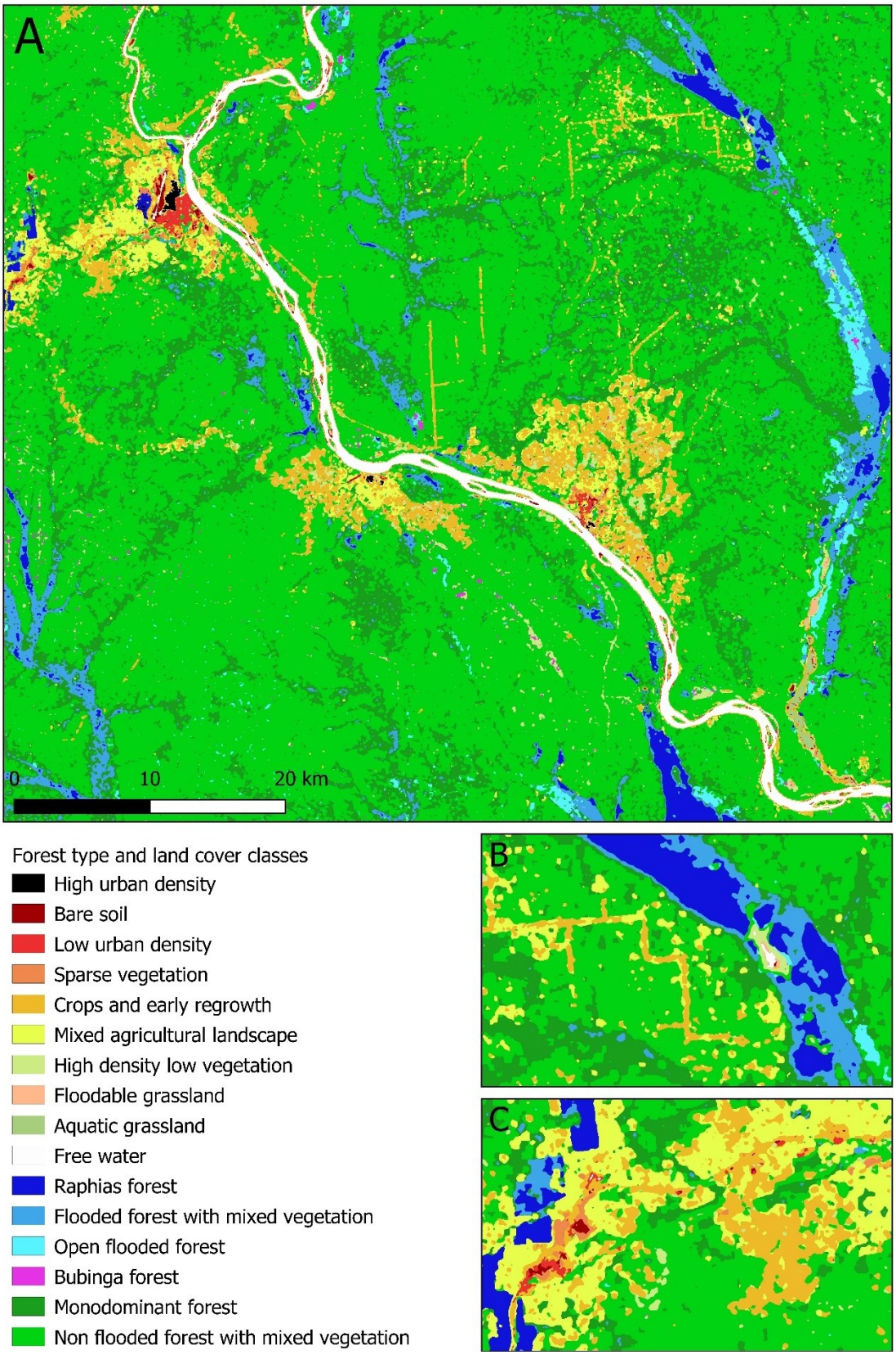

Figure 54 : *A) PTC(2,5,10)_All+A classification map of all ROI. B) Zoom on an old logging area close to flooded forest stands. C) Zoom on a heavily deforested area west of Ouésso.*

Conclusion

The objective of this thesis was to explore C-band SAR imagery for mapping in tropical forest types by remote sensing. It also aimed to test different classification methods and compare their respective results and limitations. For this purpose, more than 200 SAR-based features were computed from four years of the Sentinel-1 archive. The three classification methods that were compared are object-based, pixel-based without using textural metrics and pixel based-using textural metrics. The different models were trained using 400 training polygons collected from the photo-interpretation of optical and radar satellite images and previous classifications.

An innovative typology was created based on the OFAC classification. This was modified to better match the limited detection capability of Sentinel-1. This typology contains sixteen classes including six forest classes.

The final product of this study is a comprehensive land cover map at ten meter resolution based only on the use of SAR-C images. A map of forest cover change was also produced and was quantitatively and qualitatively compared to optical image-based classifications. Based on these maps and their validation, several conclusions can be observed, to introduce further steps.

The remote sensing community is used to finding critical the discrimination of forest types. using only Sentinel-1 images. To tackle this impasse, it appeared that taking into account the context surrounding a pixel rather than the value of that pixel produced better results. The object and texture approaches produced similar results, however it was found that the textural approach led to better performances.

Deforestation hotspot detection can also be effectively detected based on SAR-C imagery in the Pokola region although the deforested areas are overestimated compared to the recently produced forest cover change detection map based on optical imagery.

Finally, the study showed the limitations of using only SAR-C data for forest remote sensing. SAR-C data offer a limited ability to detect different forest types.

Future work in this area should therefore focus on the combined use of SAR-C data with optical or SAR-L data to refine and improve classification. It also appears crucial to rely on a field campaign allowing the acquisition of training and not rely on validation data biased by photo-interpretation.

A greater effort could be made to optimize the various algorithms and in particular to develop a supervised segmentation method for tropical forest environments.

Appendices

A1 : Various features values boxplot comparison for each class. Those values are obtained conducting a zonal statistic analysis of the 400 training polygons.

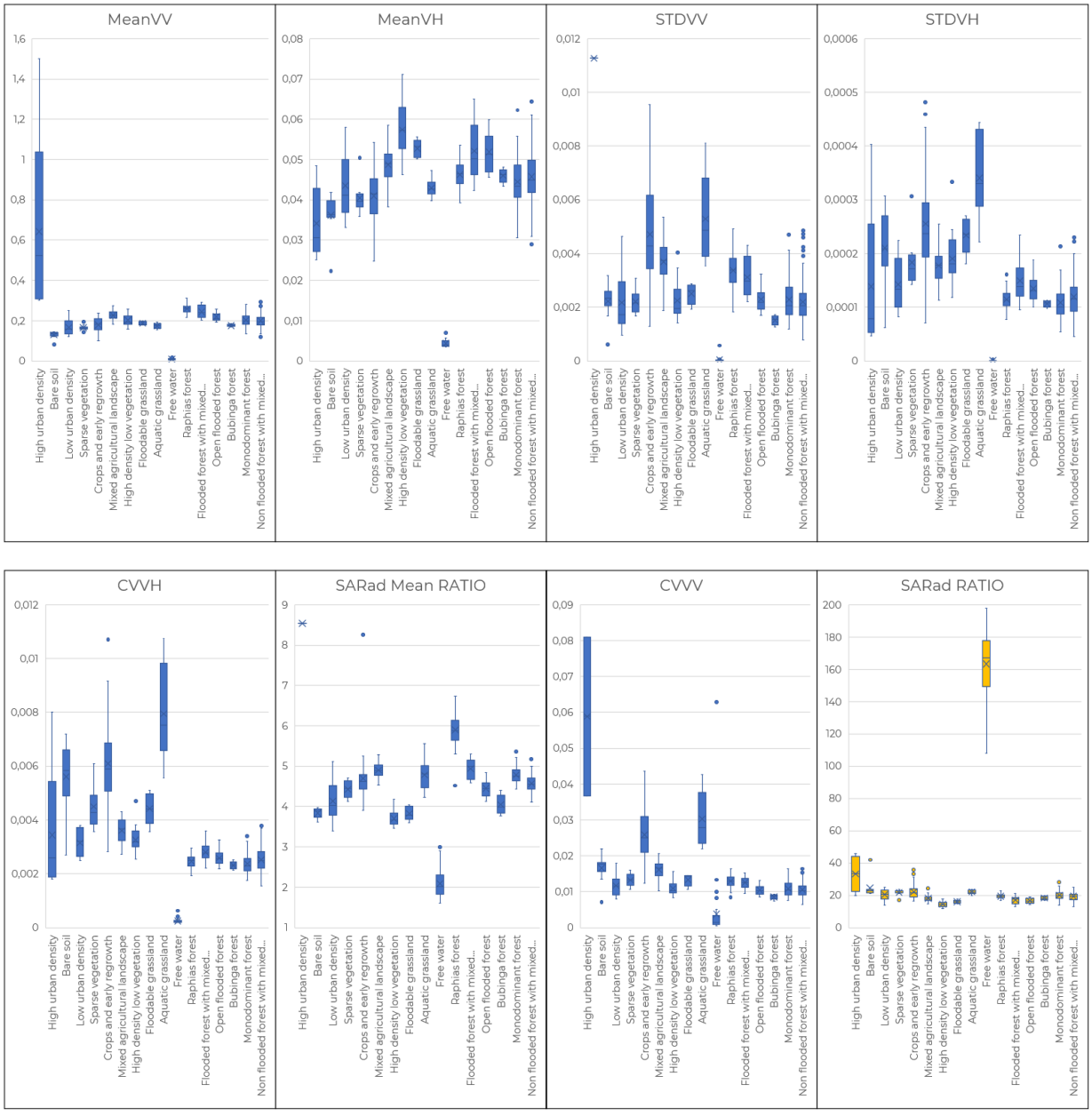

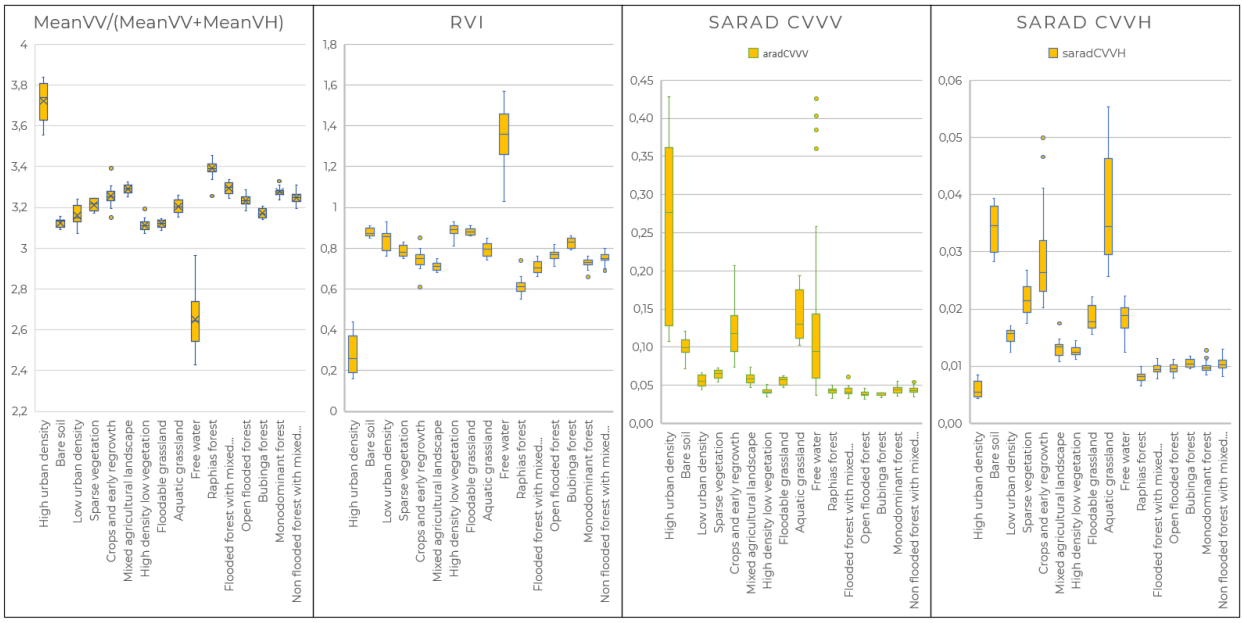
MeanVV/(MeanVV+MeanVH)
RVI
SARAD CVVV
aradCVVV
SARAD CVVH
saradCVVH
High urban density
Bare soil
Low urban density
Sparse vegetation
Crops and early regrowth
Mixed agricultural landscape
High density low vegetation
Floodable grassland
Aquatic grassland
Free water
Raphias forest
Flooded forest with mixed...
Open flooded forest
Bubinga forest
Monodominant forest
Non flooded forest with mixed...

A.2 Schematic of the OFAC official forest typology and land cover typology in central Africa (OFAC, 2022)

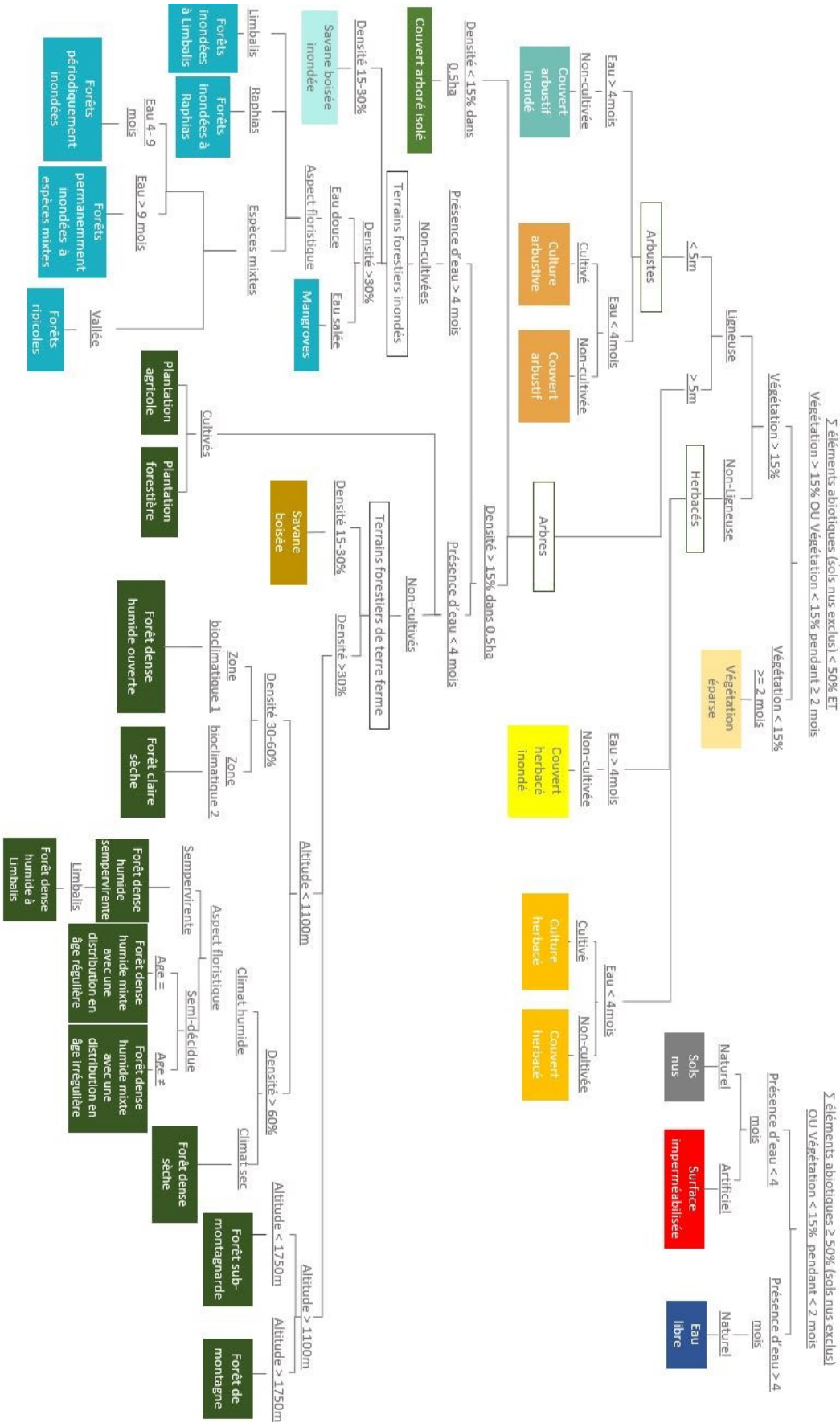

A.3 : Dalimier and al. (2022) forest type classification.

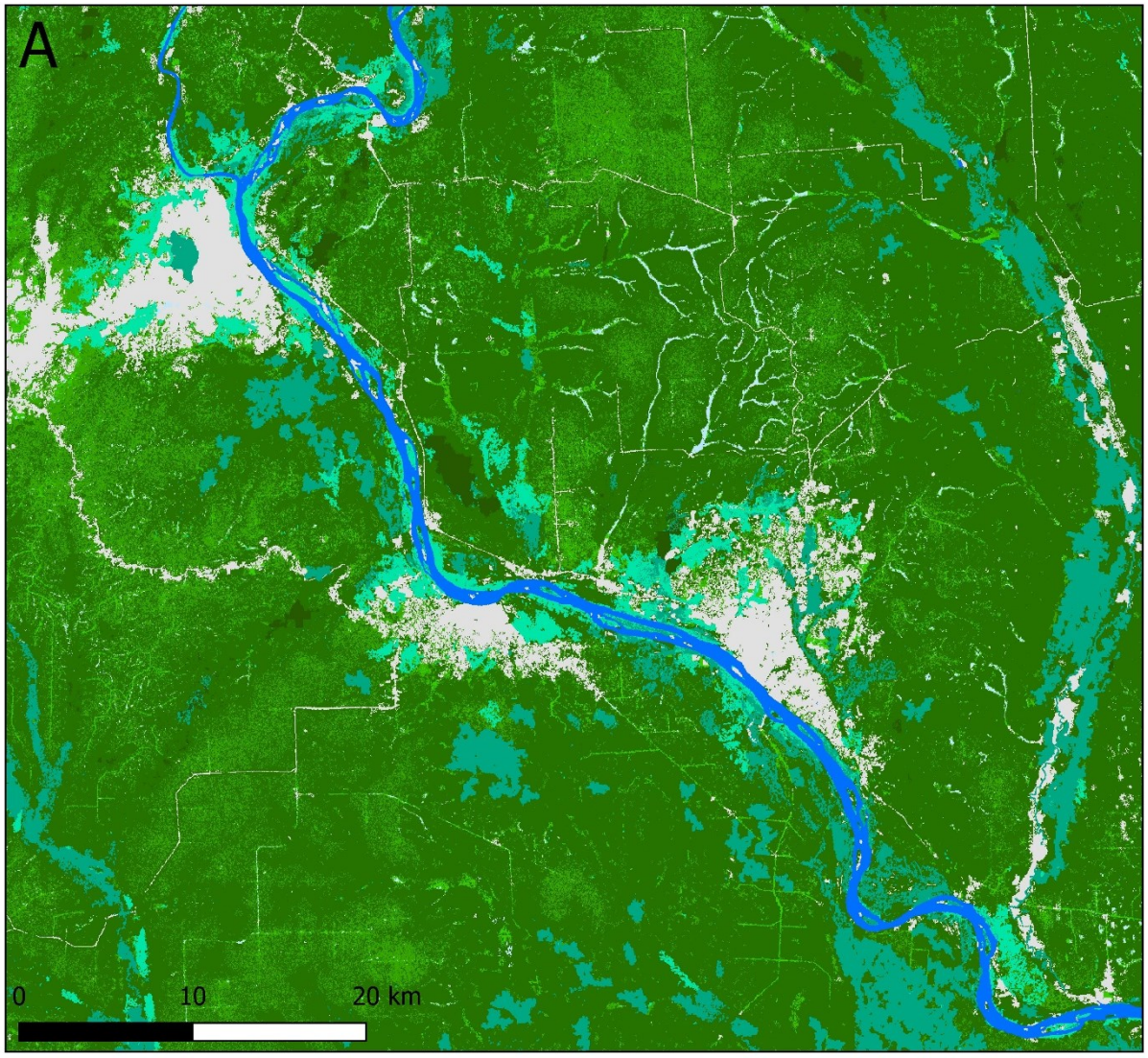

Forest type and land cover classes

- Dense monodominant evergreen forest
- Dense forest with heterogenous age distribution
- Dense forest with homogenous age distribution
- Open dense forest
- Permanentely flooded forest
- Periodically flooded forest
- Aquatic grassland
- Water
- Urban

Source : Dalimier and al. (2022)

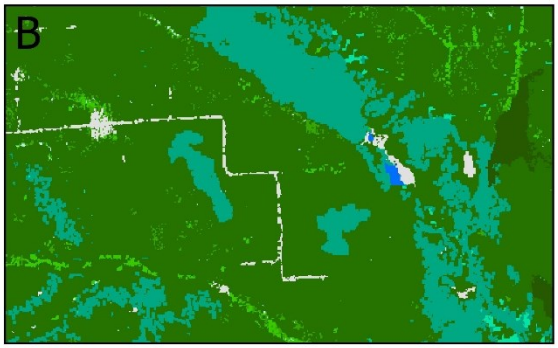

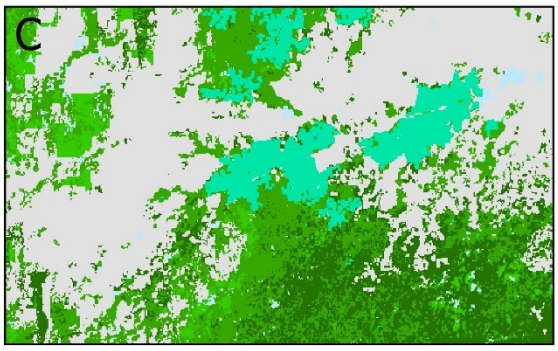

A.4 : Vancutsem and al. (2021) forest cover classification for 2020.

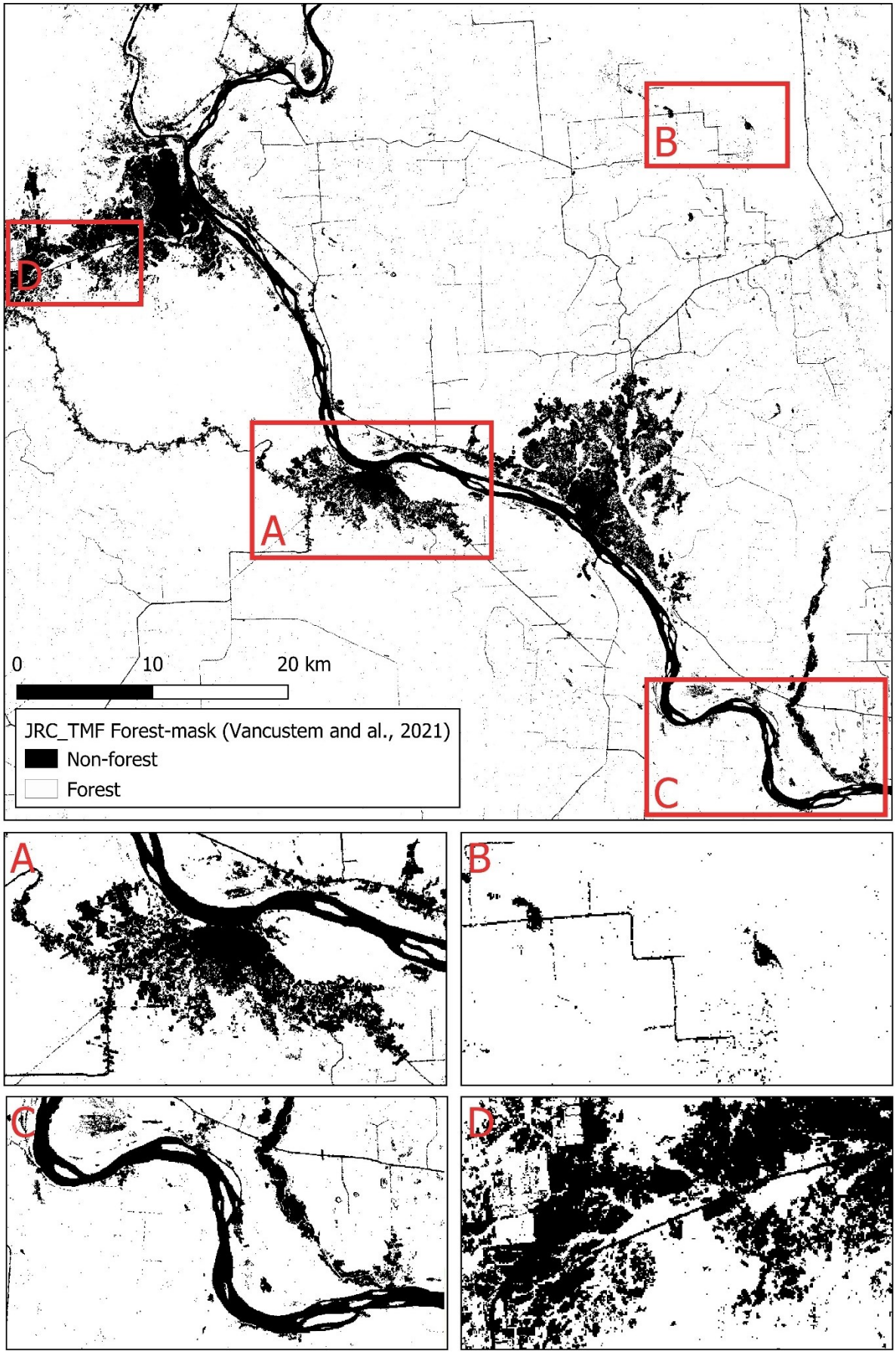

References

A. Mercier et al. (2020). « Evaluation of Sentinel-1 & 2 time series for predicting wheat and rapeseed phenological stages », ISPRS Journal of Photogrammetry and Remote Sensing, Volume 163, 2020, Pages 231-256, ISSN 0924-2716.

A. Mestre-Quereda et al. (2020). «Time-Series of Sentinel-1 Interferometric Coherence and Backscatter for Crop-Type Mapping ». JOURNAL OF SELECTED TOPICS IN APPLIED EARTH OBSERVATIONS AND REMOTE SENSING, VOL. 13.

Aly M. El-naggar (2018) «Determination of optimum segmentation parameter values for extracting building from remote sensing images». Alexandria Engineering Journal, Volume 57, Issue 4, 2018, Pages 3089-3097, ISSN 1110-0168.

A. S. Mather (1992) «The Forest Transition», Area, Vol. 24, No. 4, pp. 367-379.

A. W. Jacob et al. (2020).« Sentinel-1 InSAR Coherence for Land Cover Mapping: A Comparison of Multiple Feature-Based Classifiers »,IEEE JOURNAL OF SELECTED TOPICS IN APPLIED EARTH OBSERVATIONS AND REMOTE SENSING, VOL. 13.

Alexandre Bouvet et al. (2018) «Use of the SAR Shadowing Effect for Deforestation Detection with Sentinel-1 Time Series», Remote Sens. 2018, 10, 1250.

Amy E Duchelle et al. (2018). « What is REDD+ achieving on the ground?», Current Opinion in Environmental Sustainability 2018, 32:134–140

B. Hu et al. (2021).« Improving Urban Land Cover Classification with Combined Use of Sentinel-2 and Sentinel-1 Imagery. », ISPRS Int. J. Geo-Inf. 2021, 10, 533.

Beck, H. E., Zimmermann, N. E., McVicar, T. R., Vergopolan, N., Berg, A., & Wood, E. F. (2018). «Present and future Köppen-Geiger climate classification maps at 1-km resolution». Scientific data, 5, 180214.

Benson Kipkemboi et al. (2018).« Croptype mapping from a sequence of Sentinel 1 images », International Journal of Remote Sensing.

Biddulph and al. (2021). «Current knowledge on the Cuvette Centrale peatland complex and future research directions». Bois et Forêts des Tropiques, 350. 3-14.

C. Vancutsem, F. Achard, J.-F. Pekel, G. Vieilledent, S. Carboni, D. Simonetti, J. Gallego, L. E. O. C. Aragão, R. Nasi (2021). «Long-term (1990–2019) monitoring of forest cover changes in the humid tropics». Sci. Adv. 7, eabe1603.

C. Werner et al. (2002).« SAR Geocoding and Multi-Sensor Image Registration »

C.De Namur (1990). « Paysages quaternaires de l'Afrique centrale atlantique, page 60 : Aperçu sur la végétation de l'Afrique centrale atlantique», ORSTOM.

Dengsheng Lu, Guiying Li, Emilio Moran, Luciano Dutra & Mateus Batistella (2014). « The roles of textural images in improving land-cover classification in the Brazilian Amazon ». International Journal of Remote Sensing, 35:24, 8188-8207,

D. Kpienbaareh et al. (2021). « Crop Type and Land Cover Mapping in Northern Malawi Using the Integration of Sentinel-1, Sentinel-2, and PlanetScope Satellite Data ». Remote Sens. 2021, 13, 700.

D.S. Boyd1 and F.M. Danson (2005). « Satellite remote sensing of forest resources: three decades of research development »,Progress in Physical Geography 29, 1 (2005) pp. 1–26.

Dargie, G.C., Lawson, I.T., Rayden, T.J., Miles, L., Mitchard, E.T.A., Page, S.E., Bocko, Y.E., Ifo, S.A., Lewis, S.L. (2018). « Congo Basin peatlands: threats and conservation priorities. Mitigation and Adaptation Strategies for Global Change». 24(4), pp.669–686.

de Wasseige C., Tadoum M., Eba'a Atyi R. et Doumenge C. (2015). « Les forêts du Bassin du Congo - Forêts et changements climatiques. » Weyrich. Belgique. 128 p.

del Marmol, Alexis(2019). «Cartographie détaillée des types de formations forestières dans le bassin du Congo par télédétection optique (Sentinel-2) : concessions forestières de la Congolaise industrielle des Bois, Ouesso, République du Congo». Faculté des bioingénieurs, Université catholique de Louvain. Prom. : Defourny, Pierre ; Bontemps, Sophie.

Dipankar Mandal, Vineet Kumar, Debanshu Ratha, Subhadip Dey, Avik Bhattacharya, Juan M. Lopez-Sanchez, Heather McNairn, Yalamanchili S. Rao, Dual polarimetric radar vegetation index for crop growth monitoring using sentinel-1 SAR data, Remote Sensing of Environment, Volume 247, 2020, 111954, ISSN 0034-4257.

Dupuis, Chloé, Philippe Lejeune, Adrien Michez, and Adeline Fayolle. (2020). « How Can Remote Sensing Help Monitor Tropical Moist Forest Degradation?—A Systematic Review» Remote Sensing 12, no. 7: 1087.

Emilien Dubiez et al., CIRAD, CIFORT, AGRO Biotech Gembloux. (2014) « Tendance de déforestation dans le bassin du Congo : Comment réconcilier la croissance économique et la protection des forêts ».

ESA (no date). « Sentinel-1 SAR - Technical Guide ». Available at : https://sentinels.copernicus.eu/web/sentinel/sentinel-technical-guides

ESA (no date). « Sentinel-1 SAR - User Guide». Available at : https://sentinel.esa.int/web/sentinel/user-guides

ESA (no date). «EO portal directory: ALOS-2». Available at : https://earth.esa.int/web/eoportal/satellite-missions/content/-/article/alos-2-1

F.White (1986). « La végétation d''Afrique », ORSTOM, UNESCO. Available at : https://books.google.it/books?hl=fr&lr=&id=WHlau7HQuogC&oi=fnd&pg=PA9&dq=White+(1986)&ots=-uGAA34naX&sig=ic-hLVZKawv1ksb-IX4dCMPzK_A#v=onepage&q=White\%20(1986)&f=false

FAO (2021). « Évaluation des ressources forestières mondiales 2020: Rapport principal ». Rome. Available at : http://www.fao.org/3/ca9825fr/ca9825fr.pdf

Hansen et al. (2013) «High-Resolution Global Maps of 21st-Century Forest Cover Change», SCIENCE, 15 Nov 2013, Vol 342, Issue 6160, pp. 850-853

Haralick Robert M., Shanmugam K. and Dinstein Its'hak (1973). «Textural Features for Images Classification ». IEEE Transactions on Systems, Man, and Cybernetics, vol. SMC-3, no. 6, pp. 610-621.

Herinckx, Julien (2019). «Développement d'une méthode de traitement des séries temporelles des satellites Sentinel-1 permettant la discrimination des écosystèmes forestiers du bassin du Congo». Faculté des bioingénieurs, Université catholique de Louvain. Prom. : Defourny, Pierre ; Radoux, Julien.

Iain H. Woodhouse (2006).«Introduction to Microwave Remote Sensing».

J. Dalimier and al. (2022) «LES FORETS DU BASSIN DU CONGO - ETAT DES FORETS 2021» OFAC.

Japan Aerospace Exploration Agency (2018). «ALOS-2 Solution Book». Available at : https://global.jaxa.jp/projects/sat/alos2/pdf/daichi2_SolutionBook_3rd_En.pdf

Jean-François GILLET (2013).« LES FORETS A MARANTACEAE AU SEIN DE LA MOSAÏQUE FORESTIERE DU NORD DE LA REPUBLIQUE DU CONGO : ORIGINES ET MODALITES DE GESTION ». Available at : https://docplayer.fr/44545506-Les-forets-a-

marantaceae-au-sein-de-la-mosaique-forestiere-du-nord-de-la-republique-du-congo-origines-et-modalites-de-gestion.html

Jean-Paul Lanly (2003). «LES FACTEURS DE DÉFORESTATION ET DE DÉGRADATION DES FORÊTS». Available at : http://www.fao.org/3/xii/ms12a-f.htm

Johannes Reiche and al. (2021). «Forest disturbance alerts for the Congo Basin using Sentinel-1» Environ. Res. Lett. 16 024005

Johannes Reiche and al. (2016). «Combining satellite data for better tropical forest monitoring», GOFI GOFO-GOLC.

Jong-Sen Lee et al. (1991).« Speckle reduction in multipolarization, multifrequency SAR imagery »,TRANSACTIONS ON GEOSCIENCE AND REMOTE SENSING, VOL 29. NO 4.

Jong-Sen Lee et al. (2009).« Improved Sigma Filter for Speckle Filtering of SAR Imagery »,TRANSACTIONS ON GEOSCIENCE AND REMOTE SENSING, VOL. 47, NO. 1,

Joseph J. Erinjery, Mewa Singh, Rafi Kent (2018). «Mapping and assessment of vegetation types in the tropical rainforests of the Western Ghats using multispectral Sentinel-2 and SAR Sentinel-1 satellite imagery», Remote Sensing of Environment, Volume 216, Pages 345-354, ISSN 0034 4257

Léo Breiman (1996).« Bagging Predictors »,Machine Learning, 24, 123-140 (1996)

Léo Breiman (2001).« Random Forests »,Machine Learning, 45, 5–32, 2001

Liu, D.; Xia, F. (2010). « Assessing object-based classification: Advantages and limitations». Remote Sens. Lett., 1, 187–194.

M. Sheykhmousa et al. (2020).« Support Vector Machine Versus Random Forest for Remote Sensing Image Classification: A Meta-Analysis and Systematic Review », in IEEE Journal of Selected Topics in Applied Earth Observations and Remote Sensing, vol. 13, pp. 6308-6325.

Manuela Hirschmugl, Janik Deutscher et al. (2020). «Use of SAR and Optical Time Series for Tropical Forest Disturbance Mapping», Remote Sens. 2020, 12, 727.

Mariana Belgiu, Lucian Drăguţ (2014). «Comparing supervised and unsupervised multiresolution segmentation approaches for extracting buildings from very high resolution imagery». ISPRS Journal of Photogrammetry and Remote Sensing,Volume 96,2014,Pages 67-75,ISSN 0924-2716.

Martin BAATZ und Arno SCHÄPE (no date). «Multiresolution Segmentation: an optimization approach for high quality multi-scale image segmentation»

Megevand, Carole. (2013). « Dynamiques de déforestation dans le basin du Congo: Réconcilier la croissance économique et la protection de la forêt. » Washington, DC: World Bank.

Mercier, Audreye et al. (2019). «Evaluation of Sentinel-1 and 2 Time Series for Land Cover Classification of Forest–Agriculture Mosaics in Temperate and Tropical Landscapes» Remote Sensing 11, no. 8: 979.

Moise Tsayem Demaze (2011).« La télédétection en tant qu'outil de mesure de la réduction de la déforestation (REDD) »,REVUE TELEDETECTION, RECHERCHE ET APPLICATION, 2011, volume 9 (3-4), pp.245- 257.

NASA (no date). «Landsat Science: About» Available at : https://landsat.gsfc.nasa.gov/about

Neha Joshi et al. (2015) «Mapping dynamics of deforestation and forest degradation in tropical forests using radar satellite data», Environ. Res. Lett. 10 034014

Nicolas Deffense and al. (2020) «Benchmarking and algorithmes sélections-Progress meeting 2 ». Sens4stat(ESA)

O H am dan, H Khali Aziz & K Abd Rahman (2011). «REMOTELY SENSED L-BAND SAR DATA FOR TROPICAL FOREST BIOMASS ESTIMATION», Journal of Tropical Forest Science , July 2011, Vol. 23, No. 3 (July 2011).

OFAC (no date) « Cartographie des écosystèmes forestiers »

OFAC (no date). « Note Technique : Construction d'une typologie de l'occupation du sol et des types forestiers en Afrique Centrale ». Available at : www.observatoire-comifac.net

Pauline Gillet et al. (2016). « Quelles sont les causes de la déforestation dans le bassin du Congo ? Synthèse bibliographique et études de cas », Biotechnol. Agron. Soc. Environ. 2016 20(2), 183-194

Proforest (2011). «Interactions FLEGT-REDD+ Note d'information n°2» Available at : https://www.euredd.efi.int/news-room//asset_publisher/E6GDAHshzvwA/document/id/166014

R.E. Schapire (2013).« Explaining AdaBoost. », In: Schölkopf B., Luo Z., Vovk V. (eds) Empirical Inference. Springer, Berlin, Heidelberg.

S. Alim et al. (2014).« Ensemble Learning with Multiple Classifiers and Polarimetric Features for Polarized SAR Image Classification »,Photogrammetric Engineering & Remote Sensing, Number 3 / March 2014, pp. 239-251(13).

S. Kusano, M. Sato and Y. Yokota (2011). « Data interpolation and resampling for a synthetic aperture radar data », 2011 IEEE International Geoscience and Remote Sensing Symposium, pp. 652-655.

Sens4stat-ESA (2021). «Algorithm Theoretical Basis Document: EO Data Pre-Processing».

Sentinel Hub (no date). « Sentinel-1 GRD ». Available at: https://docs.sentinel-hub.com/api/latest/data/sentinel-1-grd/

Sotiris Kotsiantis (2011).« Combining bagging, boosting, rotation forest and random subspace methods »,Artif Intell Rev (2011) 35:223–240.

Souza, Jr, Carlos M., João V. Siqueira, Marcio H. Sales, Antônio V. Fonseca, Júlia G. Ribeiro, Izaya Numata, Mark A. Cochrane, Christopher P. Barber, Dar A. Roberts, and Jos Barlow. 2013. «Ten-Year Landsat Classification of Deforestation and Forest Degradation in the Brazilian Amazon» Remote Sensing 5, no. 11: 5493-5513.

Spracklen, Ben, and Dominick V. Spracklen (2021). «Synergistic Use of Sentinel-1 and Sentinel-2 to Map Natural Forest and Acacia Plantation and Stand Ages in North-Central Vietnam», Remote Sensing 13, no. 2: 185

Stéphane Mermoz et al. (2015). «Decrease of L-band SAR backscatter with biomass of dense forests, Remote Sensing of Environment», Volume 159, Pages 307-317, ISSN 0034-4257.

Tchatchou B, Sonwa DJ, Ifo S et Tiani AM. (2015). « Déforestation et dégradation des forêts dans le Bassin du Congo : État des lieux, causes actuelles et perspectives. » Papier occasionnel 120. Bogor, Indonésie : CIFOR.

The Congo Basin Forest Partnership (2005).«The Forests of the Congo Basin, A PRELIMINARY ASSESSMENT»

Thibault Catry et al. (2018). « Apports de la combinaison d'images satellites optique et RADAR dans l'étude des maladies à transmission vectorielle : cas du paludisme à la frontière Guyane française – Brésil », Confins 2018, 37.

Tropical forest type and land cover mapping from SAR-C multi-year time series (Sentinel-1)

Pokola area, Sangha Province (Rep. of Congo)

Thibauld Collet

The Congo Basin Forest is one of the most preserved forest ecosystems on the planet in terms of species diversity and density (Gillet and al., 2016). Besides its role as a biodiversity reserve, the Congo Basin has an important function as long-term carbon storage especially in the wetlands and peatlands from the Cuvette Centrale. The Cuvette Central area is the biggest peatland complex in the world and is mostly lying in the Republic of Congo and the Democratic Republic of Congo. It gathers all the high organic content wetlands of the Congo River and its tributaries. The quantity of carbon contained within the forest and forest soil differs depending on the forest density, soil water content, tree species and tree heights (Biddulph and al., 2021). This highlights the importance of forest type mapping for carbon stock monitoring. Those considerations make the region one of the most critical forest areas to monitor in the climate change context and the recent decrease in biodiversity.

The Copernicus programme provides a large number of continuous data that are available in radar (Sentinel-1) imagery both very high resolution. Those data have the potential to constitute a good data source for forest type and land cover remote sensing.

This master thesis will explore the regional Congo Basin regional context and Sentinel-1 remote sensing capabilities. The materials and the methodology used will be described. The results and limitations will be discussed. Finally, a complete land cover map will be presented.

The final product of this study is a comprehensive land cover map at ten meter resolution based only on the use of SAR-C images. A map of forest cover change was also produced and was quantitatively and qualitatively compared to optical image-based classifications. Based on these maps and their validation, several conclusions can be presented.

UNIVERSITÉ CATHOLIQUE DE LOUVAIN
Faculté des bioingénieurs
Croix du Sud, 2 bte L7.05.01, 1348 Louvain-la-Neuve, Belgique | **www.uclouvain.be/agro**